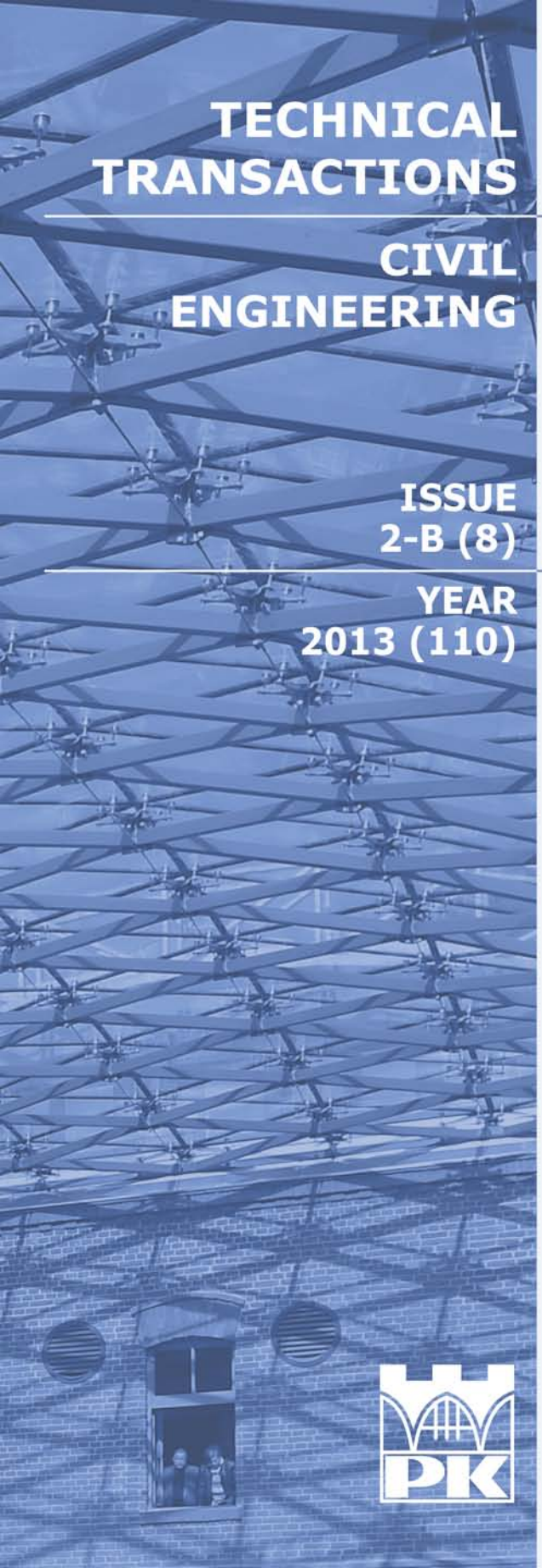

TECHNICAL TRANSACTIONS
CZASOPISMO TECHNICZNE

CIVIL ENGINEERING
BUDOWNICTWO

ISSUE 2-B (8)
ZESZYT 2-B (8)

YEAR 2013 (110)
ROK 2013 (110)

WYDAWNICTWO POLITECHNIKI KRAKOWSKIEJ

TECHNICAL TRANSACTIONS | CZASOPISMO TECHNICZNE

CIVIL ENGINEERING | BUDOWNICTWO

ISSUE 2-B (8) | ZESZYT 2-B (8)
YEAR 2013 (110) | ROK 2013 (110)

Pierwotną wersją każdego Czasopisma Technicznego jest wersja on-line
www.czasopismotechniczne.pl www.technicaltransactions.com

Civil Engineering Series
2-B/2013

Editorial Board

TECHNICAL TRANSACTIONS | CZASOPISMO TECHNICZNE
CIVIL ENGINEERING | BUDOWNICTWO
2-B/2013

WIT DERKOWSKI, MATEUSZ SURMA*

SHEAR CAPACITY OF PRESTRESSED HOLLOW CORE SLABS ON FLEXIBLE SUPPORTS

NOŚNOŚĆ NA ŚCINANIE SPRĘŻONYCH PŁYT KANAŁOWYCH NA PODPORACH PODATNYCH

Abstract

It is widely believed that reduction of unfavorable effects of shear stress in the HC slab's web can be achieved by filling the cores with concrete or through the arrangement of the monolithic layer or concrete topping. The *fib* guidelines are practically the only document which allows for determining the shear capacity of HC slabs, including the influence of concrete topping or core filling – a description of this design model and the calculation analysis are presented in the paper. In order to determine the effect of concrete topping on the behaviour of prestressed HC slabs on flexible supports, a number of calculation analyses were performed. The results of the calculations and the conclusions resulting from it are presented in the paper.

Keywords: Hollow Core, flexible support, Slim Floor, concrete topping, precast slabs

Streszczenie

Powszechnie uważa się, że zmniejszenie niekorzystnego wpływu stycznych naprężeń ścinających w żeberku płyty można osiągnąć poprzez wypełnienie betonem kanałów w skrajnych fragmentach płyty HC lub ułożenie monolitycznej warstwy nadbetonu. Wytyczne fib są praktycznie jedynym dokumentem pozwalającym określić nośność stropów SF z uwzględnieniem wpływu nadbetonu lub wypełnienia kanałów – w artykule opisano ten model obliczeniowy. W celu określenia wpływu nadbetonu na pracę sprężonych płyt HC na podporach podatnych, wykonano szereg analiz obliczeniowych, których wyniki, wraz z wnioskami z nich wynikającymi, przedstawiono w niniejszym artykule.

Słowa kluczowe: Hollow Core, podpora podatna, Slim Floor, nadbeton, płyty prefabrykowane

* Ph.D. Eng. Wit Derkowski, M.Sc. Eng. Mateusz Surma, Institute of Builiding Materials and Structures, Faculty of Civil Engeneering, Cracow University of Technology.

1. Slim Floor Structures

Slim Floors (SF) are structures made of Hollow Core (HC) slabs supported on slender beams where the beam height is usually slightly greater than the height of the precast slab element.

When designing these structures, the fact that deformation of the slabs occurs with the increase of deflection of supports should be taken into account. As a consequence, a complex stress state arises in the slabs – additional transverse normal and shear stress appears in the precast unit (Fig. 1). HC slabs tend to move alongside the beams. On the other hand, the adhesive forces and friction between the slab ends and the beam tend to prevent this displacement which generates incidental stress (Fig. 2). This leads to cracking of the joint between the filling concrete and the beam or between the filling concrete and the slab end. Opening of these cracks reduces the stiffness of the connection and eventually, shear flow between the slab end and the beam is transmitted mainly by the interface between the beam and the soffit of the slab [1].

If the HC slabs are supported so low on the beam that bending of the beam gives rise to transverse tensile stress at the bottom of the slab, the soffit of the slab tends to crack longitudinally. Longitudinal cracks reduce the transverse bending stiffness of the slabs.

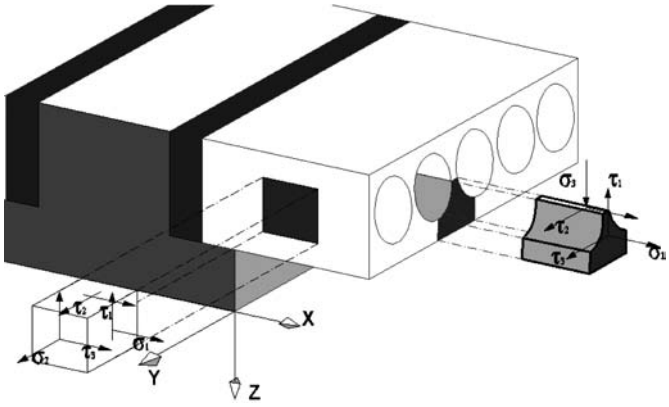

Fig. 1. Stress components in HC web

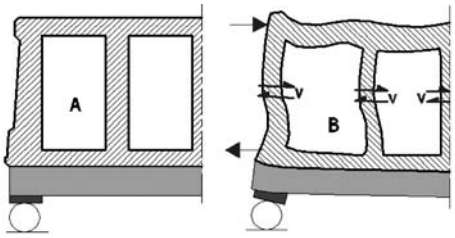

Fig. 2. Deformation of the HC cross-section as a result of deflection of the beam: A – before deflection, B – frame effect

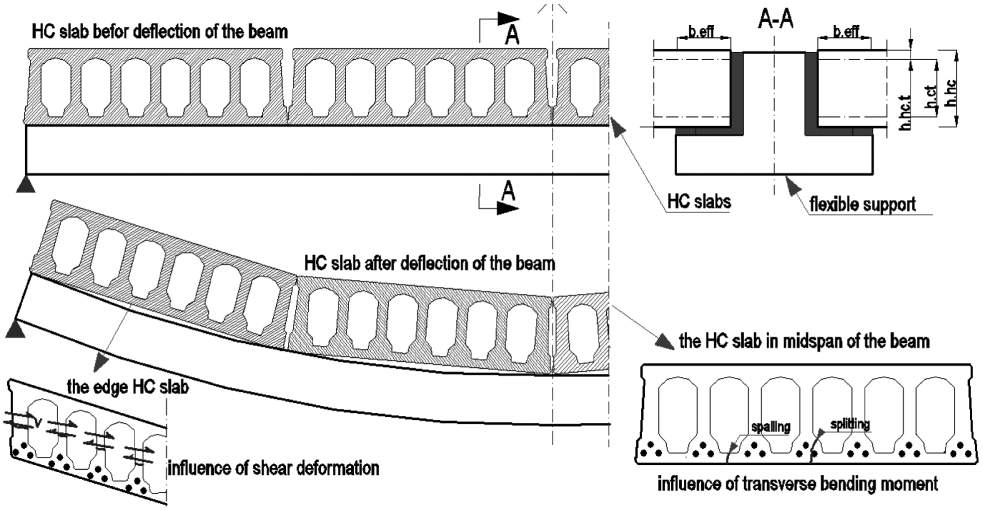

Fig. 3. Behavior of HC slabs on the flexible support

Sometimes the cracks under grow along the strands. It reduces the bond between the strands and the concrete – this has a negative effect on the shear capacity of the slab.

As a result of the deflection of the beam, the difference in work schema of the HC elements, depending on its position along the beam, appears (Fig. 3). The element in the midspan of the beam is subjected mainly to transverse bending moments. While the deflection of the beam occurs, the HC slabs are supported only in the area of their outermost webs [2]. The edge slabs are subjected to shear deformation, which is the main reason for reducing the shear capacity. On the basis of a series of experimentally full-scale tests [3], it has been shown that the failure of the floor always begins from the outermost slabs. The results of the transverse loads state in the SF structures are cracking and shear failure of the HC slabs in their weakest area – non-reinforced edge webs and reduction of the shear capacity [6].

Despite the frequent implementation of these types of structures, the existing standard EN 1168 [7] gives only a brief record of the need to take into account the reduction in design shear capacity, but does not give any calculation procedure [5] may be useful for the design of these types of structures. These recommendations are based on a series of studies carried out in Finland [4] and were created on the basis of the calculation model by Leskelä and Pajari [8]. It is a model of the composite beam and HC slab. This model is a development of the concept of HC elements based on rigid supports and is based on a classical Euler-Bernoulli beam theory. The model for the rigid supports is based on the assumption that the HC elements failure mechanism is due to shear [2, 9].

2. Concrete topping in composite beam model

Reduction of unfavorable effects of shear stress τ_2 in the HC slab's web can be achieved by the applied technological treatments e.g., filling the cores of the outermost slabs with concrete or arrangement of the monolithic layer or concrete topping.

The effects of these treatments are included in the model given in *fib* recommendations [5] by multiplying the basic shear stress component τ_2 by the reduction factor β_f (for filling cores) and β_{top} (for concrete topping). The failure criterion is achieving the tensile strength value of concrete f_{ctd} by the main stress σ_1 ($\sigma_1 < 0$).

$$\sigma_{ps} = \frac{\sigma_1}{2} + \sqrt{\left(\frac{\sigma_1}{2}\right)^2 + \tau_1^2 + \left[\beta_f \left(\tau_{2,top} + \beta_{top} \cdot \tau_{2,imp}\right)\right]^2} \tag{1}$$

where:

$\tau_{2,top}$ – shear stress component of the weight of topping concrete,
$\tau_{2,imp}$ – shear stress component of the additional loads.

Normal compression stress σ_1 and transverse shear stress τ_1 (vertical) are given by the formulae described in (2) and (3):

$$\sigma_1 = -\frac{P_t}{A} + \frac{-P_t \cdot e_p + M_t}{I_y} \cdot z \tag{2}$$

$$\tau_1 = \frac{V_z \cdot S_y}{I_y \cdot b_w} \tag{3}$$

A more difficult issue is the identification of transverse shear τ_2 (horizontal) in the HC web, emerging from the longitudinal compressive transverse shear flows ν in the composite cross-section, consisting of the beam, the concrete grouting of the joint and the upper flange of HC slab, working at the length b_{eff} (4).

$$v = \frac{e_{sl.top} \cdot (\mathrm{EA})_{sl.top}}{(\mathrm{EI})_{com}} \cdot V_b \tag{4}$$

where:

$(\mathrm{EA})_{sl.top}$ – axial stiffness of the whole upper flange,
$e_{sl.top}$ – centroidal distance of the top flange of the HC slab from the centroid axis of the composite cross-section,
EI_{com} – bending stiffness of the composite cross-section,
V_b – shear force of the beam due to imposed load.

On the basis of the compressive transverse shear flows, the value of the transverse shear stress τ_2 can be determined. The model acknowledges τ_2 at the length $x = b_{cr}$, as the average value of the stress for the h_{sl} distance.

$$\tau_2 = \frac{3}{2} \cdot \frac{v \cdot b_{sl}}{2 \cdot b_w \cdot x} = \frac{3}{4} \cdot \frac{v \cdot b_{sl}}{b_w \cdot b_{cr}} \tag{5}$$

where:

b_w, b_{sl} – sum of webs' width in the HC slab, width of the HC slab,
$v \cdot b_{sl}$ – transverse shear force from the slabs supported on both sides of the beam,
$2 \cdot b_w \cdot x$ – cross-section of HC webs supported on both sides of the beam.

The influence of concrete topping is taken into account by a reduction factor given by the formula:

$$\beta_{top} = \frac{\upsilon_{web}}{\upsilon_{top} + \upsilon_{web}} = \frac{\dfrac{0.5 \cdot F_{web}}{\Delta x}}{\dfrac{0.5 \cdot F_{top}}{\Delta x} + \dfrac{0.5 \cdot F_{web}}{\Delta x}} = \frac{F_{web}}{F_{top} + F_{web}} \leq 1.0 \tag{6}$$

where υ_{top} and υ_{web} are horizontal flow shear strength, carried by the reinforced concrete topping and slab' webs. The sum of the impacts of these streams reduces the total shear stress, given by the formula $\upsilon = 2\Delta Nx/\Delta x$ (Fig. 4a) [11].

Value of the shear flows υ_{web} and υ_{top}, could be calculated by the formula:

$$\upsilon_{web} = \frac{4}{3} \cdot \frac{b_{w.sl}}{b_{sl}} \cdot b_{cr} \cdot \tau_2 \tag{7}$$

$$\upsilon_{top} = \min\left[\left(\frac{A_{sv} \cdot f_{yk}}{s} \cdot \mu\right), \left(0.2 \cdot f_{ck} \cdot h_{top}\right)\right] \tag{8}$$

In analogy, design formulas for the F_{top} and F_{web} forces can be written, which are the longitudinal shear capacity per unit length beam in the vertical plane of the composite action between the beam and slab elements, divided respectively for concrete topping and for the slab's webs:

$$F_{web} = \frac{4}{3} \cdot L_e \frac{b_{w.sl}}{b_{sl}} \cdot \sqrt{2} \cdot \frac{f_{ctm}}{\beta_f} \tag{9}$$

$$F_{top} = \min\left[\left(2 \cdot L_e \frac{A_{sv} \cdot f_{yk}}{s} \cdot \varpi\right), \left(0.2 \cdot f_{ck} \cdot h_{top} \cdot L_e\right)\right] \tag{10}$$

In the above formulae, L_e represents the span of the considered element in the direction of the longitudinal axis of the girder, $b_{w.sl}$ is a total width of webs, and b is the width of the precast element. A_{sv} and f_{yk} are respectively the cross section area and yield strength of reinforcing bars in concrete topping, spaced along the beam with a distant of s. Not only reinforcement in concrete topping layer, but also its thickness, surface roughness and cracked concrete strength affect the value of the coefficient β_{top}. The *fib* guidelines assumed the constant coefficient of friction with a value equal to $\mu = 2.0$ [5].

β_{top} – reduction factor in concrete topping – reduces the shear stress τ_2 when the minimum reinforcement in concrete topping are bars with a diameter of minimum 5 mm spaced at 150 mm and the reinforcement is so anchored to take the tensile force that appears after cross scratches [3]. Based on the FEM analysis [6], it was found that the typical reinforcement in concrete topping (grid 15 × 15 mm, ø = 6 mm) increases the value of the horizontal shear force in the webs by 1–3%, and a strong reinforcement in concrete topping (10 × 10 mm mesh, diameter = 10 mm) with 5–12%.

The continuous reinforcement in the area of the support in concrete topping introduces a level of unintended fixing on the support plates which can lead to cracking (Fig. 4b). Type A cracks are not dangerous, but crack types B and C reduce the load plate shear HC. If the model of the composite beam with a layer of unreinforced concrete topping is used with regard to the

same effective width of plates without concrete topping as the HC b_{eff}, additional concrete layer can negatively affect shear capacity on the plates. It seems probable that the reinforcement in the concrete topping layer, parallel to the axis of the plate HC, can reduce the deformation of elements in the direction of the girder, thereby positively affecting the shear capacity [6]. In the light of these studies, for slabs with longer spans, a concrete topping layer is a better option to increase the shear capacity of the HC element than filling the cores. Although topping generates additional load, it increases the stiffness of the slab in the SLS [8]. Positioning of the concrete topping layer is particularly often used for HC slabs with large spans.

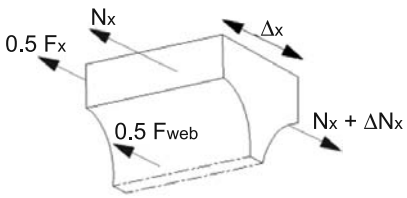

Fig. 4a. Shear strengths balanced the influence of the shear stresses

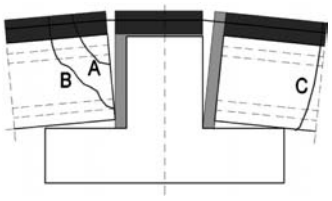

Fig. 4b. Cracking in the HC slab due to unintentional clamping moment in the support

By providing an adequate adhesion of the top surface of the concrete slabs to the concrete topping, one can achieve a positive impact on the reduction of transverse shear stress in the web and an increase in the capacity of the shear elements. However, the presence of a concrete topping can also have negative consequences, i.e. by increasing the surface of the compressed flange, increasing the total flow of the longitudinal tangential stresses [8].

3. Parametric design analysis

In order to determine the impact of the various parameters of the design model described above, a large number of calculations were performed.

The subject of the first analysis was to determine the effort HC slab (expressed by the ratio of principal stresses σ_{ps} to the design value of the tensile strength of concrete f_{ctd}) for a variety of cooperation between the HC element and the concrete topping: HC without any topping, full composite action between the HC and the reinforced concrete topping, full composite action between the HC and the unreinforced concrete topping and the topping layer treated only as a ballast. For example, the results obtained for the slab HC 320 are shown in Fig. 5.

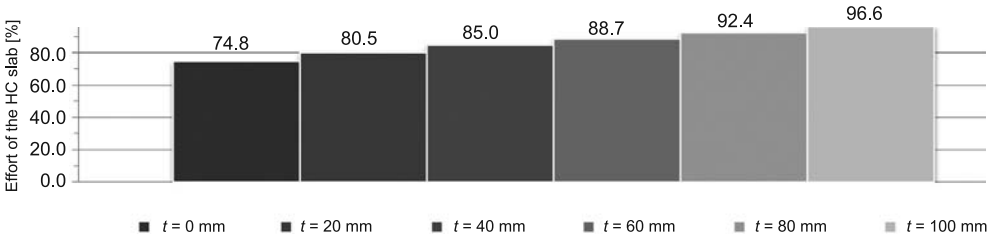

Fig. 5. Effort of the HC slab (320 mm) according to the thickness of concrete topping

Moreover, in the next calculations, the influence of the thickness of the concrete topping (variable from 0 mm to 100 mm) on the effort of the composite slab, as well as the effect of the value of the coefficient of friction between the upper edge of the HC element and the topping, were considered – see Fig. 6. The impact of the order of concreting the vertical joints and laying the concrete topping has been also analyzed. To estimate the influence of the topping reinforcement ratio on the effort of the HC slab's web, other calculations were made. The results are presented on Fig. 7.

The summary of the results for different types of HC elements, working in various conditions is given on Fig. 8–11.

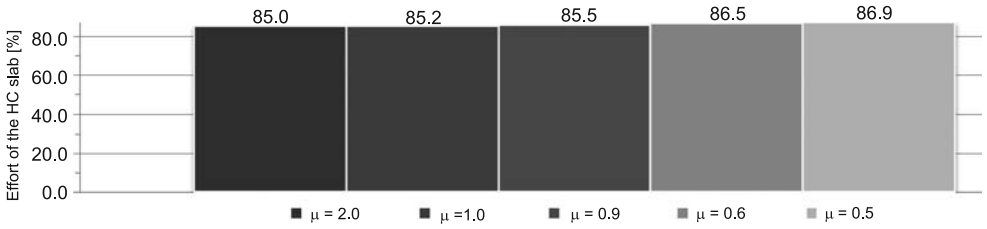

Fig. 6. Effort of the HC slab (320 mm) according to the value of the friction coefficient between the concrete topping and the precast unit

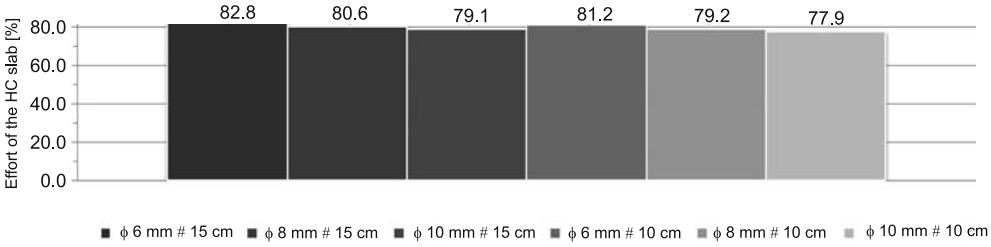

Fig. 7. Effort of the HC slab (320 mm) according to amount of supplementary reinforcement in the concrete topping

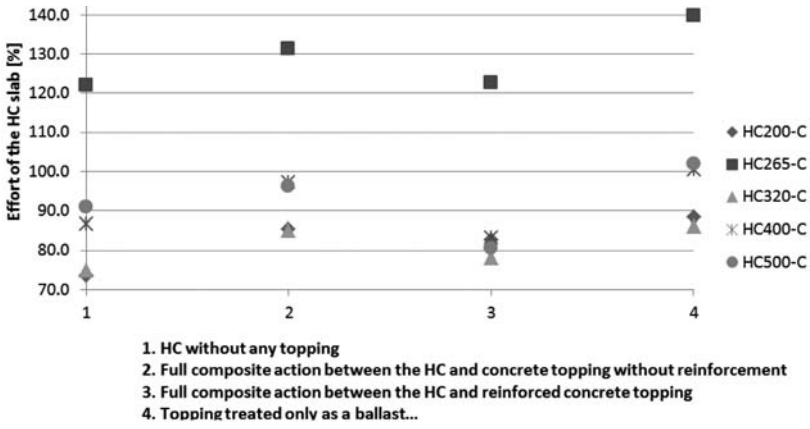

Fig. 8. Effort of the different types of HC slabs with a small number of the webs according to different behaviour of the topping and precast unit

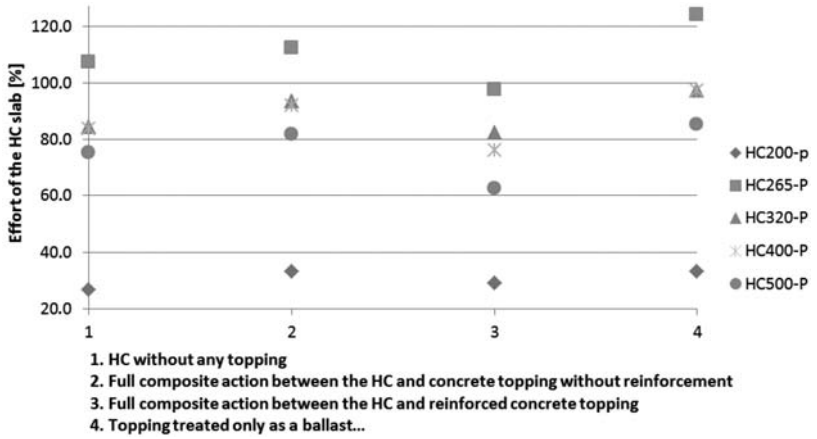

Fig. 9. Effort of the different types of HC slabs with a large number of webs according to different behaviours of the topping and precast unit

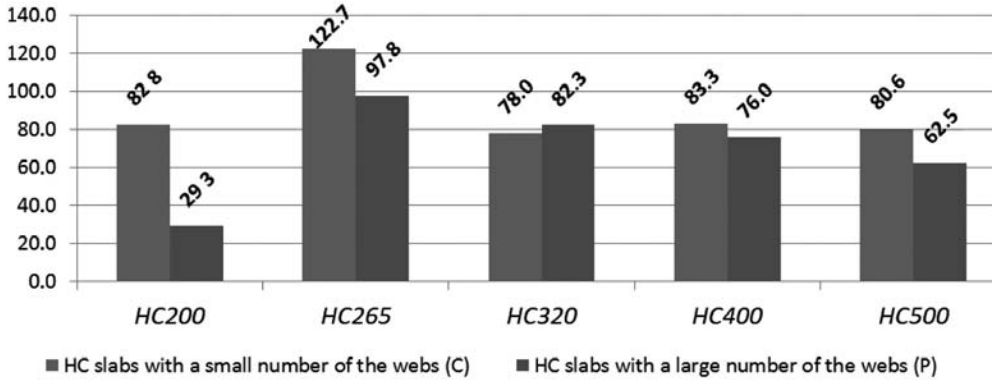

Fig. 10. Effort of the different types of HC slabs with small and large numbers of webs with topping layer

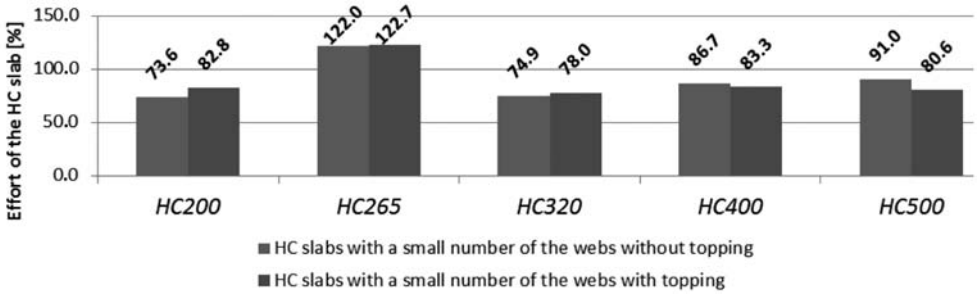

Fig. 11. Effort of the different types of HC slabs with a small number of webs with and without topping layer

4. Discussion of conducted studies

The fib recommendations are based on a series of studies, carried out in Finland by M. Pajari, which were accompanied by a quite gently worded conclusion: "If the composite beam model is applied using the same effective width as for slabs without topping, the topping has a negative effect on shear capacity. It is possible that a reinforcement parallel to the slab units in the concrete topping may have a positive effect on the shear capacity of HC slabs by reducing shear deformation of HC slab in the direction of the beam" [6].

Only one experimental floor specimen was tested out within the scope of the Finnish studies mentioned above for HC slabs with reinforced concrete topping (HC 265 with a topping height of 60 mm). A comparison of the test results obtained for HC slabs with and without concrete topping showed that a topping layer increased shear capacity of the HC slab ca. 50% [12].

Experimental research carried out in Finland and Germany (1990–2009) for the HC slabs without topping showed that these elements supported on a slender beams have a lower shear capacity than one on rigid supports and the difference of their effort reaches 30–60% [13].

On the basis of computational analyses which were carried out using calculation procedures set exactly in the *fib* recommendations, the following conclusions can be drawn:

- The effort of the HC webs under shear increases with the addition of a concrete topping layer and is aggravated by an increase in its thickness. Although the fact of the incidental loads from self-weight of the topping is indisputable, it seems that the increase of the cross-sectional dimensions of the composite beam should lead to a decrease in its effort. It should be noted that in his research, M. Pajari [6] drew attention to the negative consequences of laying the topping, such as increasing the compression zone resulting in an increase in the shear longitudinal stream in the web.
- Analysis of the influence of the coefficient of friction between the concrete topping and the upper surface of the precast element (varying from 0.5 to 2.0) showed the negligible effect of this parameter on the slab's effort, such as the impact of the order of the vertical joints concreting and pouring of the topping layer.
- The concreting sequence of vertical joints between the slab and the beam is coincident with the expectation, but it does not substantially affect the slab's effort.
- The modification (reduction) of the effective width of the topping on precast elements due to the different classes of concrete of precast slabs and the topping layer does not significantly affect the effort of the slab.

By modifying the reinforcement work described in F_{top} formula (10), by selecting the maximum and not the minimum value of the two given functions, the following conclusions can be drawn:

- The increase in the reinforcement ratio for the topping slightly improves the working conditions of the composite beam. The topping reinforcement may reduce the deformation slab in the direction of the beam, thereby positively affecting its shear capacity. The relationship between the height of the slab and the type of its cross-sectional shape and the increase in shear capacity due to the presence of reinforced topping can be observed. For slabs with a small number of webs and circular cores, the topping layer reduces the effort only for elements with a height higher than 400 mm. However, for slabs with a large number of webs and slender cores, a positive effect of topping is already observed in the elements with a height higher than 265 mm.
- Assuming a simplified cross-section geometry of the precast element, especially for slabs with circular cores, is not meaningless for the calculation result. Shear capacity decreases for the

bigger flange height, but at the same time the topping has a positive impact and slightly increases the shear capacity of the slab. This behavior is observed for all types of HC elements.

5. Conclusions

The results obtained from the analytical calculations, which took into account the presence of the concrete topping, do not fully correspond to the common belief about the positive impact of the topping, as well as to the results of experimental tests [6]. The conducted analysis showed also that the shape of the element's cross-section strongly influences its shear capacity. The increase in the reinforcement ratio for the topping slightly improves the working conditions of the whole slab.

According to the authors of this paper, there is a justifiable need for further experimental research in the field of Slim Floors working with topping and for attempts to modify the design model described for such structures.

References

[1] Pajari M., Koukkari H. *Shear resistance of PHC slabs supported on beams I: Tests*, Journal of Structures Engineering, nr 9, 1998.

[2] Pajari M. *Shear resistance of PHC slabs supported on beams II: Analysis*, Journal of Structures Engineering, nr 9, 1998.

[3] Pajari M., *Design recommendations for Hollow Core supported on beams*, VTT Research Rapport RTE37-IR-2/1995, Espoo, 1995.

[4] Pajari M. *Shear resistance of prestressed Hollow Core slabs on flexible supports*, VTT Publications 228, Espoo, 1995.

[5] *fib Bulletin 6 Special design considerations for precast prestressed Hollow-Core floors*, 2000.

[6] Pajari M. Yang L. *Shear capacity of Hollow Core slabs on flexible supports*, VTT Research Notes 1587, Espoo, 1994.

[7] EN 1168:2005+A3 2011 Precast concrete products – Hollow core slabs.

[8] Leskelä M., Pajari M., Re*duction of the vertical shear resistance in Hollow-core slabs when supported on beams*, Proceedings of Concrete`95 Conference, Brisbane, Australia 1995.

[9] Pajari M., *Design of prestressed Hollow Core slab*, VTT Research Rapport 657, Espoo, 1989.

[10] Mercx W., Walraven J.C., *The bearing capacity of prestressed Hollow Core*, Delft, 1983.

[11] Mattock A.H., Hawkins N.M. She*ar transfer in reinforced concrete-recent research*, PCI Journal, nr 1, 1972.

[12] Pajari M. Prest*ressed Hollow Core slabs supported on beams. Finnish shear tests on floors in 1990–2006*, VTT Working Papers 148, Espoo, 2010.

[13] Roggendorf T., *Zum Tragverhalten von Spannbeton-Fertigdecken bei biegweicher Lagerung*, Dissertation, Aachen 2010.

TECHNICAL TRANSACTIONS | CZASOPISMO TECHNICZNE
CIVIL ENGINEERING | BUDOWNICTWO
2-B/2013

JUSTYNA JASKOWSKA-LEMAŃSKA, DANIEL WAŁACH*

METHODS OF REINFORCING HISTORICAL WOODEN CEILINGS ON THE EXAMPLE OF THE PALACE COMPLEX IN GORZANÓW

METODY WZMACNIANIA ZABYTKOWYCH STROPÓW DREWNIANYCH NA PRZYKŁADZIE ZESPOŁU PAŁACOWEGO W GORZANOWIE

Abstract

Modern design and implementation does not only concern newly created and designed buildings, but also buildings that already exist, including historical buildings. The necessity of maintaining their authenticity with minimum interference in the historical substance of the building requires the application of modern design and materials solutions. This problem pertains to most renovated and modernized historical buildings, including the palace complex in Gorzanów, which is located in Lower Silesia in the Kłodzko Valley. Within the framework of adapting the building to modern requirements while maintaining its historic nature, solutions making it possible to preserve richly decorated wooden ceilings, despite the increase of operational loads in palace rooms, are sought after. For this purpose, analysis of the load-bearing capacity of wooden ceilings has been conducted, including architectural and construction inventory, material studies, and the modeling of various possible ceiling reinforcement solutions. The work presents the results of the conducted analysis, and methods of reinforcing wooden structures by means of modern materials and technological solutions have also been discussed.

Keywords: wooden structures, ceiling reinforcement, historical wooden ceilings, CFRP composites

Streszczenie

Nowoczesne projektowanie i realizacje dotyczą nie tylko nowo powstałych i projektowanych obiektów budowlanych, ale również obiektów już istniejących, w tym obiektów zabytkowych. Konieczność zachowania ich autentyzmu przy minimalnej ingerencji w zabytkową tkankę obiektu wymusza zastosowanie nowoczesnych rozwiązań projektowych i materiałowych. Problem ten dotyka większości remontowanych i modernizowanych obiektów zabytkowych, w tym również zespołu pałacowego w Gorzanowie, który zlokalizowany jest na Dolnym Śląsku w Kotlinie Kłodzkiej. W ramach dostosowania obiektu do współczesnych wymagań, przy jednoczesnym zachowaniu jego zabytkowego charakteru, poszukuje się rozwiązań pozwalających na zachowanie bogato zdobionych drewnianych stropów mimo zwiększenia obciążeń użytkowych w pałacowych pomieszczeniach. W tym celu przeprowadzono analizę nośności drewnianych stropów, która objęła inwentaryzację architektoniczno-budowlaną, badania materiałowe oraz modelowanie różnych możliwych rozwiązań wzmocnienia stropów. W pracy przedstawiono wyniki przeprowadzonej analizy, a także omówiono metody wzmacnianie konstrukcji drewnianych przy pomocy nowoczesnych materiałów i rozwiązań technologicznych.

Słowa kluczowe: konstrukcje drewniane, wzmacnianie stropów, zabytkowe stropy drewniane, kompozyty CFRP

* M.Sc. Eng. Justyna Jaskowska-Lemańska, Ph.D. Eng. Daniel Wałach, Department of Geomechanics, Civil Engineering Geotechnics, AGH University of Science and Technology.

1. Introduction

The reinforcement of building structures, including historic buildings, currently constitutes an important problem for both renovators and designers. The development of technologies results in the application of newer solutions and materials which allow for the fulfillment of the requirements posed during conservational renovations. They make it possible to maintain authenticity with minimum interference to the historic substance of the building. It should be remembered, however, that the application of modern technologies carries risks relating to lack of experience in the design of structures with their use.

Historical palace complexes are an essential part of the landscape of Lower Silesia, however, the last decades have been a time of slow degradation for many of them. This is often the result of a lack of clear property rights as well as the necessity of performing large modernizing work in order to achieve a useful state.

Gorzanów is a picturesque town, situated in the center of the Kłodzko lands. In 1573, a renaissance palace and park complex was built there. During the XVII century, the monumental palace was partially rebuilt in the baroque style. Currently, the palace consists of four wings surrounding an inside courtyard, and its representative body can be seen from the Palace rooms in the basement have been covered with barrel vaults with lunettes with sharp vault seams. The upstairs rooms had renaissance polychrome beam-framed floors, which were remodeled in the XVIII century in the central wing to plafonds with polychrome with antique and contemporary themes [4, 8].

a) b)

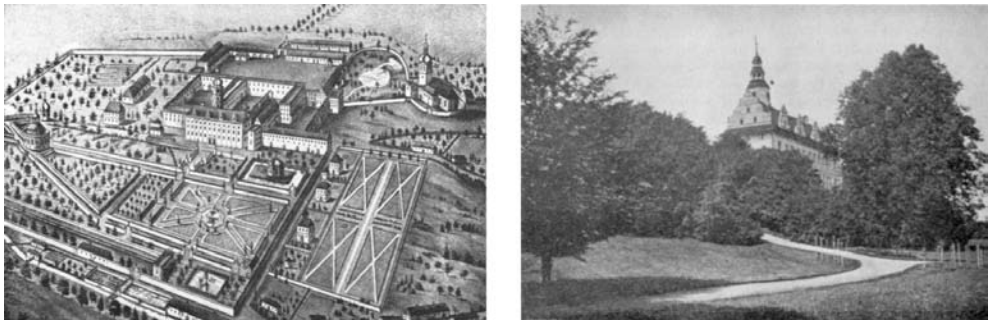

Fig. 1. Palace and park complex in Gorzanów [10]: a) urban layout from the XVII century, b) archival photograph from the beginning of the XX century

After the Second World War, the settled populace from the eastern borderlands stopped caring for the building, and in extreme cases, even used valuable elements of palace furniture for its own purposes. After 60 years of neglect, the current state of the palace can be best described as a ruin [3]. In 2010, one of the owners made an attempt to secure the roof structure. However, badly performed renovation work caused further devastation of the building. Currently, the palace is subject to protective works, and revitalization of the entire area of the palace and park complex is planned in the future. One of its elements will be the adaptation of the main palace body for commercial purposes.

a) b)

Fig. 2. Palace and park complex in Gorzanów – state as of the year 2012: a) exterior eastern facade [10], b) interior eastern facade

2. Analysis of registered damage

In order to determine the current technical state of the building, an inventory of present damage was taken. The most damage was registered in the central part of the palace – the east wing, in which part of the roof was destroyed as a result of badly performed renovation works (Fig. 2b). Also in the west part, in which residential rooms could still be found up to 2011, much damage resulting from a lack of roofing was observed. The north and south wings were kept in a much better state, due to the good state of the roofing.

The main cause of most of the registered damage was the harmful impact of water on structural elements, including, above all, on the historical wooden ceilings. This was caused by many gaps in the roofing and by the complete lack of a roof on the central part of the palace. The absence of a roof is as a consequence of badly performed renovation work. Originally, the palace roofing was made from stone roofing tiles, however, these were replaced with ceramic roofing tiles during renovation work. During renovation, the rafter framing structure was not reinforced despite the biological corrosion present in it. Excessive loading of the rafter framing with material with a greater weight caused this part of the roof to collapse. This, in turn, caused the destruction of ceilings of lower floors found below the collapsed part of the roof (Fig. 5a).

The lack of maintenance work on roof flashing at the point of contact of valley rafters and dormers has resulted in local but intensive impact of water on the structure of the wooden ceilings. As a result of the total degradation of the ceiling of the highest floor, the above impact was transferred in a straight line to the ceilings of successive floors causing their destruction, as illustrated on Fig. 3a and 3b.

Furthermore, it was observed that a significant part of wooden ceiling elements exhibits local damage caused by biological corrosion. This was caused by many years of use, the absence of the appropriate climatic conditions and of ceiling maintenance, as well as by the direct impact of water. The greatest damage to ceilings is present in areas where elements are supported, e.g. points of support of ceiling beams on walls (lack of the appropriate anti-moisture insulation), and also in other areas, locally. This was confirmed by sagging measurements of selected ceilings.

a) b)

Fig. 3. Damage to ceilings of successive floors caused by the local impact of water: a) damage on the II floor, b) damage on the I floor

a) b)

Fig. 4. Biological corrosion of ceilings: a) corrosion caused by a lack of the appropriate atmospheric conditions, b) corrosion caused by the direct impact of water

a) b)

Fig. 5. Ceiling damage: a) absence of ceilings that collapsed along with the roofing, b) fire damage

Sagging measurements of wooden ceiling beams were performed for rooms in which ceilings were preserved in their entirety or were not damaged for the most part. 12 wooden beams located in 6 rooms were subject to measurement. Sagging measurement was conducted using laser rangefinders and a leveled geodetic staff. The results of measurements are presented in graphic form on Fig. 6–7. The X axis shows the distance between successive measuring points, and the Y axis shows vertical distance between measuring points located underside of the beam and reference level. Measuring points are located at an interval of every 50 cm over the entire span of the beam, assuming shifting of extreme measuring points from the wall face by approx. 30–50 cm. Conducted sagging measurements and macroscopic assessment made it possible to determine the nature of the operation of beams and places of their deterioration. Based on measurements, two characteristic types of dislocations can be distinguished – sagging in the center of the beam span resulting from own weight and static load, a natural phenomenon for such a structural system, as well as depressions in areas near supports (e.g. seatings of ceiling beams) that may result from deterioration of the wooden element and significant deflections of walls from verticality. The following charts present results of measurements for two ceilings with varying degrees of sagging.

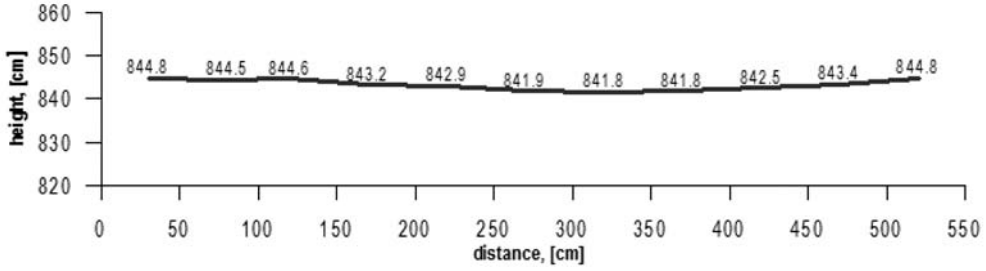

Fig. 6. Exemplary beam sagging at the center of its span

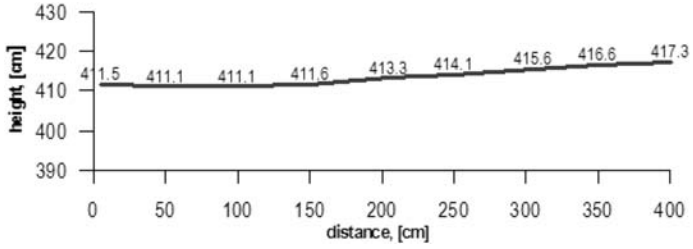

Fig. 7. Exemplary depression in the area near a support

Many years of the absence of protection against water has also caused significant dampness of both interior and exterior walls. This has caused detachment and loosening of plasters, destruction of wall surfaces, and destruction of wall elements themselves.

Table 1

Results of destructive and non-destructive tests

Parameter		Number of samples [pcs.]	Shape and dimensions of sample [mm]	Average value	Standard deviation	Value for 12% moisture content	Characteristic value
Moisture	%	12	20 × 20 × 30	9.33	0.28	12	–
Density	kg/m^3	18	20 × 20 × 30	407.72	28.77	–	–
Compressive strength along fibers	MPa	10	20 × 20 × 30	42.99	5.30	38.41	30.62
Compressive strength transverse to fibers	MPa	8	20 × 20 × 30	9.25	3.1	8.26	3.72
Flexural strength	MPa	3	20 × 20 × 300	74.61	12.97	66.92	47.64
Modulus of elasticity along fibers	GPa	3	–	8.86	–	7.92	–

3. Material studies

In order to assess the technical state of structural wooden elements and the load-bearing capacity of existing ceilings, material samples were collected for non-destructive and destructive laboratory tests.

Destructive tests were conducted according to standards PN-77/D-04227, PN-77/D-04229, PN-79/D-04102, PN-79/D-04103; and the following parameters were determined on their basis: dampness, density, compressive strength along fibers, compressive strength transverse to fibers, flexural strength. In the case of the modulus of elasticity, tests on small samples without flaws were abandoned in favor of tests on full-dimensional elements. Obtained values of individual parameters are presented in table 1. Based on obtained results, the class of wood was determined according to standard PN-B-03150:2000 as C18. The decisive parameter that classified the tested material in a given class of wood proved to be the modulus of elasticity.

Fig. 8. Elements collected for tests

The bending test was conducted as a non-destructive laboratory test on ceiling elements at their actual size. The maximum concentrated force for which studied elements fulfilled the limit use state condition (max $u = L/167$) was determined. The method of conducting tests has been presented on Fig. 9, and obtained results are listed in Table 2. The results of the test show a dependency between the state of the wood and its load-bearing capacity. However, results should not be compared directly, because the tested elements had differing cross-sections.

Fig. 9. Testing of beams in technical scale – view of test apparatus

Table 2

Results of non-destructive material tests

Series	Shape and dimensions of beam [mm]	Macroscopic assessment of state	Sagging [mm]	Force [kN]
Beam I	165 × 155 × 2000	Good	12.08	28.13
Beam II	169 × 150 × 2000	Very good	12.14	33.08
Beam III	159 × 156 × 2000	Biological corrosion	12.35	22.10
Beam IV	130 × 115 × 2000	Good	12.26	13.52
Beam V	164 × 129 × 2000	Very good	12.02	26.24

4. Methods of reinforcing wooden structures

Methods of structure reinforcement can be divided in terms of the nature of their work into:

- a new system of load-bearing elements, in the case where the existing structure is capable of carrying its own load (Fig. 10),

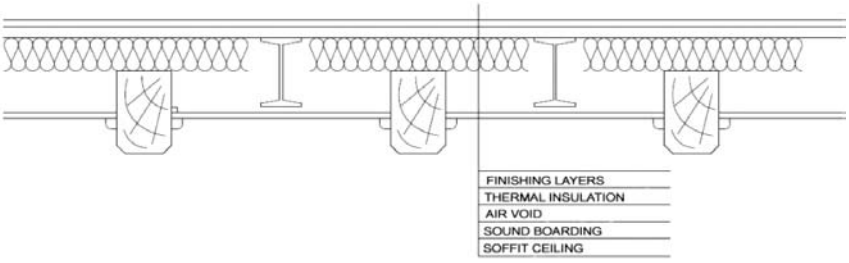

Fig. 10. Exemplary solution of independent reinforcement of a wooden ceiling

- a suspended system, which is simultaneously responsible for carrying useful loads as well as the weight of the historical wooden structure itself (Fig. 11),

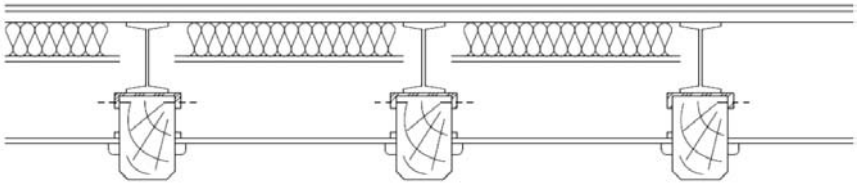

Fig. 11. Exemplary solution of suspended reinforcement of a wooden ceiling

- systems based on cooperation of the reinforcement with the existing structure (Fig. 12),

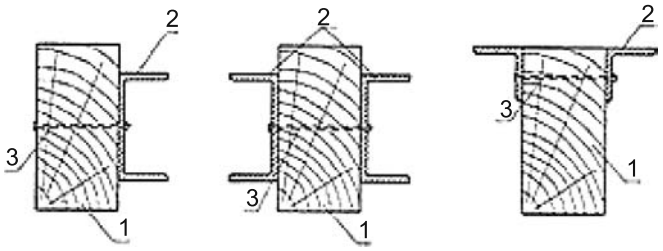

Fig. 12. Exemplary solution of systems based on cooperation of the reinforcement with the existing structure; 1 – Ceiling beam, 2 – Rolled section, 3 – Steal connection

These last systems are most often used due to technological and material diversity as well as due to the exploitation of the existing load-bearing capacity of the structure [1].

Over the years, a series of solutions for reinforcement of wooden structures using conventional construction materials has been developed. The material most often used for reinforcement is steel elements – from steel rods glued in specially prepared grooves in the beam, through substitute rod lattices, steel shackles and cover plates, to brackets made from rolled sections and replacement of part of the element. Such reinforcements are usually visible in the structure, which significantly limits the capability of applying them in historical elements. In certain cases, it is possible to create a coupled structure, e.g. ceiling on wooden beams coupled with a reinforced concrete slab. Such a solution is possible for application when wooden beams are capable of carrying tensile stress, compressive stress will then be carried by the reinforced concrete slab. Conventional solutions also include structural reinforcement based on hydrophobization of elements, which leads to general improvement of the technical parameters of wood [1, 2, 9].

The development of technologies makes it possible to fashion new solutions, with the application of composite materials, among others. These are plastics that most often consist of two phases: a continuous phase (called the matrix) and a dispersed phase, constituting the reinforcement. Currently, fibrous composites with polymer matrices (thermoplastic and thermally hardened resins) reinforced with carbon fibers (CFRP), glass fibers (GFRP) or aramid fibers (AFRP) are most often used. Composites are joined with wood using glues, mainly resin-based glues. The main advantage of composites is the ratio of their weight and dimension to the achieved strength. They can protect a structure very well while essentially not creating any additional load. For example, the gluing of tape to the upper and lower surface of a beam may improve its load-bearing capacity by 100% and rigidity by 40% [6]. CFRP tapes are easy to "conceal" in the cross-section so that the original appearance and shape of the element is preserved. Fig. 13 shows an example of reinforcement of an historical wooden beam with tapes. Pre-stressed composite tapes give new capabilities for reinforcing existing structures. They take part in carrying loads immediately after being glued on and reduce stresses in the existing cross-section. Improvement of the load-bearing capacity of elements therefore takes place through the introduction of a stress state contrary to the stress expected during exploitation as well as through elimination of the influence of wood flaws on its strength [1, 6].

Fig. 13. Reinforcement of ceiling beams in the palace in Gorzanów

5. Analysis of reinforcement of selected structures

Within the framework of the adaptation of the palace in Gorzanów to modern requirements, solutions making it possible to preserve the richly decorated wooden ceilings while improving their useful loads are sought after. For this purpose, analysis of the capability of reinforcing selected wooden ceiling structures was conducted. The ceiling over the "Fireplace" room was analyzed in detail, and its current state has been presented on Fig. 14. Solutions that do not raise doubts concerning aesthetics and that are technologically possible for implementation have been accepted for analysis. The following methods of reinforcement were considered:

- replacement of selected wooden ceiling beams with steel elements,
- gluing of CFRP tapes into selected ceiling beams,
- direct coupling of the wooden ceiling structure with a reinforced concrete slab,
- construction of an independent reinforced concrete slab – suspended system.

a) b)

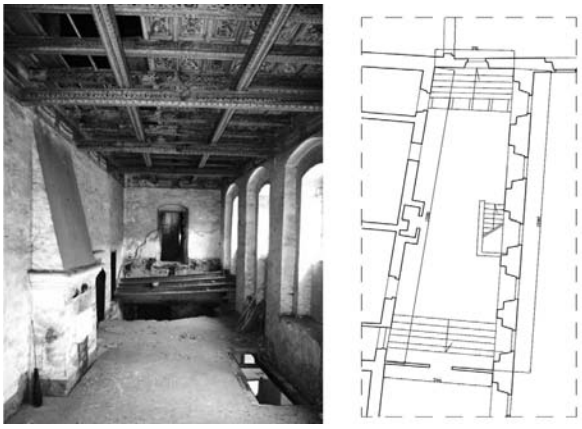

Fig. 14. „Fireplace" room: a) current state, b) projection

Calculations of the load-bearing capacity of the ceiling were carried out using Autodesk Robot Structural Analysis 2012 software. The accepted model of calculations has been presented on Fig. 15.

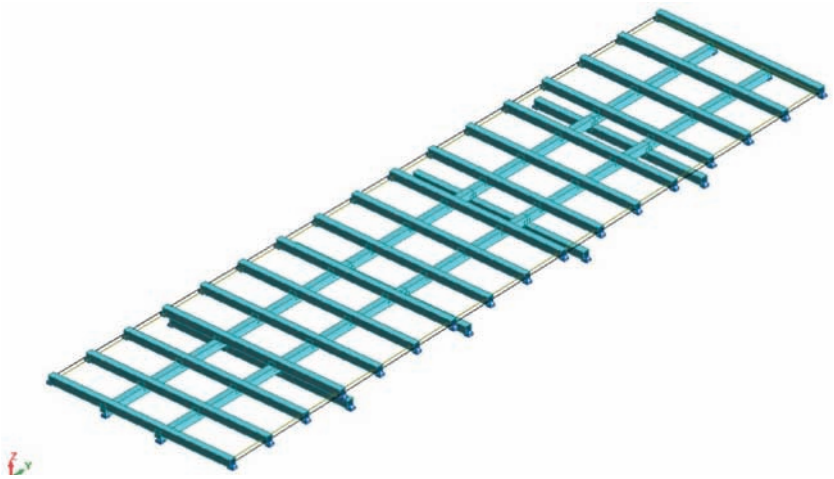

Fig. 15. Calculated model of the ceiling in the "Fireplace" room

For calculations, dimensions of wooden beams of 14.0 × 16.0 cm and a wood class of C18 were accepted based on conducted material tests. In the analyzed ceiling, 3 characteristic groups of beams were distinguished, which were subjected to effort analysis (Fig. 15). Performed calculations of the current ceiling load state (own weight and constant loads from the weight of finishing elements) showed that the efforts of the elements subjected to the greatest load from individual groups of beams do not exceed 100.0%, although the effort of beam no. 2 was as high as 99.0% (Fig. 16).

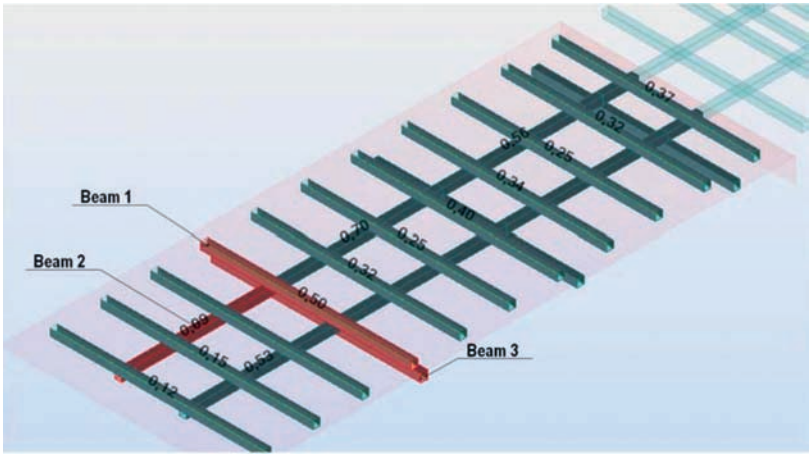

Fig. 16. Efforts of wooden structural elements of the "Fireplace" room ceiling

In the case of the application of additional load to the existing structure, resulting from among other things, the capability of adapting the rooms over the "Fireplace" room as useful rooms, the efforts of the elements carrying the greatest loads were respectively, 77.0% for beam 1, 189.0% for beam 2, and 78.0% for beam 3. This proves that the current technical state of the ceiling does not make it possible for it to carry the additional load relating to the change of use. Furthermore, the current level of effort of certain ceiling beams indicates the necessity of performing additional reinforcing works for the purpose of adapting the analyzed ceiling to modern requirements.

Analysis of ceiling reinforcement through replacement of longitudinal wooden ceiling beams (beam 2) with IPE 100 steel elements indicates (Fig. 17) that this type of structure would be capable of carrying both constant loads as well as operational loads acting on the ceiling. However, at the same time, it must be emphasized that this type of reinforcement would have to be carried out by making special grooves in existing beams into which steel sections would have to be inserted in order to maintain the existing decorations of wooden beams.

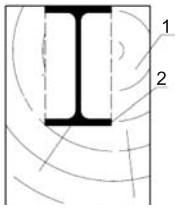

Fig. 17. Replacement of selected wooden ceiling beams with steel elements; 1 – Ceiling beam, 2 – Rolled section (IPE 100)

The application of the method of reinforcement of wooden ceiling beams with CFRP tape makes it possible to accept a higher class of wood in calculations of limit states due to the significant improvement of their strain properties. This is confirmed by the results of studies presented in paper [6] and by the author's own studies, which were conducted on ceiling beam elements acquired from the palace in Gorzanów (Fig. 8). Studies were conducted on beams into which individual CFRP carbon tapes were glued (Fig. 18), and load was applied to these beams to check the fulfillment of limit bending state requirements. Obtained results were related to tests of these same beams without reinforcement.

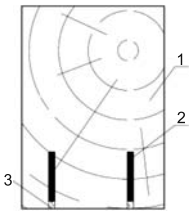

Fig. 18. Gluing of CFRP tapes into ceiling beams; 1 – Ceiling beam, 2 – CFRP tapes; 3 – Structural glue

Analysis of reinforcement of the ceiling above the "Fireplace" room through gluing of CFRP tape into individual ceiling beams indicates that this type of structure would be capable of carrying both constant loads as well as operational loads acting on the ceiling. It is to be emphasized that the improvement of the load-bearing capacity of reinforced beams is directly

dependent on the method of gluing CFRP tapes. It can therefore be accepted that the level of reinforcement can be appropriately shaped in this way with the preservation of the same elements in the ceiling.

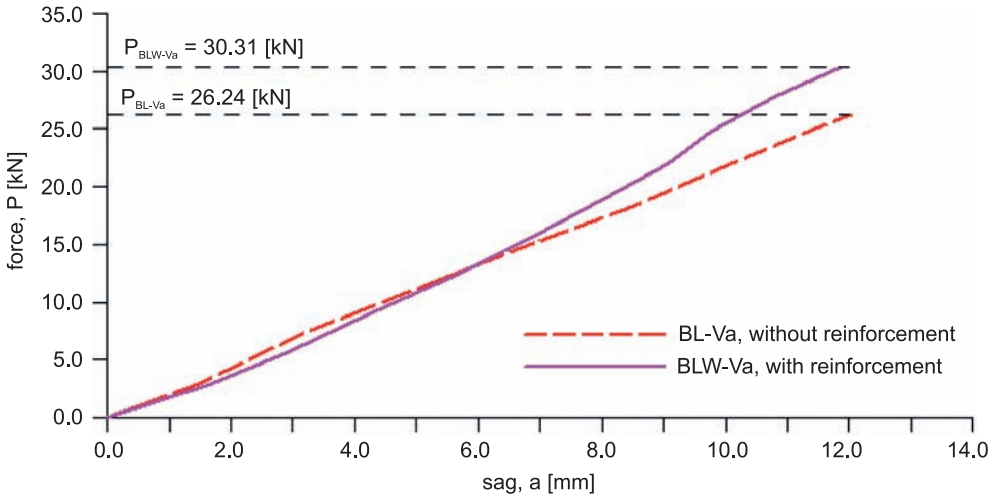

Fig. 19. Improvement of the load-bearing capacity of BL-VA beam in the scope of SGU reinforced with CFRP tape

The application of reinforcement of the analyzed ceiling through coupling of its wooden structure with a reinforced concrete slab (Fig. 20) causes excessive load on it, particularly in beam 2, in which effort rose to above 250%. Above all, this is related to a significant rise in the weight of the entire ceiling structure. In such a case, a suspended system should be implemented by resting the reinforced concrete slab on an independent structure e.g. steel (Fig. 10). The efforts of individual wooden elements in this solution are very small and arise only from carrying loads related to their own weight. It must be remembered that the implementation of reinforcement through direct coupling of a wooden structure with a reinforced concrete slab or the construction of an independent reinforced concrete slab in a suspended system causes significant loading of building walls can cannot *can or cannot?* always be used.

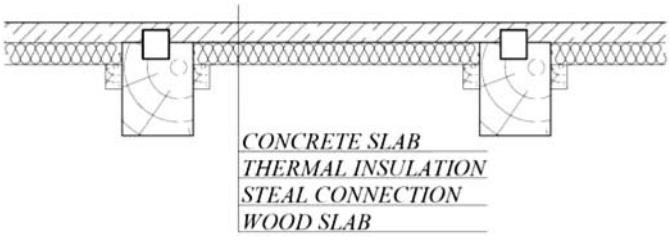

Fig. 20. Direct coupling of the wooden ceiling structure with a reinforced concrete slab

A combined list of obtained results of calculations for individual technical solutions has been presented in Fig. 21.

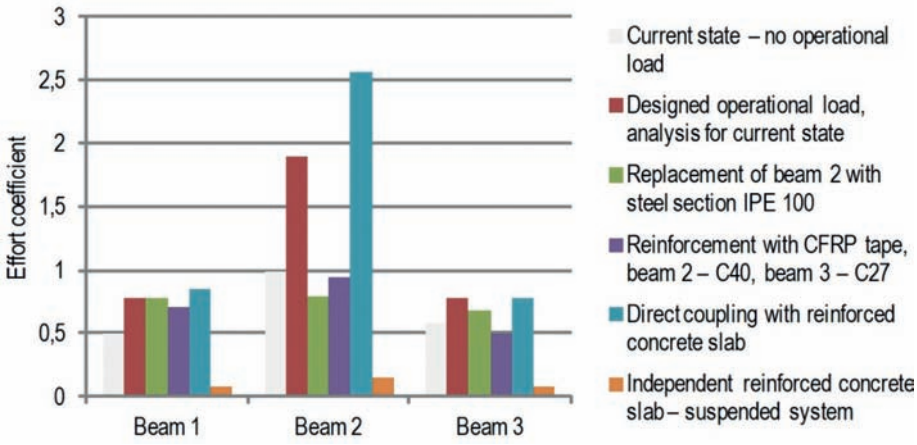

Fig. 21. Results of load-bearing capacity analysis of selected structural elements of the ceiling above the "Fireplace" room depending on the method of reinforcement

6. Conclusions

The damage inventory and conducted tests made it possible to determine the current technical state of selected ceilings found in the historical palace in Gorzanów. Based on performed calculations, it can be stated that selected wooden ceilings that have been preserved in a good state due to their historical value can be reinforced by implementing CFRP carbon fiber tapes or other technical solutions. Reinforced structures would be capable of carrying both constant loads as well as operational loads acting on the ceiling. Before the introduction of new operational loads however, load-bearing capacity analysis must be conducted individually for each ceiling – if load-bearing capacity is too low, coupling of wooden ceilings with a modern reinforced concrete slab may be considered. It should be remembered, that the implementation of certain solutions that reinforce the structure of ceilings may result in excessive loading of building walls and cause additional cracking.

Deteriorated ceilings that do not present historical value may be replaced with new ceilings by using existing seatings as support points for new beams e.g. wood or steel.

References

[1] Jasieńko J., *Połączenia klejowe i inżynierskie w naprawie, konserwacji i wzmacnianiu zabytkowych konstrukcji drewnianych*, Dolnośląskie Wydawnictwo Edukacyjne, 2003.
[2] Karyś J., *Ochrona budynków przed korozją biologiczną*, Arkady, 2001.

[3] Łuczyński R.M., *Losy rezydencji dolnośląskich w latach 1945–1991*, Atut, 2010.
[4] Mazurski K.R., *Ziemia Kłodzka – część południowa*, Sudety, 1996.
[5] Neuhaus H., *Budownictwo drewniane*, Polskie Wydawnictwo Techniczne, 2004.
[6] Nowak T., *Analiza pracy statycznej zginanych belek drewnianych wzmacnianych przy użyciu CFRP*, praca doktorska PRE nr 4/07, 2007.
[7] Nowak T., Jasieńko J., *Analiza pracy statycznej belek drewnianych wzmocnionych taśmami CFRP*, Wiadomości konserwatorskie, 26/2009.
[8] Pilch J., *Leksykon zabytków architektury Dolnego Śląska*, Arkady, 2005.
[9] Rudziński L., *Konstrukcje drewniane. Naprawy, wzmocnienia, przykłady obliczeń*, Wydawnictwo Politechniki Świętokrzyskiej, 2008.
[10] Materiały graficzne udostępnione przez Towarzystwo Miłośników Gorzanowa.

TECHNICAL TRANSACTIONS | CZASOPISMO TECHNICZNE
CIVIL ENGINEERING | BUDOWNICTWO
2-B/2013

RADOSŁAW KANSY, WITOLD CECOT*

HIGHER-ORDER FEM FOR ANALYSIS OF COUPLED PROBLEMS

MES WYŻSZEGO RZĘDU W ANALIZIE PROBLEMÓW SPRZĘŻONYCH

Streszczenie

W artykule przedstawiono zastosowanie hp-adaptacyjnej MES do analizy numerycznej problemów sprzężonych. W szczególności omówiono program *HP3D* i pewne wątki dotyczące adaptacji siatki oraz numerycznych aspektów modelowania problemów sprzężonych. Niektóre możliwości nowego programu ilustruje przykład numeryczny motywowany rzeczywistym inżynieryjnym problemem. Wskazano również na możliwe i pożądane przyszłe kierunki rozwoju tego oprogramowania.

Słowa kluczowe: hp-adaptacyjna MES, modelowanie problemów sprzężonych, termo-mechanika

Abstract

The paper presents the application of the hp-adaptive FEM to numerical analysis of coupled problems. *HP3D* code is especially discussed, as well as some topics concerning mesh adaptation and numerical aspects of modeling coupled problems on the example of weakly coupled thermo-mechanical problem. Some possibilities of the new code are illustrated by a numerical example motivated by a real engineering problem. Finally, some future possible and desirable directions of development for this code are noted.

Keywords: hp-adaptive FEM, coupled problems modeling, thermo-mechanical modeling

* M.Sc. Eng. Radosław Kansy, Ph.D. Eng. Witold Cecot, prof. PK, Institute for Computational Civil Engineering, Faculty of Civil Engineering, Cracow University of Technology..

Denotations

C – elasticity tensor
σ – stress tensor
ε – strain tensor
ε^T – thermal strain tensor
ε^S – shrinkage strain tensor
s – (concrete) shrinkage strain rate
κ – thermal conductivity
α – thermal expansion coefficient
θ – temperature
Q – heat source
δ_{ij} – Kronecker delta
f_i – body forces
u – displacements

1. Introduction

Many engineering problems are of a multi-physical nature and include different physical phenomena, e.g. mechanics and heat transfer, mechanics and acoustics, mechanics of solids and fluids, etc. The numerical analysis of such problems very often requires special treatment.

The Finite Element Method (FEM) is a widely used tool for the approximation of solutions to mechanical problems that can be defined in terms of differential equations. Its variety evolved over the decades. One of these is *higher-order FEM*, which has the main advantage of being able to perform calculations with use of high order approximation functions. This leads directly to an ability to model various problems in which the satisfactory solution is obtained with use of relatively small number of degrees of freedom.

Specialized software, such as the new *HP3D* code, allows for the modelling of various, especially coupled, problems with use of higher-order FEM. Additionally, it allows the user fairly easy application of *hp* mesh refinement. Furthermore, a very important aspect of using *HP3D* [5] is ability to model coupled problems, e.g. thermo-mechanical fields. Other issues which are significant in ground of numerical techniques are presented in this paper.

Thermo-mechanical coupling is significant in analysis of many structures and materials. For example, the issue of crack initiation and fracture propagation, humidity nursing, effective designing and the separation of the phases of forming massive concrete elements became a vast issue for activities in the individual field of engineering science [1, 10].

The issue bordering these thermo-mechanical problems is shrinkage (also expansion; in general: change in volume) field, which can have its source both in thermal field, which penetrates body and humidity field changes, which in turn strongly influences chemical reactions that lead to changes in volume.

The analyzed examples are reduced to modeling the issue of volume changes taking into account only thermal influence. This problem is in fact a weakly coupled one. Therefore, it can easily be decoupled and solved sequentially, i.e. after heat transfer steady state is obtained, stress/strain fields can be derived from the temperature field data. However,

even for such a weakly coupled case this approach seems to be a good option. Moreover, adding an additional coupling term (e.g. heat generation by friction) would change the case diametrically to strongly coupled without a significant complication of the numerical analysis undertaken in *HP3D*.

2. Classification of coupled field problems in engineering

A vast amount of processes which lie directly in the scope of interest for mechanical engineering are of coupled and often multi-physical nature [8]. In general, they have to be analyzed by sophisticated computer codes which need to allow the user to describe various fields that interact with each other and are governed by different laws and involve dependent variables. The coupled problems may be classified and characterized in several ways [2]. One may use:

- weakly coupled (also called one-way or load transfer or loose) – where dependent variables can be eliminated or
- strongly coupled (also called two-way or direct or tight) – where dependent variables usually cannot be eliminated.

These dependent variables result from either physical problems (e.g. displacement and temperature) or the mathematical formulation itself (e.g. displacement and stresses).
In addition, one may easily distinguish the domain and scale of analysis, which may be:

- multi-domain, where coupling effects occurs on an interface of two domains,
- one-domain, with the coupling in the bulk,

and

- one scale analysis, as well as
- multiscale analysis.

Considering the type of physical effects accounted for, one may distinguish the following problems:

1. Exclusively mechanical problems due to independent treatment of:
   - displacement and stress,
   - displacement, strain and stress.
2. Mechanical processes coupled with other physical effects, that induce strain distortions in solids resulting from, for example,
   - temperature change (thermo-mechanical problems),
   - shrinkage or expansion of a composite component, e.g. shrinkage of concrete, development of rust in the steel reinforcement elements within the concrete (chemo-mechanical problems).
3. Fluid-structure interaction e.g. porous media, aeroelasticity, offshore structures (fluid-solid coupling).
4. Acoustic-elastic problems.
5. Bio-heat generation and transfer.
6. Electro-mechanical problems.
7. More than two-field problems, like thermo-hydro-mechanical, welding (CFD, EM, heat, solidification), electro-magnetic-fluid.
8. Other.

The details of approximation significantly influence the computer code structure designated for analysis of coupled field problems. The most important aspects include:

1. Type of coupling:
   - multi-disciplinary, in which one code generates data for another, e.g. temperature field obtained from one code is transferred to another, where in turn the displacement field can be computed and post-processing stages executed,
   - multi-physics, in which all data is stored in one code and can fully operate on weakly or strongly coupled problems.
2. Data base (boundary conditions, subdomains) should account for the type of coupling.
3. Parallel computing may be particularly profitable in this type of modeling.

3. General description of new *HP3D* code

HP3D software was created by: prof. Leszek Demkowicz et al. [3, 5], mainly from *Institute for Computational Engineering and Science, The University of Texas, Austin*, and has a rich library [7] of finite elements: prisms, tetrahedrons and pyramids of arbitrary order up to 8^{th}. To generate the finite element mesh, first a geometry need to be introduced. This step is done with use of GMP (Geometrical Modeling Package). Definition of the domain geometry is obtained by introducing information about "geometrical element mesh" which comes, similarly as the finite elements, in the form of four available solids: tetrahedron, prism, hexahedron and pyramid (see Fig. 1). A Built-in pre and post-processor is used for creating the numerical model and visualizing results in graphical form.

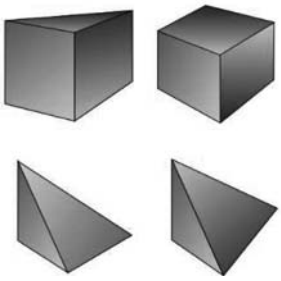

Fig. 1. GMP library members which forms geometry of the modeled object: prism, hexahedron, tetrahedron, pyramid [4]

Then, with use of transfinite interpolation (originally proposed by W. Gordon and C. Hall in 1973 in works regarding four node element and curvilinear coordinate systems applied to mesh generation), which has the important advantage of imitating the exact values of any surface function on its domain boundaries, the strict geometry of the analyzed element is reproduced. This also allows analysis of engineering problems that require very precise modeling of geometry for numerical calculations.

Geometrical blocks consist of the following parts: vertexes, edges, faces. These need to be connected by giving appropriate parameters, as follows: node coordinates (and its sequence), edges (in case of arcs, coordinates of two nodes that belong to the arc and its center), numeration of surfaces in appropriate order which constitutes order for introducing the boundary conditions, and finally, whole solids represented by the node numbers written in appropriate order.

Initial geometry blocks can be partitioned into finite elements of various order of approximation and sizes. Solution improvements obtained by mesh refinement, e.g. building four new, smaller elements from one (division of the base element can be controlled by the user, and executed in any spatial direction separately) is available in two different ways: remeshing the whole domain in three spatial directions separately/simultaneously (uniform *h*-adaptivity) or in selected elements (interactive *h*-adaptivity) by specifying their numbers.

The method of *p*-adaptation is based on the idea of rising up the approximating polynomial order. This gives the ability to model strongly elongated elements without locking effect. An example of anisotropic *hp*-refinement is shown in Fig. 2.

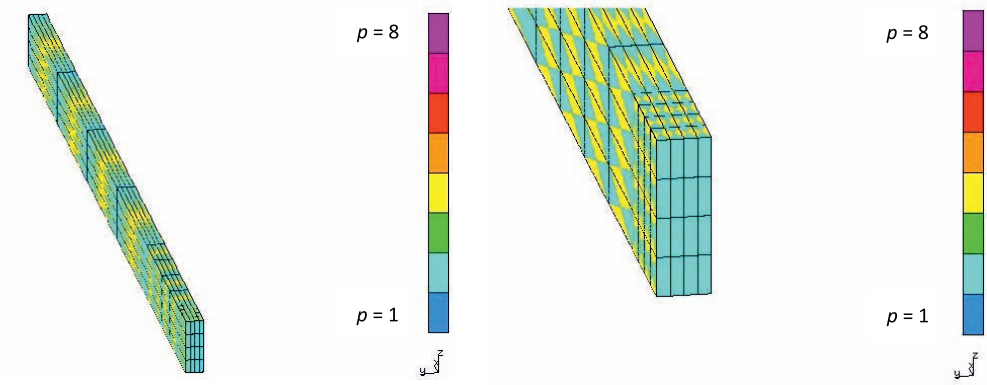

Fig. 2. Elongated elements. *hp*-adaptation in different directions

One of the main objectives of developing the *HP3D* software is introducing mesh refinement criteria (e.g. based on error estimation procedures), from which an appropriate (depending on expectations regarding the quality of solution) order of approximation and density of mesh could be concluded. Experiences and mathematical considerations show [3, 5, 6] that the best convergence (exponential) is obtained when an *hp*-adaptation is applied (see Fig. 3). These criteria should provide answers to a significant question of how to obtain an optimal mesh refinement.

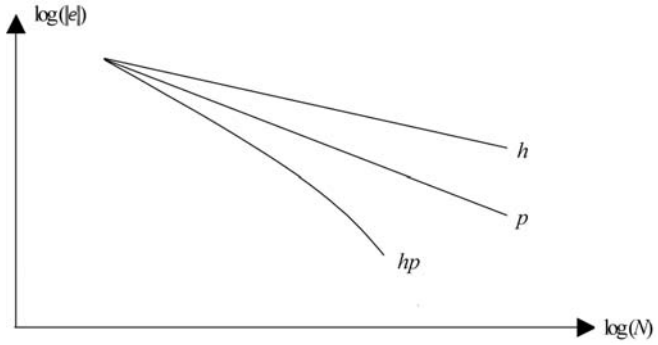

Fig. 3. Idea of convergence rate depending on type of adaptation

Since there is a distinction between geometrical elements that build geometry of the model, and finite elements that provide the solution, pre-processing and refinement procedures cooperate with the GMP module, which is responsible for continuous mapping of exact model geometry, especially after several *h*-adaptations (e.g. rounded objects stay rounded after dividing elements into smaller ones).

HP3D code allows the user relatively easy specification of own problems and procedures, especially when the analyzed issue is of a coupled nature.

4. Formulation of weakly coupled thermo-mechanical problem

The thermo-mechanical problem considered in this paper is weakly coupled. Therefore, the solution may be obtained in the following steps: determination of temperature distribution followed by mechanical analysis. The new *HP3D* code allows solution of all coupled problems in one step, this such an approach is described in this chapter.

Formulation of weakly coupled thermo-mechanics (weakly, because only the temperature field affects changes in the strain field, while deformations do not result in changes in the temperature field) in strong form (considering only elastic model of the material) comes down to the following statements:

$$-\sigma_{i,j,j} = f_i \tag{1}$$

$$\sigma_{i,j} = C_{ijkl}\left(\varepsilon_{kl} - \varepsilon^T_{kl} - \varepsilon^s_{kl}\right) \tag{2}$$

$$\varepsilon_{ij} = \frac{1}{2}\left(u_{i,j} + u_{j,i}\right) \tag{3}$$

$$-\kappa\theta_{,ii} = Q \tag{4}$$

Stated above are the equations of equilibrium (1), stress-strain constitutive law with distortions of different type (2), Cauchy strain-displacement relation (3), and finally differential form of Fourier's law of thermal conduction (4) where C_{ijkl}, κ are material parameters and f_i, Q are given functions. The strain distortions (following will be treated as imposed strains in the procedure) are as follows:

$$\varepsilon^T_{ij} = \alpha\theta\delta_{ij} \tag{5}$$

$$\varepsilon^s_{ij} = s\delta_{ij} \tag{6}$$

where s is the example of concrete shrinkage strain rate [9], i.e.

$$s = \varepsilon_{c,as} = \varepsilon_{c,aso}(f_{cm})\beta_{as}(t) \tag{7}$$

$$\varepsilon_{c,aso}(f_{cm}) = -\alpha_{as}\left(\frac{\frac{f_{cm}}{f_{cmo}}}{6+\frac{f_{cm}}{f_{cmo}}}\right)^{2.5} 10^{-6} \tag{8}$$

$$\beta_{as}(t) = 1 - \exp\left[-0.2\left(\frac{t}{t_1}\right)^{0.5}\right] \tag{9}$$

and α_{as} is a coefficient depending on the type of cement used, f_{cm} [MPa] is the average strength of concrete after 28 days ($f_{cm} = f_{ck} + 8$ MPa)), $f_{cmo} = 10$ MPa, $t_1 = 1$ day.

The boundary conditions for mechanical fields:

$$\sigma_{ij} n_j = q_i \Big|_{\delta\Omega_t} \tag{10}$$

$$u_i = h_i \Big|_{\delta\Omega_u} \tag{11}$$

and for thermal quantities:

$$\kappa \frac{\partial \theta}{\partial n} = S \Big|_{\delta\Omega_F} \tag{12}$$

$$\theta = T \Big|_{\delta\Omega_T} \tag{13}$$

The corresponding weak form can be stated as follows:
find $u \in H_0^1(\Omega) + \hat{h}$ and $\theta \in H_0^1(\Omega) + \hat{T}$, such that:

$$\begin{cases} \int_{\Omega}^{-} \nu_{i,j} C_{ijkl} u_{k,l} d\Omega - \int_{\delta\Omega_t}^{-} \nu_i q_i ds + \int_{\delta\Omega_t}^{-} \nu_{i,i} s ds, \quad \forall \nu_i \in H_0^1(0) \\ \int_{\Omega}^{-} \psi_{,i} \kappa \theta_{,i} d\Omega = \int_{\sigma\Omega_F}^{-} \psi Q ds, \quad \forall \psi \in H_0^1(\Omega) \end{cases} \tag{14}$$

After discretization one obtains the following system of linear algebraic equations (at this level, weak coupling can be seen as a zero element, responsible for coupling mechanical field with temperature, present in the second row of the stiffness matrix):

$$\begin{bmatrix} B_{uu} & B_{u\theta} \\ 0 & B_{\theta\theta} \end{bmatrix} \begin{bmatrix} d_u \\ d_\theta \end{bmatrix} = \begin{bmatrix} L_u \\ L_\theta \end{bmatrix} \tag{15}$$

where d_u, denotes degrees of freedom for displacements and temperature fields, and L_u, L_θ are components of the load vector.

5. Numerical example

The example considers a facade precast member made of polystyrene with thin layer of plaster on it. The real element was built-in the structure and undergone cracking (see Fig. 4). The motivation to model this issue was to implement a weakly coupled problem into *HP3D* code. Weakly coupling was taking into account thermal influence of solar heat, which probably lead to damage of the element.

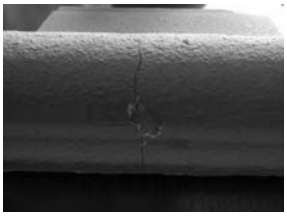

Fig. 4. Facade precast member which undergone cracking

To allow analysis of weakly coupled problems, some changes had to be done to the *HP3D* code. Correctness of these was confirmed by solution of selected benchmark problems and then the software was used to analyze the described real-life problem. The whole part of the element was modeled, although the element was cut from the bigger precast member of facade – this fact is represented in the kinematic boundary conditions.

The following thermal conditions were used: steady state due to the uniform temperature increment inside the domain by ΔT = 20°C (assumed on the basis of daily temperature differences); linear formula (5) for resulting thermal strain ε_{ij}^{T}; adiabatic thermal boundary conditions are assumed only on the exterior face of the element (see Fig. 5 – green color), since only this face stays in contact with the environment.

Material parameters are the same for both materials: thermal expansion coefficient $\alpha_T = 70x\frac{10^{-6}m}{m}°C$, Young modulus E = 3 GPa and Poisson ratio ν = 0.35.

The following kinematic boundary conditions were assumed: fixing on every side surface and internal one (sticking to the wall) – blue color in Fig. 5. Free displacements were allowed only at the external face of the member – green color in Fig. 5.

Results did not exclude that the cause of cracking was the high tensile stress in the element due to the heat exposure. Nevertheless, to state more comprehensive conclusions, further analysis must be done.

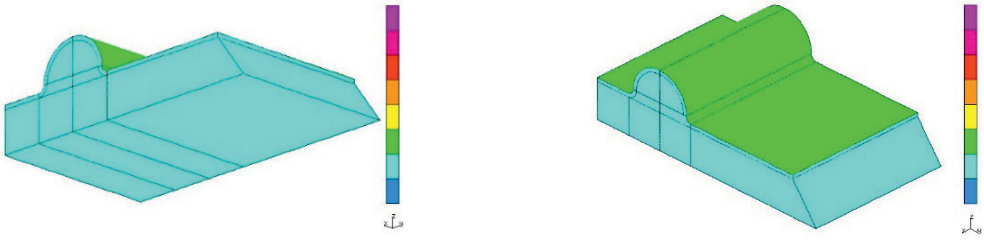

Fig. 5. Kinematic and thermal boundary conditions – see description in the text

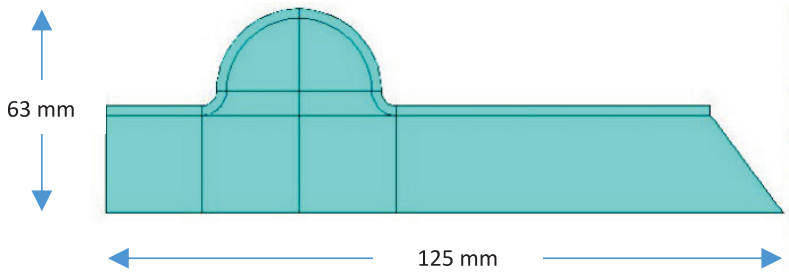

Fig. 6. Dimensions of the model: depth – 80 mm. Thickness of plaster – 3 mm

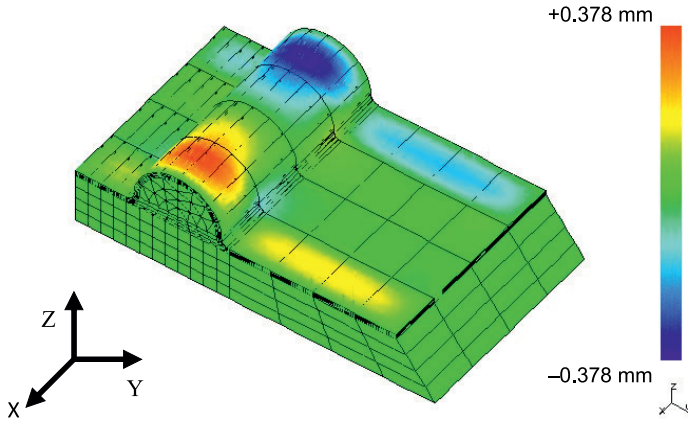

Fig. 7. Displacements at *x* – direction

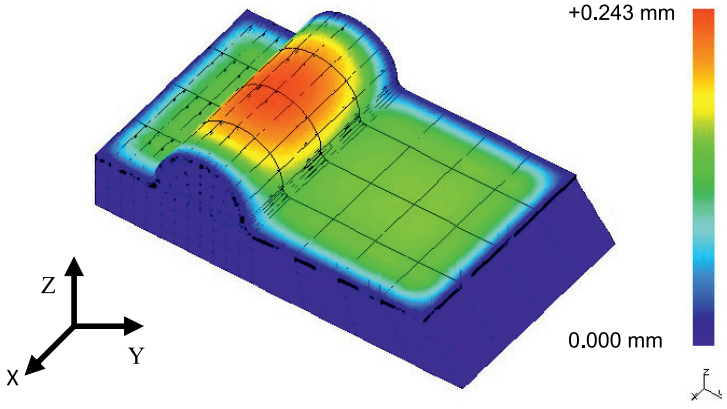

Fig. 8. Displacements at *z* – direction

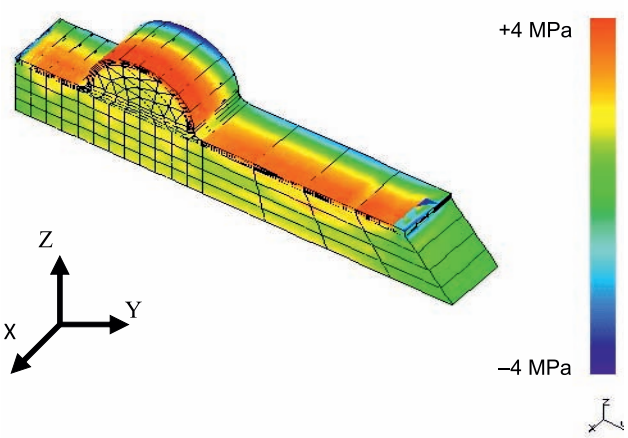

Fig. 9. σ_x strains in longitudinal cross-section

6. Concluding remarks

Development of *hp-adaptive FEM* can contribute to a significant efficiency increase of software used to solve complex engineering issues. To make computations more reliable, algorithms of automatic *hp* adaptation need to be constantly improved and introduced to practice. Effective error estimators should efficiently benefit from *hp* adaptation indicating places where the mesh should be refined and what type of refinement should be performed (*h* – division of elements; *p* – increase in order of approximation; *hp* – both at once).

Solving weakly and strongly coupled problems is also a current challenge. One such problem was presented in the paper [12] and in our future research, the problem of stress/strain fields determination in braking systems induced by heating up of friction pair will be considered. In this case, strongly coupled, nonlinear phenomena are to be considered. The influence of temperature field on mechanics is obvious, whereas the essentially very complex process of energy dissipation, resulting in heat generation, is a direct consequence of friction between two or more elements of the braking system. Therefore, such thermal phenomena have their origin in analysis of nonlinear contact problems.

This research was supported by the European Union through the European Social Fund within; Cracow University of Technology program – top quality teaching for the prospective Polish engineers, University of the 21st century; project(contract no.UDAPOKL.04.01.01-00-029/10-00).

References

[1] Andreasik M., *Naprężenia termicznoskurczowe w masywach betonowych,* praca doktorska, Kraków 1982.

[2] Cecot W., Serafin M., *On coupled field problem*, Technical report, Institute for Computational Civil Engineering L-5, Cracow University of Technology, 2012, http://l5.pk.edu.pl/images/BN/2012_12_a_ICCE_report.pdf.

[3] Demkowicz L., Kurtz J., Pardo D., Paszynski M., Rachowicz W., Zdunek A. *Computing with* hp-*adaptive Finite Elements. Vol. 2. Frontiers: Three-Dimensional Elliptic and Maxwell Problems with Applications*, Chapman&Hall/CRC, 2007.

[4] Demkowicz L., Cecot W., Gatto P., Kim K., Paszynski M., *Short Course on 3D hp-Adaptive Finite Elements and Discontinuous Petrov-Galerkin Method*, Conference seminar materials, HOFEIM (Higher-order Finite Element and Isogeometric Methods), Kraków 2011.

[5] Demkowicz L., *Computing with* hp-*adaptive Finite Elements. Vol. 1. One and Two Dimensional Elliptic and Maxwell Problems*, Chapman&Hall/CRC, 2006.

[6] Demkowicz L., Rachowicz W., Devloo Ph., *A fully automatic* hp-*adaptivity*, Journal of Scientific Computing, 17, 2002, 127-155.

[7] Gatto P., *Modeling bone conduction of sound in the human head using hp-finite elements*, Ph.D. thesis, ICES, 2012.

[8] Hameyer K., Driesen J., Gersem H. De, Belmans R., *The classification of coupled field problems*, IEEE Transactions on Magnetics, (35), 1999, 1618-1621.

[9] Kiernożycki W., *Betonowe konstrukcje masywne. Teoria. Wymiarowanie. Realizacja*, Polski Cement, 2003.

[10] Klemczak B., *Wykorzystanie metod komputerowych w przewidywaniu ryzyka zarysowania konstrukcji masywnych*, Przegląd Budowlany 9/2006, 16-21.

[11] Paszynski M., *Graph grammar-driven parallel adaptive PDE solvers*, AGH, University of Science and Technology Press, 2009.

[12] Yevtushenko A.A., Kuciej M., *One-dimensional problem of friction during braking: The history of development and actual state*, International Journal of Heat and Mass transfer 55, 2012, 4148-4153.

TECHNICAL TRANSACTIONS | CZASOPISMO TECHNICZNE
CIVIL ENGINEERING | BUDOWNICTWO
2-B/2013

MAGDA KIJANIA, TERESA SERUGA, IGA REWERS*

EFFECT OF SOME FACTORS ON SECOND ORDER EFFECTS IN REINFORCED CONCRETE COLUMNS

WPŁYW WYBRANYCH CZYNNIKÓW NA EFEKTY II RZĘDU W SŁUPACH ŻELBETOWYCH

Abstract

This paper presents the results of an analysis of reinforced concrete columns in which there are differences in the value of the second order effects obtained from the method of nominal stiffness (MNS) and the method of nominal curvature (MNC) based on Eurocode 2. Some of the factors such as cracking, ratio of reinforcement, cross-section of a column, and relation of an axial force N_{Ed} to a design axial resistance of section $N_{Rd,}$ were analysed. It was shown that the choice of the method for calculating the second order effect is crucial and can impact the design of columns significantly.

Keywords: concrete columns, second order effects, method based on nominal stiffness, method based on nominal curvature, effective length, cracking

Streszczenie

W artykule przedstawiono wyniki prac i własne analizy dla żelbetowych słupów, w których widoczne są różnice wartości efektów II rzędu, określonych metodami nominalnej sztywności i nominalnej krzywizny wg EC2. Analizując wpływ zarysowania elementów, stopnia zbrojenia, przekroju słupa i stosunku siły podłużnej do siły krytycznej na efekty II rzędu, pokazano, że dobór metody obliczeń efektów II rzędu może znacząco wpływać na wyniki wymiarowania słupów.

Słowa kluczowe: słupy żelbetowe, efekty drugiego rzędu, metoda nominalnej sztywności, metoda nominalnej krzywizny, długość wyboczeniowa, zarysowanie

* M.Sc. Eng. Magda Kijania, Ph.D. Eng. Teresa Seruga, M. Sc. Eng. Iga Rewers, Institute of Building Materials and Structures, Faculty of Civil Engineering, Cracow University of Technology.

1. Introduction

In the analysis of slender reinforced concrete columns subjected to longitudinal force and bending moment, the influence of deformations of the structure on internal forces should be considered. Second order effects are these additional effects, bending moments or eccentricities.

Depending on the kind of construction, with the aim of considering these effects, a global analysis is made – whole construction calculations (which should also take into account the influence of cracking, creep and non-linearity of material properties). The other method is to use a local analysis of isolated members (columns).

The following article concentrates on columns, which can be treated as isolated. The procedure in this case can be simplified to two basic steps:

- static analysis of the whole construction, based on the rule of stiffness (first order analysis),
- checking the slenderness of each column and comparing it with the proper limit values of slenderness. If the slenderness exceeds the limit value, additional moments (eccentricities) caused by deformations of members should be calculated (second order analysis).

There is an increase of bending moments due to second order effects in compressed concrete members. The final value of M_{Ed} moment, which is taken to calculations, consists of:

$$M_{Ed} = M_{0Ed} + M_2 \tag{1}$$

where:

M_{0Ed} – 1st order moment, including the effect of imperfections,
M_2 – nominal 2nd order moment.

In Eurocode 2 [17] three methods used for second order effects analysis are indicated:

- general method – based on non-linear second order analysis,
- simplified method – based on nominal stiffness (MNS),
- simplified method – based on nominal curvature (MNC).

The general method of calculating load-bearing capacity for columns considering second order effects has not been specifically defined in Eurocode 2. It can be assumed that this name is used to describe approaches in which the deformation of the column is not assumed at the beginning. Therefore, it is determined by analysis of subsequent cross-sections at the column length. There is a necessity in this approach to use computer programmes, like in the method described and verified experimentally by M.E. Kamińska and A. Czkwianianc in their paper [1].

Papers [2, 8] inform that methods of analysis of columns apply only to isolated members of constant cross-section and reinforcement, which are subjected to loading only at their ends.

In p. 5.8.5 of Eurocode 2 [17] there is a statement that methods based on nominal stiffness as well as the one based on nominal curvature can be used for isolated members. In 5.8.8.1 (1) of [17] it is said that the nominal curvature method is "primarily suitable for isolated members with constant normal force and a defined effective length l_0". Its usability is restricted by p. 5.8.8.3 of Eurocode 2 to members of constant, symmetrical cross-section with symmetrical reinforcement.

In the Polish National Annex to Eurocode 2, any of the simplified methods (MNS or MNC) were designated as binding ones. The lack of criteria of choosing the proper method

is an important problem due to the fact that the results of calculations of second order effects with two methods mentioned above can be significantly different in lots of cases.

The example described in B. Westerberg paper [14] can be an illustration for this statement. The paper consists of the analysis of the 6.0 m long cantilever column with a cross-section of 0.8 × 0.6 m, subjected on its top side to a transverse force H_{Ed} = 200 kN in the plane of higher stiffness. In the plane of lower stiffness, the column was loaded with a vertical force N_{Ed} = 3000 kN with an eccentricity of e = 0.2 m. Among the material assumptions, the design value of concrete compressive strength was taken as f_{cd} = 20 MPa and design yield strength of reinforcement as f_{yd} = 435 MPa. Second order moments have been calculated with two methods – MNS and MNC (independently in both planes of the column) and the reinforcement calculated for those cases was compared. In the plane of higher stiffness, moments obtained from second order effects calculated by MNS are 1.4 times higher than those from MNC, whereas for the plane of lower stiffness, the factor of the difference increases to 2.4 (that is: for MNS: 1265 kNm, for MNC: 525 kNm).

The relation of second order moments (calculated in the plane of lower stiffness with two methods) to the value of $\omega = A_s f_{yd}/(A_c f_{cd})$ and in comparison to M_{Rd} is shown in Fig. 1 [14].

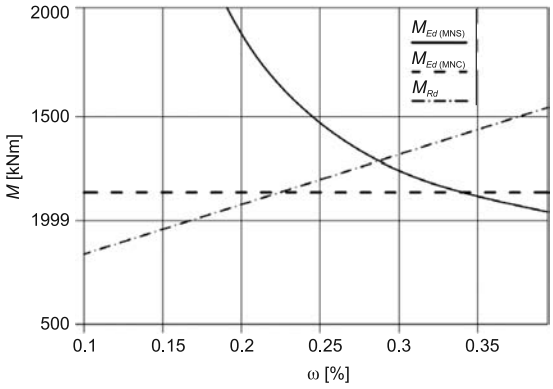

Fig. 1. The relation of second order moments (MNS, MNC) and M_{Rd} to the value of reinforcement intensity ω (for y – axial bending) [14]

The difference between second order effects, calculated with MNS and MNC, can also be noticed on the graphs presented by M.E. Kamińska in paper [5]. Graphical results of calculations of second order eccentricities for columns are presented for various cases: with slenderness l_0/h = 10, 20, 30 i 40, with reinforcement ratio $\rho_{L1} = \rho_{L2}$ = 0,0164 and $\rho_{L1} = \rho_{L2}$ = 0.0027, for strength classes for concrete B20 i B60 and for RB500W for steel. Calculations were performed based on EC2 from the year 2002 as well as PN-02 [16] and were compared with the results from the analytical method.

It can be noticed that the differences between second order effects calculated with MNS and MNC are significant, especially for columns made of lower concrete grades (B20), lower reinforcement ratio ($\rho_{L1} = \rho_{L2}$ = 0.0027) and higher slenderness (l_0/h = 30; 40) with e_0/h = 0.1. The values of second order effects from MNS are then higher than those from MNC; for example for l_0/h = 30 the eccentricity e_2/h for MNS is two times bigger than from MNC.

It is necessary to underline that the values of eccentricities from MNC shown in the graphs presented in the paper [5], are in lots of cases similar to the results obtained from the analytical method. On the other hand, the results from other methods (including MNS) differentiate more, depending on the column slenderness.

K. Koziński, in the paper [7], compared the second order effects obtained from the experimental studies with the results from analytical calculations using various methods: MNS, MNC according to EC2 [17], ACI method [15] and PN-02 method [16]. The results for 16 columns subjected to compression with eccentricities on both axes were analysed. The effective length of the columns was equal to 2.81 m, the cross-sections: 150 × 150 mm; 150 × 300 mm; 150 × 450 mm; 150 × 600 mm. The studies were conducted by subjecting the columns to the assumed loads with eccentricities equal to 50 mm and 150 mm and with the plane deviation angles equal to 22,5° and 45°. The reinforcement ratio of the analysed columns was constant with the value of 2.74%, steel used was RB500W. The columns were made of high concrete grades – the compression strength after 28 days was $f_{cm,cube}$ = 122.8 MPa.

K. Koziński claimed that, on the basis of calculations and the experimental results, the differences between the values obtained from various methods are significant and the second order effects from MNS (similar to those from PN-02) are several times over-estimated. The results of calculations according to ACI were the closest to the experimental data of transverse shifts of the tested columns. The MNC results were less accurate, however, still not so different from the measured values.

The comparing analysis of the influence of the chosen factors on the second order effects in RC columns calculated with the method of nominal stiffness and the method of nominal curvature are presented in the second part of the article. In each case, the action of N_{Ed} and M_{Ed} (strong – axis bending) was considered.

2. Simplified methods of calculating second order effects

2.1. Method of nominal stiffness (MNS)

Method of nominal stiffness is based on the critical force due to the buckling calculated for the nominal stiffness of the analysed member. It is advisable that the material non-linearity, creep and cracking, which have an impact on the behaviour of the structure members, are taken into consideration. The design moment in the members subjected to the bending moment and an axial force which includes the effect of the first and second order effects, can be shown as a bending moment increased by the factor described below:

$$M_{Ed} = M_{0Ed} + M_2 = M_{0Ed} + M_{0Ed} \cdot \frac{\beta}{\frac{N_B}{N_{Ed}} - 1} = M_{0Ed} \cdot \left(1 + \frac{\beta}{\frac{N_B}{N_{Ed}} - 1} \right) \tag{2}$$

where:

M_{0Ed} – 1st order moment, including the effect of imperfections,
M_2 – nominal 2nd order moment,
N_B – buckling load based on nominal stiffness,

N_{Ed} – design value of axial load,
β – factor which depends on distribution of the 1st and 2nd order moments.

2.2. Method of nominal curvature (MNC)

The method of nominal curvature allows for the calculation of the second order moment based on the assumed curvature distribution (which responds to the first order moment increased by the second order effects) on the length of the member. The distribution of the total curvature can be either parabolic or sinusoidal.

The value of the II order moment can be calculated as:

$$M_2 = N_{Ed} \cdot e_2 \tag{3}$$

where:

N_{Ed} – design value of axial load,
e_2 – deflection calculated by taking into account such parameters as creep, intensify of the reinforcement and also distribution of the reinforcement over the height of the cross-section.

$$e_2 = \frac{1}{r} \cdot \frac{l_0^2}{c} \tag{4}$$

where:

c – factor depending on the curvature distribution,
l_0 – effective length,
$1/r$ – curvature.

Considering the formula (4), the determination of the l_0 value is particularly important because it influences on the e_2 eccentricity with the second power.

In the aim of determining the curvature of members with a constant, symmetrical cross-section, Eurocode 2 allows the equation:

$$\frac{1}{r} = K_r \cdot K_\varphi \cdot \frac{1}{r_0} \tag{5}$$

where:

$1/r_0$ – basic curvature:

$$\frac{1}{r_0} = \frac{f_{yd}}{0.45 \cdot E_s \cdot d} \tag{6}$$

f_{yd} – design yield strength of reinforcement steel,
E_s – design value of modulus of elasticity of reinforcement steel,
d – effective depth of the cross-section if the reinforcement is located on both sides of the cross-section or substitute effective depth if part of the reinforcement is placed along the cross-section depth, parallel to the bending plane,
K_φ – factor for taking account of creep,

$$K_\varphi = 1 + \beta_\lambda \cdot \varphi_{ef} \geq 1,0 \tag{7}$$

K_r – correction factor depending on axial load,
β_λ – factor for taking account of characteristic compressive cylinder strength of concrete and slenderness ratio.

A β_λ coefficient (β_λ symbol was used to differentiate between β coefficient in MNS equations) is determined as:

$$K_\varphi = 1 + \beta_\lambda \cdot \varphi_{ef} \geq 1,0 \tag{8}$$

where:

f_{ck} – characteristic compressive cylinder strength of concrete after 28 days,
λ – slenderness ratio.

A K_r coefficient, which allows for the decreasing of the curvature of the element for higher axial forces values is calculated as:

$$K_r = \frac{n_u - n}{n_u - n_{bal}} \leq 1.0 \tag{9}$$

where:

n_u – $1 + \omega$,
ω – intensity of reinforcement, $A_s f_{yd}/(A_c f_{cd})$,
n – relative axial force, $n = N_{Ed}/(A_c f_{cd})$,
n_{bal} – relative axial force n in the case in which the the maximum limit value of a moment is achieved. According to the EC2 the value $n_{bal} = 0.4$ can be established,
A_c – area of concrete cross section.

The description of how the K_r coefficient depends on the n_{bal} is included in p. 4.3 of this paper.

3. Effective length of columns as a function of their flexibility in nodes

According to the EC2 [17], the effective length l_0 is determined to consider the shape of the deflection curve (caused by buckling). It is the length of a column with joints on both ends, subjected to constant axial force, with the same cross-section and buckling load as the analysed member. Eurocode 2 includes examples of different buckling modes and the corresponding effective lengths for isolated members with constant cross-sections.

For frames with the regular mesh of columns and beams, Eurocode gives relationship defining the l_0 lengths for isolated members. The general equation is:

$$l_0 = \beta \cdot l \tag{10}$$

where:

β – factor of buckling,
l – clear height of compression member between end restraints.

The β coefficient is calculated according to Eurocode equations numbered (11) and (12), depending whether the structure is braced or not.

For braced members:

$$\beta = 0.5 \cdot \sqrt{\left(1 + \frac{k_1}{0.45 + k_1}\right) \cdot \left(1 + \frac{k_2}{0.45 + k_1}\right)} \tag{11}$$

For unbraced members:

$$\beta = \max \begin{cases} \sqrt{\left(1+10\cdot\dfrac{k_1\cdot k_2}{k_1+k_2}\right)} \\ \left(1+\dfrac{k_1}{1+k_1}\right)\cdot\left(1+\dfrac{k_2}{1+k_2}\right) \end{cases} \tag{12}$$

where:

k_1, k_2 – relative flexibilities of rotational restraints at ends 1 and 2.

They are calculated using an equation:

$$k = \frac{\theta}{M}\cdot\frac{EJ}{l} \tag{13}$$

where:

θ – rotation of restraining members for bending moment M,

EJ – bending stiffness of compression member.

This relationship after simple transformation can be explained as follows:

$$k = \frac{\alpha_{rs}\left(\dfrac{EJ_a}{l_a}+\dfrac{EJ_b}{l_b}\right)}{k_i\cdot\alpha_{rr}\cdot\sum\dfrac{EJ_r}{l_{eff}}} \tag{14}$$

where:

$\sum\dfrac{EJ_r}{l_{eff}}$ – sum of relative stiffness of beams (bracing members) in a node in an analysed plane,

$\dfrac{EJ_a}{l_a}, \dfrac{EJ_b}{l_b}$ – relative stiffness of column above and below the node,

k_i – coefficient equals 3.0 for pin-ended and 4.0 for restrain,

α_{rs}, α_{rr} – reduction coefficients considering stiffness decrease of beams or columns due to cracking, described below.

If there is a possibility that the compressed member which adheres to the analysed element has an impact on the rotation caused by buckling, it should be included in the calculation of the k coefficient. Therefore symbols a and b have been added to the above mentioned equation – they stand for compressed members (columns) above and below the analysed node.

The influence of cracking can be considered using various approaches with different precision and labour demands, as described in paper [13] for example. The most accurate method is based on determining the stiffness distribution which responds to the moment caused by subjected loads. It is evaluated in a finite number of nodes on the beam length, and the rotation angle caused by the moment in the node is calculated later. However, this method demands sophisticated numerical calculations which can be completed only with the use of computer programmes. A simpler approach is based on the idea of calculating the lowest cross-section stiffness on the length of the beam after its cracking. The most simplified method is to use the decreasing coefficients for stiffness of the members. Respectively, for the full stiffness the coefficients equal to 1.0, while the highest decrease of stiffness is described with the lowest values of these coefficients.

From the comparison of stiffness reducing coefficients presented below, the conclusion is that in many cases, the ratio α_{rc}/α_{rb} equals 0.50.

The approach based on decreasing stiffness is used for example in the ACI-318 [15], where the reduction of stiffness is assumed as follows:

- columns $\alpha_{rc} = 0.70$,
- beams $\alpha_{rb} = 0.35$.

The same values of reduction factors due to cracking are suggested by W. Starosolski in paper [11].

J. MacGregor [9, 8] claims that columns before failure are usually not as cracked as beams, therefore he determines the reduction factors as:

- columns $\alpha_{rc} = 1.00$ without any reduction,
- beams $\alpha_{rb} = 0.50$.

According to another paper by J. MacGregor and S. Hage [10, 8], concrete member stiffness can be reduced by factors:

- columns $\alpha_{rc} = 0.80$,
- beams $\alpha_{rb} = 0.40$.

It seems interesting to analyse how the change of stiffness of beams and columns caused by cracking influences the stiffness of the node or the β coefficient and therefore the second order effects [4].

4. Parametrical analysis

The following part presents a comparative analysis of the influence of certain factors on second order effects in the reinforced concrete columns in braced and unbraced structures. The analysis takes into consideration the following factors: the stiffness of cracked elements (both beam and column), ratio of the reinforcement, area of the cross-section of the column and the relation between design axial force N_{Ed} and design axial resistance of section N_{Rd}.

The subject of this analysis is an isolated column of a frame structure (of typical dimensions for these structures). Two columns with different slenderness (element I and II) in braced structure and one column (element I) in unbraced structure were analysed, assuming the same material characteristics: concrete grade of C30/37 and steel RB500W.

Dimensions, static scheme and support conditions of columns were assumed as is shown on the Fig. 2. In the case of the unbraced structure, the horizontal displacement of beams was allowed (node 2). The dimensions of the cross-section of beams (30 × 60 cm) and the distance between the faces of the supports (5.95 m and 3.00 m) were established. The column I has dimensions of the cross-section: 40 × 50 cm and its height (between the faces of the supports) equals 4.10 m. The respectively dimensions of the column II are: 30 × 40 cm (cross – section) and 6.50 (height).

For comparative purpose, in those analyses in which the following parameters were constant, it was assumed that the results of static analysis did not include the influence of the deformations of structure (equal for restrained and unrestrained structure). The bending moment in the top node 150 kNm and in the bottom one 60 kNm, an axial force 1450 kN and the reinforcement 4φ16 were established.

The support flexibility of the node /1/ $k_1 = 0.1$ (pin – ended) was assumed. It is because of the fact that in reality, the realization of fully fixed support for which the adequate value

is k = 0 (theoretic limit for fully fixed support), is really rare [17]. The support flexibility of the node /2/ was calculated from the relation (11) or (12). The effective creep coefficient φ_{ef} = 1.32 in the braced structures and φ_{ef} = 1,24 in the unbraced structure were established. The value c_0 = 8 was taken into the MNS method for both braced and unbraced structures. In the first case, due to the constant equivalent moment and in the later, due to the fact that this value generates the highest second order effects.

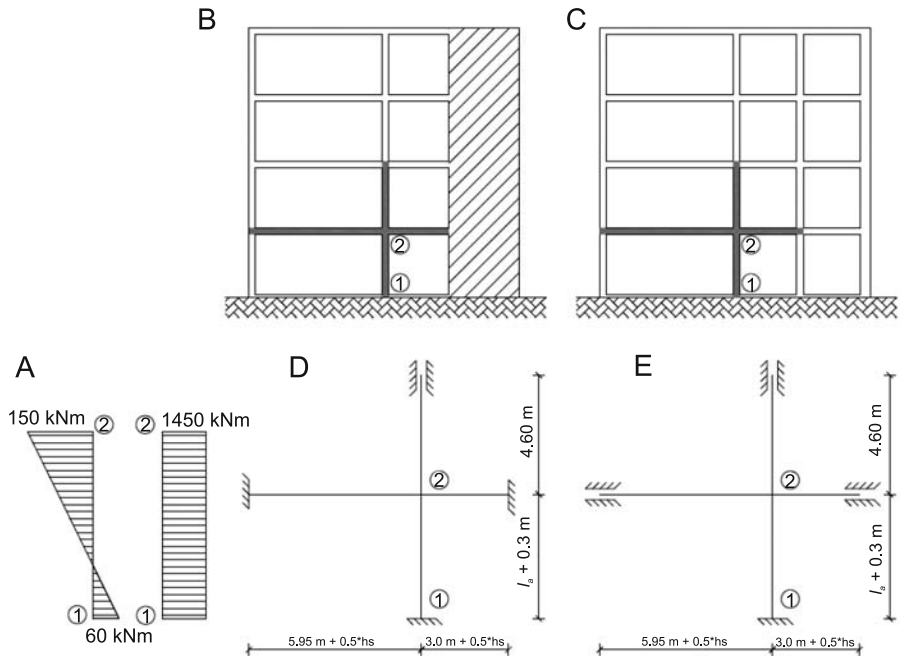

Fig. 2. Forces in the analysed column 1–2 (A) and the static scheme of the part of the braced structure (B, D) and unbraced structure (C, E)

4.1. The influence of cracking on values of the second order effects

Changes in stiffness of the cracked elements and its influence on the support flexibility /2/ and β (11), (12) coefficient and consequently on the size of the second order effects were analysed.

In the analysis, four combinations of stiffness reducing coefficients were taken into consideration, for both braced and unbraced structures:

- case 1 – uncracked beam and column,
- case 2 – uncracked beam and cracked column,
- case 3 – cracked beam and uncracked column,
- case 4 – both beam and column cracked.

Values of the second order effects were calculated according to Eurocode 2 [17] using MNS and MNC. Results of the analysis are presented in Tables 1 and 2 and in graphs 3 and 4 for braced and unbraced structures, respectively.

4.1.1. Analysis of a column in a braced structure

In the isolated member of the braced structure, moments with the second order effects for each case (calculated using both methods) are similar. They differ from 3 to 5 percent for column I and from 6 to 9 percent for column II. Case 3 (cracked beam and uncracked column) generates the largest moments with the second order effects. In cases 2 and 4, when the column was also assumed as cracked, these moments with the second order effects decrease. It can be concluded that taking into consideration a possibility of cracking of beams or columns, does not have a significant influence on the results. It is not necessary to evaluate the decrease of the columns stiffness which is caused by cracking, because such assumption increases the safety reserve. Due to the fact that differences of the results for cracked and uncracked beams (cases 1 and 3) are not significant, the stiffness of the beam could be set at a level of 40–50 percent and furthermore, the exact calculations of the stiffness can be omitted.

Table 1

Moments with the second order effects in relation to cracking of members in braced structures for columns I and II

nb.	factor of stiffness		effective length l_0 [m]		equivalent moment [kNm]		moment including 2nd order effect MNS [kNm]		moment including 2nd order effect MNC [kNm]	
	beam	column	I	II	I	II	I	II	I	II
1	1.00	1.00	2.53	3.73	75.17	79.51	86.08	125.83	93.65	116.07
2	1.00	0.70	2.46	3.67	74.93	79.32	85.24	124.02	92.49	114.97
3	**0.35**	**1.00**	**2.76**	**3.98**	**76.02**	**80.41**	**89.15**	**135.16**	**97.80**	**121.37**
4	0.35	0.70	2.68	3.87	75.72	80.04	88.05	131.22	94.06	116.27

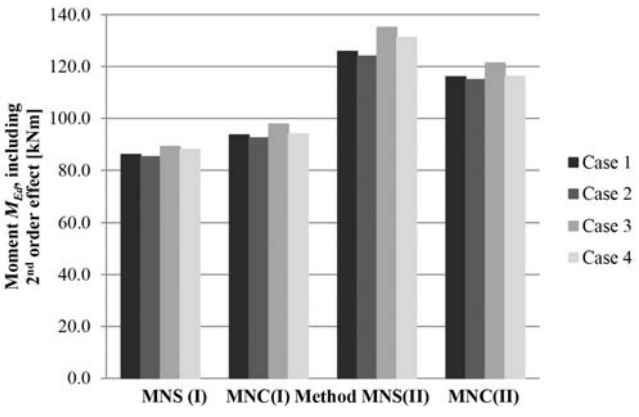

Rys. 3. Results of the analysis of the influence of members' cracking on the second order effects

In the analysis of the braced construction, some inconsequences can be observed and these result from the statements in Eurocode 2. The value of limit slenderness λ_{lim} is 3–4 times bigger than the slenderness of member I and 1.5 times bigger than the slenderness of member II. This means that according to EC2, the second order effects should not be taken into consideration. Designers are allowed to not check the second order effects by comparing the slenderness with the limit value and calculating the concrete column as a thick one. However, the values of the second order effects are greater than 10% of the first order moment (equivalent moment). For element I ($\lambda = 17 \div 19$) the second order effects are 13–17 percent of the equivalent moment for MNS and 23–28 percent for MNC. For the element II ($\lambda = 32 \div 35$) the ratio equals 56–63 percent for MNS and 45–50 percent for MNC.

4.1.2. Analysis of a column in an unbraced structure

In the analysis of the isolated member of the unbraced structure, the calculated moments, which include second order effects, differ significantly, as shown on Fig. 4, for cases 1–4. In each case, higher values of the effects are obtained from the MNS. In both methods, the calculated moments are higher when considering cracking in the beam only (case 3). The difference between the final moment in the uncracked structure (case 1) and in the structure with the cracked beam (case 3) is more than 20% for MNS and about 8% for MNC.

A conclusion should be made that considering cracking of the beam in unbraced structures is very important. However, it is not necessary to take into account cracking of a column for the same reason as in the braced structures. To avoid over-reinforcement of the column, the best option is to calculate the exact stiffness of the beam. There is also a possibility of assuming the stiffness of the cracked beam as retaining 45–50 percent of the stiffness of the uncracked member. However, the influence of the beams' cracking on their stiffness and a flexibility of nodes and therefore on the effective length of columns, should not be omitted.

Table 2

Values of moments with the second order effects in relation to cracking of elements in unbraced structures

nb.	factor of stiffness		effective length l_0 [m]	equivalent moment [kNm]	moment including 2nd order effect MNS [kNm]	moment including 2nd order effect MNC [kNm]
	beam	column				
1	1.00	1.00	5.26	169.07	286.42	239.06
2	1.00	0.70	5.12	168.58	278.21	235.39
3	**0.35**	**1.00**	**6.01**	**171.79**	**340.62**	**259.81**
4	0.35	0.70	5.67	170.56	313.97	239.15

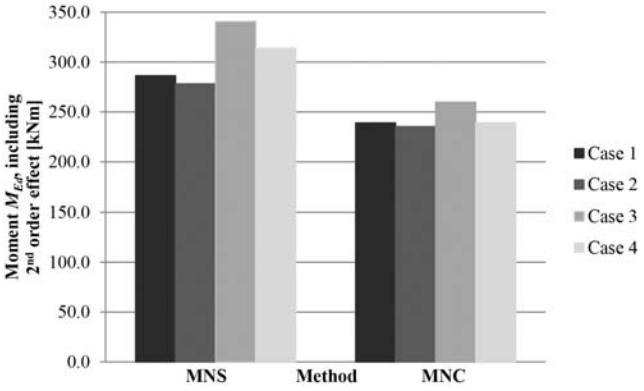

Fig. 4. Results of the analysis of the influence of members' cracking on the second order effects

The differences between the results from MNS and MNC can be easily observed. The values of the moments with the second order effects from MNC and MNS are respectively 70–100 and 40–50 percent greater than the first order moment in columns.

In the analysis of the braced structure, the second order effects are similar for both methods, whereas for the unbraced construction, the second order moments from MNS are 30% higher than those from MNC. According to this remark, the proper choice of method for evaluating the second order effects in an unbraced structure has a significant effect on the design of the column.

4.2. Influence of reinforcement ratio and cross-section of a column on the second order effects

The following analysis presents the influence of the reinforcement ratio in a column in braced construction on the second order effects. The static scheme and support conditions in the column were assumed as on Fig. 2: the bending moment 150 kNm in the top node and 60 kNm in the bottom one and an axial force equals 1450 kN. Material characteristics: concrete grade C30/37 and steel RB500W. The cross-section of the beam is 30 × 60 cm and the distances between the faces of its supports are 5.95 m and 3.00 m. Support flexibility of the node /1/ k_1 = 0.1 and of the node /2/ was calculated from the relation (11). Effective creep coefficient φ_{ef} = 1.32 and c_0 = 8.

The only change is the cross-section dimensions, which are equal to 30 × 40 cm, 40 × 40 cm and 40 × 50 cm, respectively. The analysis is conducted assuming the stiffness reduction factor for a beam as α_{rb} = 0.35 and full stiffness of the column. The reinforcement ratio range is from 0.2% up to 0.99% with a step 0.1%.

Calculations were made with both methods, MNC and MNS. Results are presented in Table 3 and Fig. 5.

Results from both methods differ distinctly. In Fig. 5, they are presented in relation to the equivalent moment, which is a constant value. In the analysed cases, differences

between moments with the second order effects calculated with both methods reach 50%. Moments from MNS decrease with the increasing reinforcement ratio and the largest decrease happens in the column with the smallest cross-section. The reinforcement ratio does not influence values of the second order effects obtained from MNC. The moment is almost equal, small differences in the graph are caused only by changes of the reinforcement diameter.

The largest second order effect from MNS is for the column with the smallest cross-section, whereas it is entirely the opposite in MNC – the highest second order effects are for the largest column.

The other conclusion is that differences between columns of cross-sections of 30 × 40 cm and 35 × 45 cm are higher than the differences between 35 × 45 cm and 40 × 50 cm. The reason for such a situation is a K_r coefficient, which according to Eurocode 2 is limited to the value of 1.0. The column with the smallest cross-section has a coefficient $K_r = 0.74$, the middle column $K_r = 0.95$ and for the largest column, the calculated coefficient was higher than 1,0, therefore it was assumed as 1.0 – according to the equation (9) of Eurocode 2 and Fig. 6. That is why the difference between moment values for middle and the largest column is slight.

Table 3

Moments with the second order effects values [kNm] determined with MNC and MNS in dependence of the reinforcement ratio and column cross-section (in braced construction)

reinforcement ratio [%]	dimensions of the column [cm]					
	40 × 50		35 × 45		30 × 40	
	Moment M_{Ed}. including 2nd order effect [kNm]					
	MNS	MNC	MNS	MNC	MNS	MNC
0.20	99.10	98.09	108.23	97.47	123.13	92.96
0.30	92.86	98.15	99.81	97.56	111.64	93.20
0.40	89.32	98.20	94.91	97.64	104.45	93.41
0.50	87.04	98.24	91.70	97.72	99.78	93.62
0.60	85.44	98.28	89.44	97.79	96.43	93.81
0.70	84.26	98.32	87.75	97.85	93.92	93.99
0.80	83.60	98.36	86.45	97.91	91.96	94.16
0.90	82.64	98.39	85.40	97.96	90.38	94.32
0.99	82.10	98.42	84.63	98.01	89.21	94.46

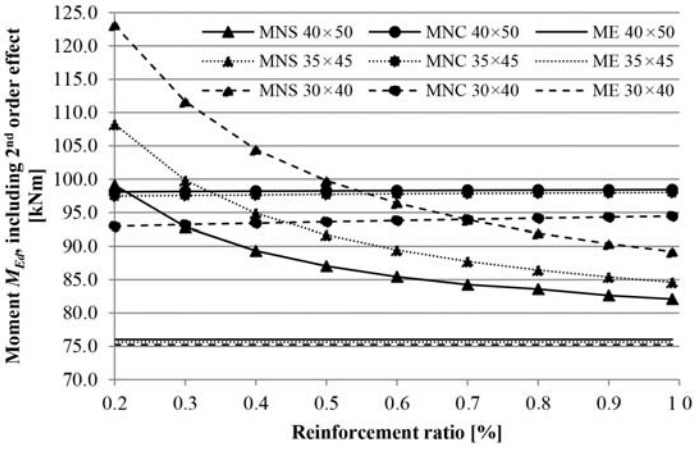

Fig. 5. Moments with the second order effects values determined with MNC and MNS in dependence of the reinforcement ratio and column cross – section. ME – equivalent moment

4.3. Influence of reinforcement ratio and relation of the force N_{Ed}/N_{Rd} on the second order effects in MNS and MNC

Data for the analysis of the column in the braced structure are similar to p. 4.2 and Fig. 2: the bending moment 150 kNm in the top node and 60 kNm in the bottom one. Material characteristics: concrete grade as C30/37 and steel RB500W. The cross-section of the beam is 30 × 60 cm and the distances between the faces of its supports are 5.95 m and 3.00 m. The cross-section of the column is 40 × 50 cm and its height is 4.10 m. The support flexibility of the node /1/ k_1= 0.1 and of the node /2/ was calculated from the relation (11). The effective creep coefficient was φ_{ef}= 1.32 and c_0 = 8. The reinforcement ratio ranges from 0.25% to 0.99%. Relation N_{Ed} to the design axial resistance of section N_{Rd} also differs. Results are presented in Tables 4 and 5 and on the Fig. 8.

Table 4

Moments with the second order effects calculated with MNS in relation to the reinforcement ratio and a longitudinal force value of a column in a braced structure

MOMENT M_{Ed} INCLUDING 2nd ORDER EFFECT [kNm] – MNS						
reinforcement ratio [%]	**relation between N_{Ed} and N_{Rd} force [%]**					
	1	**20**	**40**	**60**	**80**	**99**
0.25	66.9	82.8	98.6	113.8	128.5	142.8
0.50	66.6	78.4	90.9	103.6	116.3	129.0
0.75	66.5	77.0	88.3	99.8	111.6	123.5
0.99	66.5	76.4	87.2	98.2	109.6	121.1

Table 5

Moments with the second order effects calculated with MNC in relation to the reinforcement ratio and a longitudinal force value of a column in a braced structure

MOMENT INCLUDING 2ND ORDER EFFECT [kNm] – MNC						
reinforcement ratio [%]	**relation between N_{Ed} and N_{Rd} force [%]**					
	1	**20**	**40**	**60**	**80**	**99**
0.25	66.9	84.0	101.4	107.3	105.2	95.3
0.50	66.9	85.0	102.6	108.7	106.8	96.7
0.75	67.0	86.0	103.8	110.2	108.3	98.1
0.99	67.0	86.9	104.9	111.6	109.8	99.5

The key parameter in MNC is the K_r coefficient, which takes into account the decrease of the curvature for higher axial force values (Fig. 6). This coefficient should not exceed 1 (EC2 [17]). If $n < n_{bal}$, calculated K_r coefficient is higher than 1, the assumption that $K_r = 1$ should be made. The curvature value $1/r$ is constant. If $n_{bal} = n$, the coefficient $K_r = 1$, while if $n_{bal} < n < n_u$ the K_r coefficient is lower than 1 and the curvature $1/r$ decreases to zero. Values of the second order effect also decrease to zero, and the gradual closing of the cracks contributes to the reduction of their amount. This impact can also be observed in the results of analyses using MNC (Tab. 5 and Fig. 7).

For analysed columns, for the initial range of N_{Ed}/N_{Rd} (Fig. 7), values of the moments with the second order effects increase with an increase of the reinforcement ratio and an increase of the relation N_{Ed}/N_{Rd}, and differences between MNS and MNC are slight. With the increase of an effort, the results obtained from both methods start to diverge. Differences between MNS and MNC increase with an increase of the reinforcement ratio to relation $N_{Ed}/N_{Rd} \approx$ 50% for the reinforcement ratio $\rho = 0.25\%$ and $N_{Ed}/N_{Rd} \approx 80\%$ for $\rho = 0.99\%$ (higher values of the moments with second order effects obtained initially from MNC). When the effort of

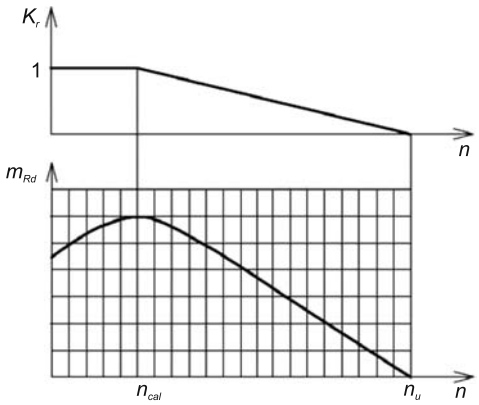

Fig. 6. K_r coefficient in relation to interaction curve $m_{Rd} - n$ according to [6]

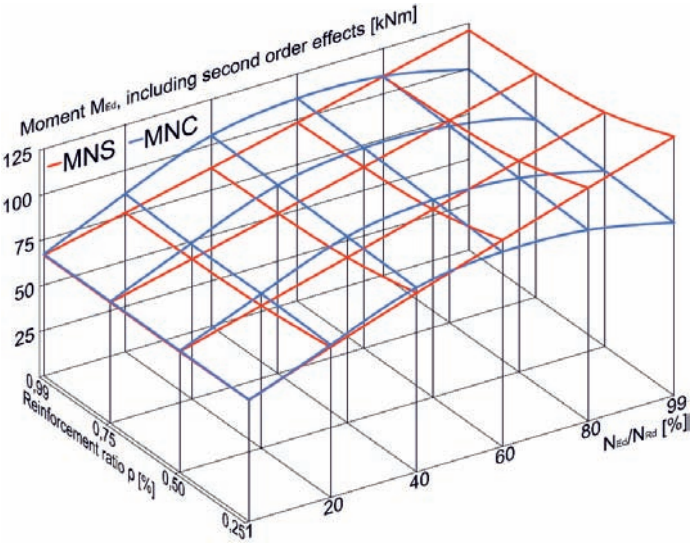

Fig. 7. Moments with the second order effects in dependence of the reinforcement ratio ρ and longitudinal force value, calculated with MNS and MNC

the column increases, the differences between values from both methods are greater (but they decrease with an increase of the reinforcement ratio). Then higher values of the moments with second order effects are obtained from MNS. It is worth mentioning that according to [12], the coefficient which causes deflection of compressed member to increase $(1/[1–(N_{Ed}/N_B)])$ as in equation (2) is exactly (up to 2 percent) for values of N_{Ed} below 60 per cent buckling force N_B.

In the analysed range of the reinforcement ratio in column I (in the braced structure), the biggest differences between moments with second order effects, calculated with MNS and MNC, are obtained when the effort of the column is the biggest and those differences equal from 20 to 50 percent.

5. Conclusions

Eurocode 2 and Polish standards statements do not indicate any criteria for the choice of a proper method for the calculation of second order effects. Results of moment M_{Ed}, which can be obtained from both methods, differ significantly from what has been presented in the conducted comparative analysis. The range of the presented analyses does not allow for the formulation of some general conclusions, however, the remarks are compatible with observations by the Authors of [5, 7, 14], quoted in p.1. MNC provides the second order effects closer to the experimental data [5, 7], however, attention should be paid to the statement 5.8.8.3 of Eurocode 2 [17], which restricts using MNC only for columns with a symmetrical, constant cross-section and symmetrical reinforcement.

The from presented results imply that, stiffness reduction factor considering cracking of beams in braced structures raise the second order effects, however not considerably. From the presented literature and the author's own analysis it can be concluded that the above

mentioned factor can be assumed to be about 50%. In unbraced structures, the influence of this coefficient is significantly larger and a real, exact cracking of the beam should be considered. In both cases, when there is no necessity for high accuracy of calculations, cracking of a column, which decreases the second order effects, can be omitted.

The reinforcement ratio influences the second order effects in a braced structure only in MNS (the second order effect decreases with the increase of the reinforcement ratio), while in the MNC there is no relation. The highest second order effects calculated with MNS are obtained for columns with the smallest cross-section and they decrease with the increasing dimensions of the column's cross-section. In MNC, the situation is the opposite, the highest values of the second order effects are for columns with the largest cross-section, but the differences were not as significant as in the MNS.

The values of the second order effects depend on the longitudinal force. In MNC, they initially grow and then the influence of closing cracks can be observed as the second order effects decrease. In MNS, the second order effects increase consistently. In the presented analysis, the values of M_{Ed}, which were obtained from both methods, differ even by 50%.

The conducted analysis of a braced structure reveals some inconsequences, caused by Eurocode 2 statements. For columns with a slenderness even 3 or 4 times lower than the limit slenderness, the calculated second order effects were 13–17% and 23–28% for MNS and MNC, respectively. Therefore, as exceeding 10% they should not be omitted. For columns with slenderness closer to the limit values, the second order effects are distinctly higher.

The comparative analysis proves that the choice of method for evaluating the second order effects can have a considerable impact on the results of calculations of members subjected to compression. When both simplified methods (MNS and MNC) are allowed to be used in order to calculate the second order effects in Poland, even though they generate different results, some comments which limit the range of the usages should be formulated. This can help designers choose the right method.

References

[1] Czkwianianc A., Kamińska M., *Metoda nieliniowej analizy żelbetowych elementów prętowych*, PAN, KILiW, IPPT, Warszawa 1993.

[2] Czkwianianc A., Kamińska M., *Nośność przekrojów obciążonych momentem zginającym i siłą podłużną*, [w:] *Podstawy projektowania konstrukcji betonowych i żelbetowych według Eurokodu 2*, praca zbiorowa pod redakcją M. Knauffa, DWE, Wrocław 2006.

[3] Fingerloos F., Hegger J., Zilch K., *Eurokod 2 fur Deutchland. DIN EN 1992-1-1 Bemessung und Konstruction von Stahlbeton- und Spannbetontragwerken. Tiel 1–1. Kommentierte Fassung*, Berlin–Wien–Zurich 2012.

[4] Iskra (Rewers) I., Kijania M., Praca magisterska, Politechnika Krakowska 2012.

[5] Kamińska M.E., *Stan graniczny nośności elementów zginanych, ściskanych i rozciąganych*, [w:] *Komentarz naukowy do PN-B-03264:2002*. ITB, Warszawa 2003.

[6] Knauff M., *Obliczanie konstrukcji żelbetowych wg Eurokodu 2*, Wydawnictwo Naukowe PWN, Warszawa 2012.

[7] Koziński K., *Nośność i odkształcalność dwukierunkowo mimośrodowo ściskanych smukłych słupów żelbetowych z betonów wysokiej wytrzymałości*, praca doktorska, Politechnika Krakowska 2011.
[8] Kukulski W., Sulimowski Z., *Stan graniczny nośności z udziałem efektów odkształceń konstrukcji*, [w:] *Podstawy projektowania konstrukcji betonowych i żelbetowych według Eurokodu 2*, praca zbiorowa pod redakcją M. Knauffa, DWE, Wrocław 2006.
[9] MacGregor J.G., *Discussion of Determination of Effective Length Factors for Slender Concrete Columns*, ACI Journal, Proceedings, Vol. 70, No. 5, 1973.
[10] MacGregor J.G., Hage S.E., *Stability analysis and design of concrete frames*, Proceeding ASCE, Journal of the Structural Division, Vol. 103, No. ST10 1977.
[11] Starosolski W., *Konstrukcje Żelbetowe według Eurokodu 2 i norm związanych – tom 3*, PWN, Warszawa 2012.
[12] Timoshenko S.P., Gere J.M., *Teoria stateczności sprężystej*, Arkady, Warszawa 1963.
[13] Wandzik G., *Projektowanie ściskanych elementów żelbetowych wg Eurokodu 2 – kryterium smukłości i długość efektywna*, Materiały Budowlane. Konstrukcje – Technologie – Rynek, nr 1/2013.
[14] Westerberg B., *Second order effects in slender concrete structures. Background to the rules in EC2*, TRITA-BKN. Rapport 77, Betongbygnad, Stockholm 2004.
[15] ACI 318-08, *Building Code Requirements for Structural Concrete and Commentary*.
[16] PN-B-03264:2002 – Konstrukcje betonowe, żelbetowe i sprężone. Obliczenia statyczne i projektowanie, PKN, Warszawa 2002.
[17] PN-EN 1992-1-1:2008 – Eurokod 2 Projektowanie konstrukcji z betonu. Część 1-1.

TECHNICAL TRANSACTIONS | CZASOPISMO TECHNICZNE
CIVIL ENGINEERING | BUDOWNICTWO
2-B/2013

BEATA KUTERA, GRZEGORZ KACPRZAK*

THE PILE STIFFNESS IN A PILED-RAFT FOUNDATION

SZTYWNOŚĆ PALA W FUNDAMENCIE PŁYTOWO-PALOWYM

Streszczenie

Artykuł przedstawia próbę zastosowania teorii sprężystości do oceny sztywności pala w fundamencie zespolonym płytowo-palowym w celu oszacowania osiadań konstrukcji. Zaprezentowano dwie metody obliczenia: uproszczony model komputerowy oraz rozwiązanie analityczne. Wyniki skonfrontowano z rezultatami badań polowych.

Słowa kluczowe: fundament płytowo-palowy

Abstract

The paper presents the trial of the theory of elasticity application to estimate pile stiffness in a combined piled-raft foundation. Two methods were applied: a simplified numerical model and closed-form analytical solution. Results were compared with the field tests.

Keywords: combined piled-raft foundation

* Eng. Beata Kutera, Ph.D. Eng. Grzegorz Kacprzak, Institute of Roads and Bridges, Faculty of Civil Engineering, Warsaw University of Technology.

Symbols

K_r – raft stiffness [MN/m]
K_p – pile group stiffness [MN/m]
K_{FPP} – combined stiffness of a piled raft [MN/m]

1. Introduction

Because of difficult ground conditions some areas in the city centres stayed undeveloped, despite their convenient location. This is the case of Warsaw's Żoliborz glacial tunnel valley. Lack of land in the city centre and development of foundation technologies resulted in increasing interest of developers in sites located in this area. One of such investments was the inspiration and basis for this article.

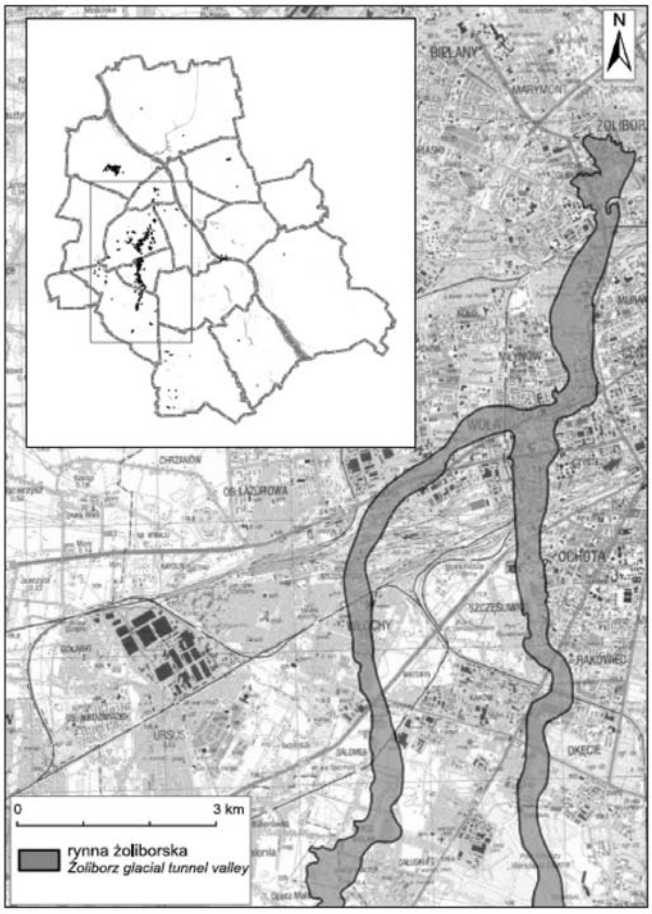

Fig. 1. Extents of Zoliborz glacial tunnel valley in Warsaw [1]

Development of tall buildings on weak soil requires taking into account both load bearing capacity (Ultimate Limit State) and settlement values (Serviceability Limit State). Raft foundation provides sufficient bearing capacity, but does not resolve the problem of strains exceeding maximum allowable values, or uneven settlement.

Typical solution is to design additional pile supports to transfer load directly to deeper, stronger soil layers. In conventional design procedures it is assumed that total load has to be transferred by the piles – contribution of raft to foundation bearing capacity is ignored. The design of piled-raft foundation takes into consideration contribution of both piles and raft to the total foundation stiffness, leading to more economical design than traditional approach.

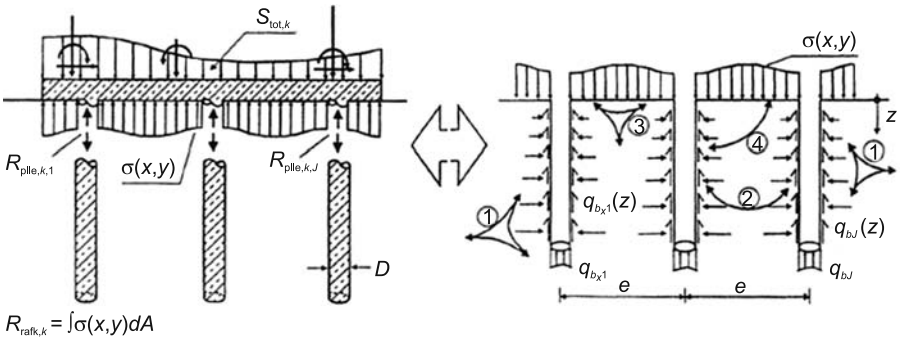

Fig. 2. Soil-structure interaction effects for a piled-raft foundation [2]

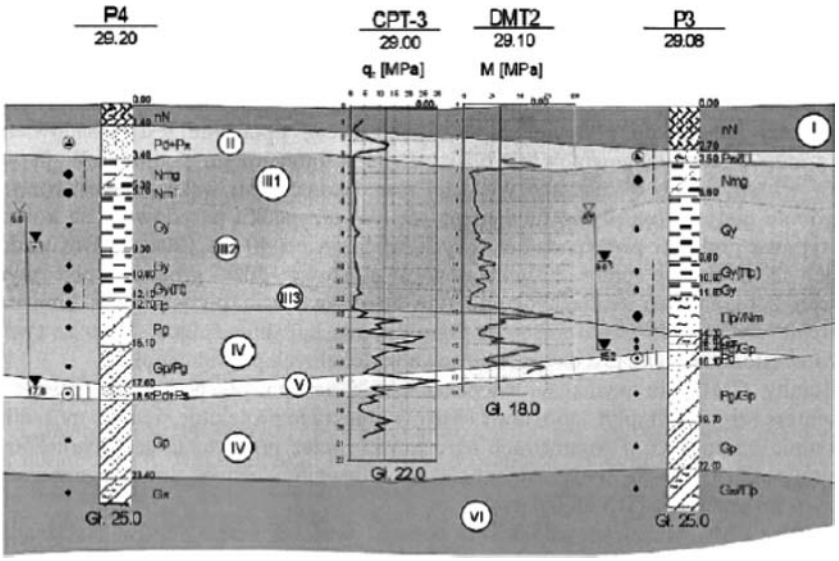

Fig. 3. Geotechnical cross-section presenting subsoil layers [2]

Unfortunately, neither former Polish standard PN-83/B-02482, nor European standard EN 1997 provides designers with guidelines concerning estimation of settlement of piled-raft foundation. Taking into account interaction of piles, raft and soil is a complicated task, indeed, as it has not been fully investigated, despite thorough research.

Of course it is possible to build a complete model of soil and piled-raft structure to be analysed with Finite Element Method. Theoretically, calculated displacements and stresses are more precise than computed by other methods. However, it should be noted that numerical errors and difficulties connected with modelling of soil behaviour may significantly influence reliability of the results, while complexity of a model extends time of modelling itself as well as the following calculation.

The paper presents alternative methods: analytical estimation of piled-raft stiffness and simplified model consisting of a plate on elastic supports, analysed then in a popular computer program ABC Płyta. Both methods require estimation of raft stiffness and single pile stiffness. Raft stiffness is quite easy to calculate; the major problem is how to estimate pile's behaviour.

As results of field tests are available [3], it is possible to compare results of theoretical modeling with real values. Geometry, load value and soil parameters applied in analysis comply with physical model and results of geotechnical research.

2. Raft stiffness

Raft stiffness may be defined as a ratio of imposed stress to resulting settlement. Provided modulus of compressibility of the soil layers are known, consolidation under predicted load may be easily estimated.

Modulus of compressibility of the layer of gyttja was estimated in CPT and dilatometer tests to be approximately 15 MPa. The total estimated settlement of a 10-meters thick layer of compressible organic soils under 120 kPa load equals 40 mm. The total raft stiffness is:

$$K_r = \frac{120\,\text{kPa} \cdot 25\text{m}^2}{40\,\text{mm}} = 75\,\text{MN/m}$$

It can also be represented as stiffness of the soil below the foundation:

$$K_r = \frac{120\,\text{kPa}}{40\,\text{mm}} = 3\,\text{MPa/m}$$

3. Pile stiffness

Determining stiffness of a pile requires deriving mathematical relation between imposed load and settlement. Traditional approach bases on calculating maximum bearing capacity and resulting settlement, but leads to linear stiffness of a pile support, which does not comply with load-settlement curve observed in field loading tests. Furthermore, the estimated stiffness is lower than real. In usual range of loads full bearing capacity will never be mobilized and the pile stiffness will be greater. According to Gwizdała [9], pile reaches its limit load at

settlement of 0.10 D (D is a pile diameter), while in fact the range of loads imposed is usually much lower than maximum values.

Even though it is well-known that soils do not behave as elastic materials, the theory of elasticity is a useful tool to calculate stresses and displacement in soil masses. The key requirement is to define elastic "constants" for an appropriate range of stress in analysed soil mass [6]. According to tests, elastic "constant" for ground have no constant values – modulus G and E depend on current state of stress and strain in soil. It can be observed in triaxial compression test, when one of the results is $E(\varepsilon)$ relation.

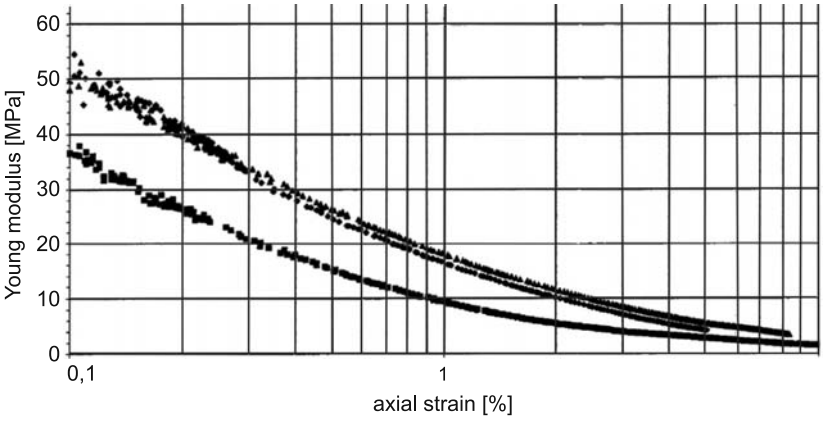

Fig. 4. $E(\varepsilon)$ relation – laboratory triaxial compression tests result

Possible solution of pile head settlement was derived by Randolph and Wroth, presented in [6]. The solution applies to a single pile in a homogenous soil, with a shear modulus increasing linearly with depth.

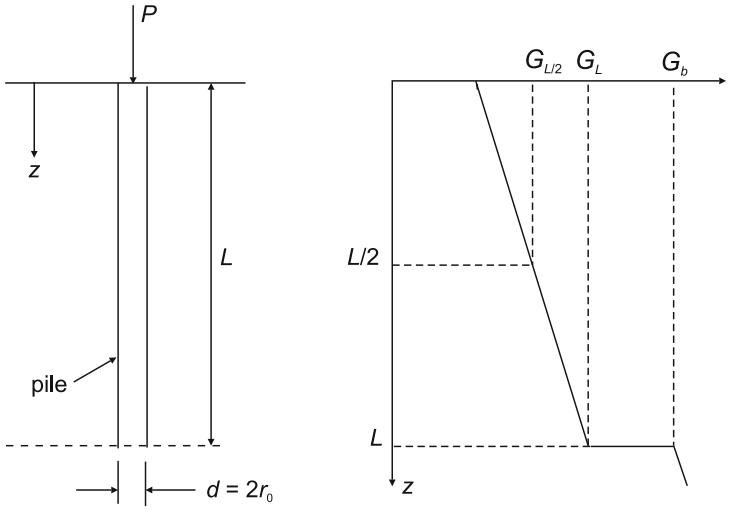

Fig. 5. Single axially loaded end bearing pile [6]

The pile head settlement d is given by a following formula:

$$\frac{P}{\delta r_0 G_L} = \frac{\dfrac{4\eta_r}{(1-\nu)} + \dfrac{2\pi\rho}{\zeta}\dfrac{\tanh(\mu L)}{\mu L}\dfrac{L}{r_0}}{1+\dfrac{1}{\pi\lambda}\dfrac{4}{(1-\nu)}\dfrac{\eta_r}{\xi}\dfrac{\tanh(\mu L)}{\mu L}\dfrac{L}{r_0}} \tag{1}$$

where:

P – applied load,
r_0 – radius of pile shaft,
r_b – radius of pile base,
G_L – shear modulus of soil at depth L,
G_b – shear modulus of soil at pile base (in end bearing piles),
v_v – Poisson' ratio of soil,
$\eta_r = r_b/r_0$,
$\xi = G_L/G_b$,
$\rho = G_{L/2}/G_L$,
$\lambda = E_p/G_L$.

$$\mu L = \frac{L}{r_0}\cdot\sqrt{\frac{2}{\zeta\lambda}},$$

$$\zeta = \ln\left(\left[0,25+\left(2,5\rho(1-\nu)-0,25\right)\xi\right]L/r_0\right).$$

Solution is derived from a differential equation of pile compression [10]:

$$(EA)_p\frac{d^2w(z)}{dz^2} - k(z)w(z) = 0 \tag{2}$$

where:

$$k(z) = \frac{\pi B q_s}{w(z)} \tag{3}$$

is a Winkler constant for depth z. It should be noted that equation (2) is a simplified one; it ignores influence of soil compression around the pile shaft.

In a homogenous soil, a modulus k is constant along the pile shaft.

Poisson's ratio was assumed according to [7] to be 0.5 for undrained and 0.3 for drained conditions. It is claimed that laboratory tests do not give reliable values of Young's modulus to be used in case of pile analysis – it should be back-calculated on the basis of pile load tests. However, for the need of theoretical analysis, results of triaxial tests were implemented.

Unfortunately, analysis of Young's modulus was limited by range of triaxial test results, as the solution is provided only for strain exceeding 0.1%. Evaluation of smaller strains is possible using geophysical techniques and the results of such tests were not available yet. Relation between E and ε was therefore determined as an exponential function. For the full range of strain hyperboloid functions are more appropriate [9]. Iterative calculations based on equation (1) resulted in a non-linear curve of pile head displacement plotted against imposed axial load. Lacking part of the plot is connected with displacements too small to be measured with triaxial testing machine equipment.

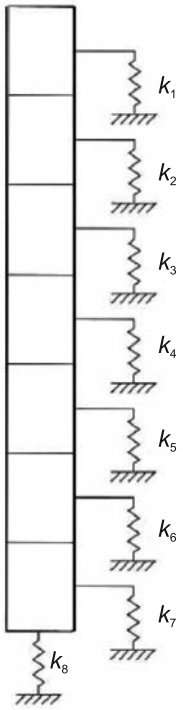

Fig. 6. Discretization of the soil along the pile shaft by Winkler springs [10]

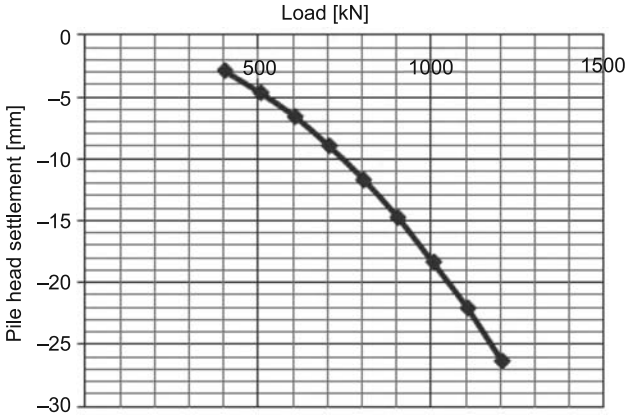

Fig. 7. Load-settlement curve for a single pile

In a piled-raft foundation loads are transferred to the soil by both piles and raft. Therefore pile head settlement equals raft settlement, a result of compression of soil layers below. Majority of settlement results from weak organic soil compression – underlying silt has insignificant effect in total settlement value. ε value was determined as a ratio of pile head settlement to total thickness of gyttja layers.

As presented in the plot (Fig. 7), stiffness of a pile has no constant value. To reflect behaviour of soil, a computer model should consider non-linearity of Young's modulus or compressibility modulus of the elastic solid. However, as stated above, the range of allowable strains is limited to 0.10 D, while in engineering practice the value is limited to c.a. 0.05 D. Taking 40 cm piles and 10 m layer of gyttja, calculated maximum strain equals merely 2 cm/10 m = 0.002 = 0.2%.

4. Modelling – ABC Płyta program

Two created models reflected geometry of the physical models constructed at site. Raft dimensions were 5.0 × 5.0 × 0.3 m – one of the rafts was supported by nine CMC columns (diameter: 0.4 m) arranged in a grid of 2.0 × 2.0 m.

Piles were introduced as single springs (assumed displacement was around 2–3 cm), and soil was characterized by Winkler coefficient 3 MPa/m.

Results of modeling are presented in Table 1, along with field tests' results. Figure 8 presents reaction forces in all of the piles.

Table 1

Settlement values in field tests and computer modelling in ABC Płyta

	Physical model		Computer model (ABC Płyta)	
	raft	piled raft	raft	piled raft
settlement [mm]	25 (16–35)	5.5 (3.9–8.6)	40	3

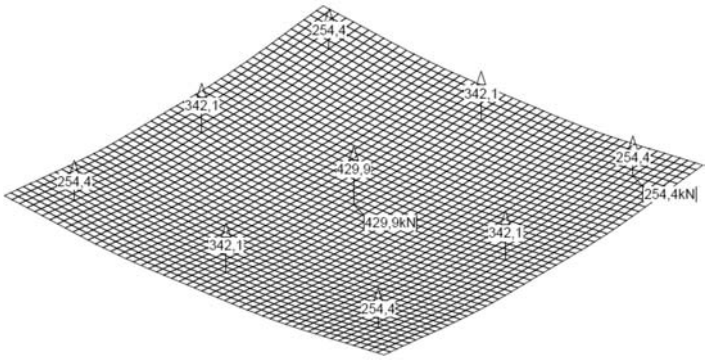

Fig. 8. Reaction forces in piles under 120 kPa load

Settlement calculated proves good correspondence with real values. Results of field tests exceeded displacements estimated in the program – this may be assigned to ignoring block deformation of the foundation in a computer model. In case of a pile group, soil between

the piles moves together with the whole piled-raft structure. Therefore effective friction along pile shafts is reduced, especially in the middle piles. Load bearing capacity of the columns is limited and contact pressure below raft increased, leading to increased settlement values. Trial of estimation of the influence of group work on a pile capacity was presented by Katzenbach in [8].

5. Analytical solution

Another method of estimating settlement of a piled-raft is based on calculating total stiffness of the foundation using simple functions of raft and pile stiffness defined separately. One of the solutions derived is the one by Randolph (Kacprzak [3]). Total foundation stiffness is defined as follows:

$$K_{FPP} = \frac{1 - 0.6 \cdot (K_r / K_p)}{1 - 0.64 \cdot (K_r / K_p)} \cdot K_p \tag{4}$$

where:

K_r – raft stiffness [MN/m],
K_p – pile group stiffness [MN/m],
K_{FPP} – combined stiffness of a piled raft [MN/m].

Pile group stiffness may be calculated as product of single pile stiffness and coefficient $n^{0.5}$, where n is number of piles in the group. Estimated raft stiffness is K_r = 75 MN/m and pile group stiffness $K_p = 143 \cdot 9^{0.5}$ MN/m. Therefore total piled-raft stiffness equals 432 MN/m and settlement associated with 3MN load – 7 mm.

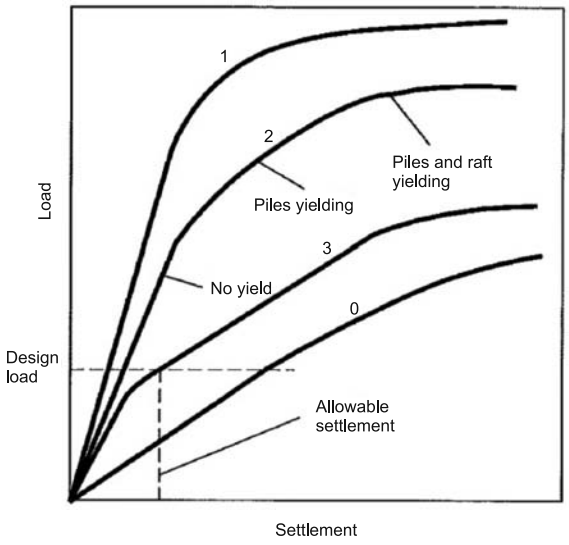

Fig. 9. Load-settlement curves depending on design approach: 0 – raft without piles, 1 – conventional piles, 2 – possible interaction of piles and raft in load transmission (safety factor for piles lowered to 1,5), 3 – full mobilization of piles' bearing capacity, full interaction [3]

Table 2

Settlement values – comparison

	Physical model	Computer model (ABC Płyta)	Analytical solution (Randolph)
settlement [mm]	5.5 (3.9–8.6)	3	7

Randolph has also provided a closed-form solution estimating load distribution between piles and raft:

$$\beta_p = \frac{1}{1+\alpha} \tag{5}$$

where:

$$\alpha = \frac{0,2}{1-0.8(K_r / K_p)} \cdot \frac{K_r}{K_p} \tag{6}$$

Results of modelling and calculation are compared with field tests in Table 3.

Table 3

Load distribution – % of load transmitted by piles

Physical model	Computer model (ABC Płyta)	Analytical solution (Randolph)
92–97%	93.9%	96.7%

6. Conclusions

Final comparison of the results of pile stiffness obtained in theoretical analysis with values measured in field load tests are presented in Tables 2 and 3. Both computer model and analytical calculation give results similar to field tests. However, it can be noticed that numerical solution results in lower value of settlement. This may be assigned to ignoring influence of the group work (introduced in Randolph's solution).

Methods presented above are easy to apply in practice and the results are close to real values measured in field test. Even though the solution provided is restricted to homogenous soil along the pile shaft, it is a common scheme for piled-raft foundation. As there is an assumption to design piles for full utilization bearing capacity (safety factor = 1), in most cases columns may reach only to the roof of the stronger layers below the single weak layers of similar low parameters. However, more field research on full-sized structures should be conducted, especially to analyse influence of superstructure's stiffness on soil-combined foundation interaction.

References

[1] Pietrzykowski P., *Eemskie gytie i kreda jeziorna z Warszawy jako przykład „mocnych" gruntów organicznych*, Biuletyn Państwowego Instytutu Geologicznego 446, Warszawa 2011.

[2] Hemsley J.A.(editor), *Design application of raft foundations*, Telford, London 2000.

[3] Kacprzak G., *Analiza porównawcza układu płyta-pal – teoria a praktyka*, Czasopismo Techniczne, 3-Ś/2011, Wydawnictwo Politechniki Krakowskiej, Kraków 2011.

[4] Kłosiński B., *O projektowaniu posadowień budynków wysokich,* Inżynieria i Budownictwo, nr 3/2009, Warszawa 2009.

[5] Kempfert H., Eigenbrod K.D., Smoltczyk U., *Geotechnical Engineering Handbook. 3.2 Pile foundations*, John Wiley & Sons, 2002.

[6] Poulos H., *Geotechnical Engineering Handbook. 1.6 Calculation of stress and settlement in soi masses*, John Wiley & Sons, 2002.

[7] Poulos H., *Methods of Analysis of Piled Raft Foundations*, A Report Prepared on Behalf of Technical Committee TC18 on Piled Foundations, International Society of Soil Mechanics and Geotechnical Engineering, 2001.

[8] Katzenbach R., Hanisch J., König G., *Kombinierte Pfahl-Plattengründungen*, Ernst & Sohn, Berlin 2002.

[9] Gwizdała K., *Fundamenty palowe*, Wydawnictwo Naukowe PWN, Warszawa 2010.

[10] Salgado R., *The Engineering of Foundations*, McGraw-Hill, New York 2008.

[11] Clancy P., Randolph M.F., *An Approximate Analysis Procedure for Piled Raft Foundations*, International Journal for Numerical and Analytical Methods in Geomechanics, vol. 17, 1993.

TECHNICAL TRANSACTIONS | CZASOPISMO TECHNICZNE
CIVIL ENGINEERING | BUDOWNICTWO
2-B/2013

IZABELA J. MURZYN, MAREK PAŃTAK*

DYNAMIC ANALYSIS OF THE PEDESTRIAN AND CYCLIST FOOTBRIDGE BETWEEN KAZIMIERZ AND LUDWINOW QUARTER IN KRAKOW

ANALIZA DYNAMICZNA KŁADKI PIESZO-ROWEROWEJ KAZIMIERZ–LUDWINÓW W KRAKOWIE

Abstract

The paper is dedicated to issues relating to the dynamics of footbridges. It includes the basic information about the dynamic characteristics of pedestrian bridges – the frequencies and modes of vibrations, stiffness, and damping. An essential part of this work is the dynamic analysis of the Kazimierz–Ludwinow footbridge in Krakow with a span of 127.20 m. The analysis was completed on the basis of a numerical model in the Autodesk Algor Simulation 2011 (Student Version) package.

Keywords: footbridge, dynamics, footbridge vibrations

Streszczenie

W artykule omówione zostały podstawowe zagadnienia związane z dynamiką mostów dla pieszych. Praca zawiera aspekty teoretyczne tego szerokiego zagadnienia oraz ich zastosowanie praktyczne w inżynierii lądowej. Zostały omówione podstawowe pojęcia z teorii drgań, które bezpośrednio przekładają się na analizę dynamiczną kładek. W dalszej części pracy została zaprezentowana analiza dynamiczna kładki pieszo-rowerowej Kazimierz–Ludwinów w Krakowie obciążonej dynamicznym oddziaływaniem użytkowników. Postacie drgań własnych zostały wyznaczone przy użyciu programu Autodesk Algor Simulation 2011 (Student Version).

Słowa kluczowe: kładki dla pieszych, dynamika kładek dla pieszych, komfort wibracyjny

* M.Sc. Eng. Izabela J. Murzyn, Ph.D. Eng. Marek Pańtak, Institute of Structural Mechanics, Faculty of Civil Engineering, Cracow University of Technology.

1. Introduction

1.1. The footbridges – basic requirements

The pedestrian bridges commonly called footbridges are the structures whose primary task is to carry pedestrians over a physical obstacle [12]. Currently, in addition to the safe conduct of traffic on the other side of the obstacle, pedestrian bridges are for their users, a kind of opportunity to enjoy the advantages of the environment with which they are associated.

Pedestrian bridges should be designed according to recommendations of the standards which require an analysis of the superstructure in the two limit states: ultimate limit state (ULS) and serviceability limit state (SLS).

The requirements of the ultimate limit state include: exhaustion of the bearing capacity for critical cross-sections of the structure; loss of stability of elements or the whole structure; material fatigue in elements or connections. The requirements of the serviceability limit state include checking of the span deflection and vibration of the structure [2]. In addition, objects in public spaces such as footbridges, should meet the requirements of the Regulations of the Minister of Transport and Maritime Economy [13, 14].

1.2. The dynamics of footbridges – basic issues

Footbridges significantly differ from the conventional bridges in how they influence the users. The footbridges users are located directly on the object deck, staying there longer than during traveling by car across the bridge and directly feels its behavior. Users are exposed to a greater feeling of structural behavior. At the design stage, the footbridges require more attention to ensure the proper functional features and comfortable use.

In addition to static analysis, a dynamic analysis is also required. The primary objective of the dynamic analysis is to determine the effect of dynamic loads on the structure's dynamic response and its influence on users. Making dynamic analysis, it should be verified that the proposed design provides a sufficiently high level of comfort. Dynamic calculations of civil engineering structures are carried out usually on a discrete model of the real system (model with lumped masses). The equation of motion has the form [6]:

$$M\ddot{q}(t) + C\dot{q}(t) + Kq(t) = P(t) \tag{1}$$

in which:

M, C, K – successively: mass matrix, damping matrix and stiffness matrix,
$q(t)$ – displacement vector,
$P(t)$ – dynamic load vector (external force).

An important stage in the dynamic analysis of the structure is modal analysis [7] that is, calculation of the mode shapes and natural vibration frequency of the structure. In modal analysis, the system of equations for the free non-damped oscillatory motion should be solved [6]:

$$M\ddot{q}(t) + Kq(t) = 0 \tag{2}$$

Next, based on the results of the preliminary analysis, it is necessary to analyze the possibility of the occurrence of resonance vibrations.

In the case of pedestrian bridges, the critical natural frequencies are within the ranges: 1.3 Hz ≤ f_i ≤ 2.3 Hz (in case of vertical vibration); 0.5 Hz ≤ f_i ≤ 1.2 Hz (in case of horizontal vibration).

1.3. Dynamic loading of footbridges

Pedestrian users impact on the construction of the bridge in a dynamic way. The user generates a load in three directions: vertical; horizontal; longitudinal [1]. An essential element of the dynamic analysis of a footbridge is to identify the frequency range of pedestrian impact.

The frequency of pedestrian impact for running, walking or jumping is within the range 1.4–3.4 Hz [1]. The basic assumption relating to the dynamic force generated by humans is their periodic character. The dynamic load vector can be represented as a Fourier series [1]:

$$F_z(t) = G + \sum_{i=1}^{n} G\alpha_i \sin\left(2\pi i f_k t - \varphi_i\right) \tag{3}$$

where:

- G – the pedestrian's weight (700–800 N).
- φ_i – the Fourier's coefficient of the i-th harmonic.
- f_k – the frequency of pedestrian activity (walking, running or jumping).
- $P(t)$ – dynamic load vector (external force).
- i – the number of the harmonic.
- n – the total number of harmonic components.
- φ_i – the phase shift of the 2nd or 3rd harmonic respectively, with respect to the 1st harmonic.

1.4. Approximate methods for estimation of impact of the dynamic load on footbridges

The approximate method for determining the impact of a single pedestrian whose stepping frequency is equal to the basic natural frequency of the vertical vibration of the structure is given in the standards BS 5400 78 (UK) and ONT 83 (Canadian).

For the footbridge which number of spans does not exceed three, the maximum vibration acceleration $a_{\max}$ is:

$$a_{\max} = 4\pi^2 f_1^2 z_{st} K \Psi \tag{4}$$

where:

- z_{st} – the deflection (caused by static load, 700 N) in the middle of the span.
- K – the configuration coefficient.
- Ψ – the dynamic response coefficient.

In order to determine the dynamic influence of more than one pedestrian on the dynamic behavior of the footbridge, the results obtained for a single user $a_{1\max}$ should be multiplied by an increasing factor of M. The value of M factor depends on the type of vibration excitation and size of the pedestrians group N_g:

- synchronized group of footbridge users walking, running or jumping: $M = N_g$,
- random impact of a free stream of pedestrians: $M = \sqrt{N_g}$.

Intentional and malicious vibration excitations are not taken into account in the design of footbridges. It should be noted that there is a real risk of its occurrence on footbridges. It is advisable to take into account these loads during footbridge superstructure designing and stress analysis [8].

2. The Kazimierz–Ludwinow footbridge in Krakow – dynamic analysis

2.1. Description of the structure

The Kazimierz–Ludwinów pedestrian and bicycle footbridge (Fig. 1) was designed between Inflancki Boulevard (Kazimierz side) and the Wolynski Boulevard (Ludwinow side) near the closed Sofitel (Forum) Hotel in Krakow. The architectural project of the footbridge was realized by the Lewicki&Latak Design Office from Krakow. The structural project was prepared by Research and Design Team Mosty–Wroclaw. The project is very interesting both in terms of its architecture and structure.

Fig. 1. Visualization of the footbridge Kazimierz–Ludwinow in Krakow

The footbridge was designed to live load according to PN-85/S-10030 standard and a vehicle of 3.5 tons total weight as an exceptional load condition [4].

The structural system includes: main span (127.20 m) consisting of two external box girders and internal "sine"-shaped box girder, abutment from the Ludwinow side; abutment and ramps from the Kazimierz side. In the plan view, the ramps are designed parallel to the bank of the Vistula River.

External box girders are load-carrying superstructure. They are designed of structural steel S355J2G3 and S460NL. The rigidity of the girders is variable along the length of the span. In accordance with the brief foredesign, the girders are fixed in abutments. Both girders have the same cross-section and are located symmetrically in relation to the longitudinal axis of the footbridge. The deck width on the external box girders is 4.0 m and is constant over the entire length of the footbridge. The height of the girders changes smoothly to 15.79 m.

The internal girder, so-called "sine", has a cross-sectional trapezoidal shape and is designed from the same steel as exterior girders. In the area of the abutment P1 (Ludwinow side), the internal girder is connected with abutment flexibly by means of the articulated non-

displaceable joint (pined joint). In the area of the abutment P2 (Kazimierz side), the girder is fixed in the abutment and the "sine"-shaped deck is lengthened by stairs descending to Kurlandzki Boulevard at the level of the bank of the Vistula River. Cooperation of external and internal girders is ensured by steel hangers, pillars and transverse beams.

The abutments were designed with architectural reinforced concrete and founded on large diameter reinforced concrete piles (1.50 m). Abutments are also integrated with the ground by means of ground anchors with multiple injected anchor bulb Anchors and piles are inclined at a ratio of 5:1.

2.2. Dynamic analysis of the Kazimierz–Ludwinow footbridge

In order to perform the dynamic analysis of the footbridge, the 3D beam FEM model using Autodesk Algor Simulation 2011 (Student Version) has been prepared. The model included the basic elements of the real system – two symmetrical exterior girders, sinusoidal internal girder pillars, hangers and transverse beams connecting and stiffening the girders.

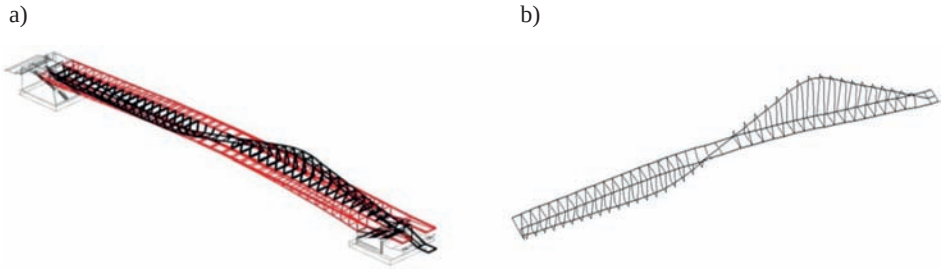

Fig. 2. Footbridge Kazimierz–Ludwinow a) axonometric view of the real structure [10], b) axonometric view of the beam computational model

All parts of the main span were modeled as beam elements. The symmetrical exterior girders and "sine" – shaped girder were modeled as beam elements, lying on the line running through the center of gravity of the girders cross-section. Pillars, hangers and transverse beams were modeled by beam elements placed along their axes in their center of gravity. The model consists of 215 nodes and 326 beam elements.

The footbridge girders were divided into 42 sections. The geometrical characteristics of the sections were calculated in accordance with the dimensions of the girder cross-section assumed in the brief foredesign [4]. In analysis, a linear elastic material model was adopted. The steel parameters were adopted in accordance with the parameters of the structural steel S355J2G3 and S4G2A.

As a result of the modal analysis, the natural frequencies and mode shapes of the footbridge were obtained. In Table 1 (below) basic frequencies less than 3.4 Hz (frequency in the range of the users dynamic action) are presented.

In order to estimate the vertical dynamic response of the structure due to pedestrian traffic, the third and fourth mode shape were selected for further analysis (these forms of vibrations are the most dangerous for the analyzed vertical vibration of the footbridge deck). Other vertical mode shapes were outside the critical range of considered pedestrian dynamic action or their form was complex and resonant vibrations have small probability of occurrence or in

the event of occurrence the vibration were quickly damped by users walking with different frequencies on the further part of the footbridge deck). It should be mentioned that the further analysis should be performed for the second horizontal mode shape with frequency f_2 = 1.14 Hz within the range of frequency of the horizontal action of walking people. These calculations were beyond the scope of the analysis performed for the purposes of this article. In Fig. 3 analyzed third and fourth mode shapes of the footbridge are presented.

Table 1

Natural vibration frequencies (in the range of the users dynamic action)

No. of mode shape	Frequency [Hz]	Period [s]	Type of mode shape
1	1.05	0.95	Vertical symmetric vibration of the side and the middle (sinusoidal) decks (one extreme)
2	1.14	0.88	Horizontal symmetric vibration of the side and the middle (sinusoidal) decks (one extreme)
3	2.06	0.49	Torsional asymmetric vibration of the middle (sinusoidal) deck (two extrema) and vertical symmetric vibration of the side decks in anti-phase (one extreme)
4	2.38	0.42	Vertical asymmetric viration of the side and the middle sinusoidal decks (two extrema)
5	2.94	0.34	Vertical symetric vibration of the side and the middle (sinusoidal) decks (three extrema)
6	2.98	0.34	Torsional asymmetric vibration of the middle (sinusoidal) deck (two extrema) and vertical asymmetric vibration of the side decks in anti-phase (two extrema)

a) b)

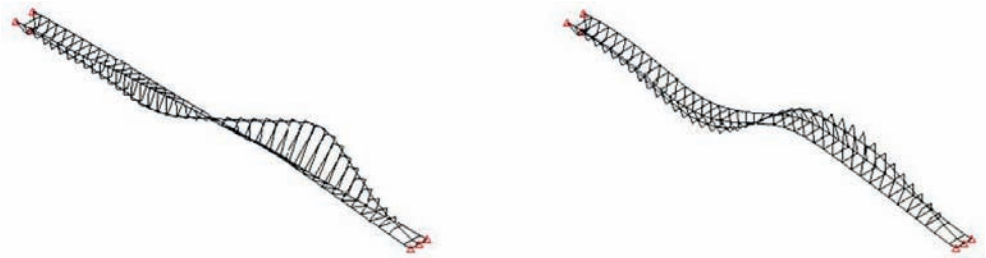

Fig. 3. Selected vertical mode shapes of the footbridge: a) third mode shape f_3 = 2.06 Hz, b) fourth mode shape f_4 = 2.38 Hz

The value of the vertical vibration acceleration was estimated according to equation (4). The deflection z_{st} caused by a static load of 700 N applied to the middle of the footbridge span is z_{st} = 0.077 mm. For K = 0.7, Ψ = 15 the vibration acceleration during a dynamic action of a single pedestrian equals:

$$a_3 = 4\pi^2 f_3^2 z_{st} K\Psi = 0.135\left[\frac{\mathrm{m}}{\mathrm{s}^2}\right], \quad a_4 = 4\pi^2 f_4^2 z_{st} K\Psi = 0.169\left[\frac{\mathrm{m}}{\mathrm{s}^2}\right]$$

Below is an example of estimation of the value of vibration acceleration caused by more than one user the group of 25 users was adopted N_g = 25. The following cases were considered:

– unsynchronized pedestrians group:

$$a_{3.25un} = Ma_3 = \sqrt{25}a_3 = 0.677\left[\frac{\mathrm{m}}{\mathrm{s}^2}\right], \; a_{4.25un} = Ma_4 = \sqrt{25}a_4 = 0.844\left[\frac{\mathrm{m}}{\mathrm{s}^2}\right]$$

– synchronized pedestrians group:

$$a_{3.25s} = Ma_3 = 25a_3 = 3.386\left[\frac{\mathrm{m}}{\mathrm{s}^2}\right], \; a_{4.25s} = Ma_4 = 25a_4 = 4.221\left[\frac{\mathrm{m}}{\mathrm{s}^2}\right]$$

The results should be compared with the requirements of the vibrational comfort criteria. Based on PN-EN 1990/A1, the limit value of vertical vibration acceleration of $0.7\left[\frac{\mathrm{m}}{\mathrm{s}^2}\right]$ was accepted. It should be noted that vertical vibrations with an acceleration of $0.7\left[\frac{\mathrm{m}}{\mathrm{s}^2}\right]$ can be felt by walking users (and very clearly by standing users) but in the case of very rare occurrences, can be accepted as permissible. Full comfort of the footbridge use will be ensured for vertical vibration acceleration less than $0.5\left[\frac{\mathrm{m}}{\mathrm{s}^2}\right]$. The results of comfort estimations are given below:

– in the case of resonant dynamic action of one pedestrian, for both analyzed natural frequency (3 and 4 mode shapes), the requirements of the vibrational comfort criteria for the vertical vibrations are fulfilled.
– in the case of dynamic action of a non-synchronized group of 25 pedestrians in case of third, torsional mode shapes f_3 = 2.06 Hz the requirements of the vibrational comfort criteria for the vertical vibrations are fulfilled. In the work the analysis of the horizontal vibration acceleration was not carried out, for the fourth natural frequency (f_4 = 2.3 Hz)
– the vertical vibration acceleration exceeds the accepted as permissible value of $0.7\left[\frac{\mathrm{m}}{\mathrm{s}^2}\right]$
– which indicates a high risk of disturbance of comfort of use of the footbridge, particularly on the "sine" – shaped deck. It should be noted that the vibration acceleration is obtained by extrapolation of the acceleration determined for case of a single pedestrian walking at a frequency of 2.3 Hz. This frequency corresponds to slow running (jogging). The occurrence of five synchronized running users (M = 5), although possible, is very rare (with low probability of occurrence) especially on the "sine" – shaped deck. Therefore, the comfort of use of the footbridge can be considered as fulfilled. A more likely case of two or three

runners does not lead to the accepted limit of vibrational comfort criteria for the vertical vibrations being exceeded. However, further analyses of the dynamic action of running users are required.

– in the case of dynamic action of a fully synchronized group of 25 persons, the requirements of the vibrational comfort criteria for the vertical vibrations were significantly exceeded (by about 6 times). However, the case of 25 synchronized pedestrians on the footbridge deck is a very rare with a very low probability of occurrence. It can be assumed that under everyday use, the comfort of using the footbridge will not be disturbed. It should be pointed out that this kind of pedestrian traffic should be forbidden on lightweight footbridges.

3. Conclusions

The results obtained during analysis were compared with the results of two analyses of the footbridge provided by the Lewicki and Latak Project Office presented in [4] and [9]. After comparison of the dynamic characteristics of the footbridge, all stages of modeling can be considered as having been performed correctly and effectively.

The natural frequencies obtained during the described analysis are within the range of the results obtained by other authors presented in Tab. 2. It should be noted that the first mode shape of vibration does not occur in the quoted results [4, 9]. It can be caused by the fact that compared dynamic analyses were carried out on various mechanical models – both with regard to the model shape, the number of the finite elements and the number of nodes. The results of modal analyses are affected by parameters related to the inertia and stiffness of the structure, which are directly changed by the simplifications adopted in the computational model (both in terms of the geometry and parameters of the material of the real system). Additional explanations for the differences in the compared results are the different mass distribution for translational and rotational degrees of freedom in both models and the different way of modeling an eccentric connections of the structural member. For a more accurate estimation of the vibration frequency and mode shapes of the footbridge, the 3D model of type e^2, p^3 (two-dimensional elements in three dimensional space) should be prepared. For the purpose of the preliminary estimation of the comfort of use of the footbridge, the accuracy of the results of the vertical vibration frequency obtained by using the described simplified computational model were accepted as sufficient.

The results of the analysis should be considered as the forecasted level of vibration accelerations encumbered with an error resulting from the estimation of the vibration damping parameter (fraction of critical damping) which also affects the coefficient Ψ in equation (4) (dynamic response coefficient).

In the analysis, the vibration damping level and the associated dynamic response coefficient from equation (4) was adopted as recommended by the literature for typical steel beam footbridges. The parameter of the vibration damping in the analyzed footbridge, due to a unique form of the construction, can be higher. In this case, the risk of instances of exceeding the acceptable level of vibration acceleration will be favorably reduced.

Further analyses of running persons and analyses of the horizontal vibrations occurring in horizontal and torsional mode shapes are required.

Table 2

The dynamic characteristics of the footbridge [9]

No. of mode shape	Frequency [Hz]	Period [s]	Description
1	1.15	0.87	Horizontal symmetric vibration of the side and the middle (sinusoidal) decks (one extreme)
2	1.20	0.83	Vertical symmetric vibration of the side and the middle (sinusoidal) decks (one extreme)
3	2.62	0.38	Vertical asymmetric viration of the side and the middle (sinusoidal) decks (two extrema)
4	2.67	0.37	Torsional asymmetric vibration of the middle (sinusoidal) deck (two extrema) and vertical symmetric vibration of the side decks in anti-phase (one extreme)
5	2.96	0.33	Vertical symetric vibration of the side and the middle (sinusoidal) deck (three extrema)
6	3.36	0.29	Torsional asymmetric vibration of the middle (sinusoidal) deck (two extrema) and vertical asymmetric vibration of the side decks in anti-phase (two extrema)

References

[1] Bachmann H., *"Lively" Footbridges – a Real Challenge*, Proceedings of the 1stInternational Conference on "Design and dynamic of footbridges – Footbridge 2002", OTUA, Paris 2002.

[2] Bilszczuk J., Kamiński T., Onysyk J., *Technical description. Construction of footbridge over the Vistula river "Kazimierz–Ludwinow" in Cracow*, Wroclaw 2009.

[3] Bilszczuk J.,W. Barcik. et al., *Design of steel footbridges, Lower Silesia Educational Publisher House (DWE)*, Wroclaw 2004.

[4] Bilszczuk J., Kamiński T., Onysyk J., *Appendix 1 to the technical description. Construction of footbridge over the Vistula river "Kazimierz – Ludwinow" in Cracow. Part I: Calculation of static and strength of the supporting structure of the main span of the footbridge*, Wroclaw 2009.

[5] Chmielewski T., Zembaty Z., *Basics of dynamic structures*, Arkady, Warsaw 1998.

[6] Clough R.W., Penzien J., *Dynamics of structures*, New York 1993.

[7] Flaga A.,*The footbridges*, WKŁ, Warsaw 2011.

[8] Flaga A., Flaga K., *Dynamic loading of footbridges caused people in different conditions of their activity. "Monograph: Design, construction and aesthetics of footbridges"*, Cracow 2003.

[9] Flaga A., Bęc J., Lipecki T., *Aerodynamic calculations of footbridge over the Vistula river "Kazimierz–Ludwinow" in Cracow*, Lublin 2009.
[10] Łatak K., Lewicki P., *Construction of footbridge over the Vistula River "Kazimierz––Ludwinow" in Cracow. Architectural drawings.*
[11] Zivanovic S., Pavic A., Reynolds P., *Vibration serviceability of footbridges unde human-induced excitation: a literature review*, Sheffield 2003.
[12] PN-85/S-10030 The bridge structures, Loads, 1985.
[13] *Regulation of the Minister of Transport and Maritime Economy of the technical conditions which should be fulfilled by public roads and their location* 2.03.1999, (Dz.U. nr 43 poz. 430), 1999.
[14] *Regulation of the Minister of Transport and Maritime Economy of the technical conditions which should be fulfilled by road engineering objects and their location* 30.05.2000 (Dz.U. nr 63 poz. 735), 2000.

TECHNICAL TRANSACTIONS | CZASOPISMO TECHNICZNE
CIVIL ENGINEERING | BUDOWNICTWO
2-B/2013

ANNA PUKOWIEC, ANNA SOBOTKA*

SUPPORT FOR MAKING DESIGN DECISIONS IN RENOVATION OF HISTORIC BUILDING

WSPOMAGANIE DECYZJI PROJEKTOWYCH W REMONCIE OBIEKTU ZABYTKOWEGO

Abstract

The design and implementation of building structure renovation works allow for a selection of constructional and material solutions, as well as organisational issues. Proper selection should take into account many different technical and economic factors, and in the case of historic buildings – conservation factors as well. This leads to suggesting various solutions. Choosing a solution should not be intuitive, but based on a multi-criteria analysis using simple or complex decision-making models. This paper discusses two constructional solutions for a flat roof in a historic building subject to renovation. An AHP method-based multi-criteria analysis has been carried out for both of them. This analysis allows for the assessment and selection of a proper solution.

Keywords: historic building renovation, multicriteria analysis, the AHP method

Streszczenie

W projektowaniu i realizacji remontów obiektów budowlanych istnieje możliwość wyboru rozwiązań konstrukcyjno-materiałowych, a także organizacyjnych. Właściwy wybór powinien uwzględniać wiele różnych czynników natury technicznej, ekonomicznej, a w przypadku obiektów zabytkowych – konserwatorskiej. Prowadzi to do proponowania rozwiązań wariantowych. Wybór rozwiązania nie powinien być intuicyjny, lecz wsparty analizą wielokryterialną wykorzystującą proste lub złożone modele decyzyjne. W artykule przedstawiono dwa rozwiązania konstrukcyjne stropodachu w remontowanym obiekcie zabytkowym, dla których przeprowadzono analizę wielokryterialną z zastosowaniem metody AHP, pozwalającą na ocenę i wybór rozwiązania.

Słowa kluczowe: remont obiektu zabytkowego, analiza wielokryterialna, metoda AHP

* Prof. Ph.D. Eng. Anna Sobotka, Eng. Anna Pukowiec, Department of Geomechanics, Civil Engineering and Geotechnics, Faculty of Mining and Geoengineering, AGH University of Science and Technology.

1. Introduction

Currently, we are observing an increasing level of interest from investors in historic building renovations. However, works of this type constitute a great challenge due to specific technological requirements, untypical conditions for execution of construction works and necessary high expenses. Therefore, proposed design and implementation concepts should be well thought out, suggested solutions should be varied, and evaluation and selection should take into account various factors. A multi-factor analysis is used in the decision-making process in various issues and is supported by different, more or less complex and popular methods [5].

Owing to the National Fund for the Revalorisation of Historic Buildings and Monuments in Krakow established in 1985, intensive revalorisation works are carried out every year in more than 100 historic buildings in the capital city of Małopolska. In 2012 this programme covered 167 objects, and the Fund appropriated 42,497,731.37 PLN for their renovation. These buildings included Fort no. 2 "Kościuszko", in which renovation works were carried out at Curtain V-I p [1, 4, 6].

The purpose of this work is to analyse and assess the concept of design solutions for the roof of fort curtain subject to renovation. Considering this, the article specifies the rules for the adaptation of historic works of military defence, which should be taken into account in design concepts. Building characteristics presented in this paper have been complemented with photographs showing the progress of construction works, as observed by authors. Two roof design proposals provided in this work have been assessed with a multi-criteria analysis using the AHP method.

2. The rules for adaptation of historic works of military defence

Many different spatial forms and structural solutions of fortification buildings have developed due to ceaseless changes in defence methods, progress in military technology and the existence of many schools of fortification and evolution of *architectura militaris* through centuries. This is also the reason why there are no applicable standards or rules for maintenance and adaptation of these objects. The issue of managing fortress complexes is an extensive matter that requires analyses in many fields of science, including the construction industry, architecture, economy, sociology, ecology, management, etc.

To simplify, we can make a few assumptions which affect the adaptation of fortress complexes. Among them we distinguish [3]:

- structural characteristics of after-fortress management guidelines resulting from the original defensive function of facility,
- preservation and technical state of facility elements,
- rules regarding protection of the value of historic facilities,
- obligatory educational and scientific functions, which should be provided by a facility,
- current legal and functional status of a fortification,
- contemporary technical and functional requirements set to building structures.

The priority in the adaptation of historic fortification is to protect them against damage whilst ensuring authentic structure of facilities. It is preferred to choose such facility adaptation method, which will guarantee:

- all-year-round facility use,
- economic calculation taking into account the costs of carrying out conservation work,
- functional programme for the use of the whole fortification,
- public availability of the facility.

In the article, the authors devote special attention to the issue of designing greenery around the facility, and to the roles it played throughout the cycle of facility service life, and the need to hide structures of this type e.g. by planting greenery directly connected with them.

Greenery surrounding forts today has little to do with historic styles. Without constant maintenance, soil fortifications turn into areas covered with wild vegetation. For the purposes of maintaining the facility as an exhibition, the most important task is to cut down trees and shrubs, and to repair damage caused by roots. During structure clearing, it is also a requirement to isolate and properly secure foliage of special historic value. While preparing an adaptation project for a given historic structure, it is extremely important to carry out historical research in order to determine the functions held by greenery in a given facility, and to make a decision regarding the extent of its reconstruction.

The study contains comparing the alternative solution, chosen from many analyzed proposals in [7], with an executed(in real) solution suggested by the designer. To the evaluation was used multicriteria analysis. This method has a lot of varieties and more and more universally is being used for analysis of different engineering problems and the decision [8, 13, 14]. The finding has historic buildings serving the decision-maker responsible for the compliance of the concept with the requirements concerning the renovation above all. Performed solving the designer is supposed to take into account a lot of important measurable and immeasurable requirement/factors to a given historic building and economic possibilities of the institutional investor.

3. Facility characteristics

Fort no. 2 "Kościuszko" is one of the oldest defensive structures of the Krakow Stronghold. It was established from 1850–1854 as a citadel fort with its centre formed by the mound built by Poles in honour of Tadeusz Kościuszko. The building is untypical of an Austrian school of fortifications due to the preservation of the mound which constitutes the central element of the whole complex. The fort plan is close to hexagonal with corner bastions. Three huge bastions were built from the west and two smaller ones from the east. The structure lacks redoubt, which was a typical element of forts at that time. Its function was performed by brick wall which was built around the Mould, surrounded by a courtyard and a cylinder of neck barracks. The fort has been included in the list of fixed vintage buildings of the City of Krakow on January 2, 1968, ref. no. A-308.

The fort section subject to renovation is Curtain V-I, constituting the southern part of fortification line. From the western side, the curtain is adjacent to Bastion V and Caponier, and from the east, it borders on the entrance road to the fort courtyard. Originally, it consisted of two longitudinal walls, each ca. 1.15m-thick, distant from each other from 12.8 m at the bastion to 14.6 m in the area of not existing now entrance gate. Inside the curtain, at both its ends, there were also rooms with barrel vaults. From the fort courtyard side there was also a ramp shielded by the wall, leading to the curtain crown.

Prior to the commencement of the works, the space between the curtain walls was filled with soil, and the curtain crown covered with growing trees and shrubs (Fig. 1). The outside walls were damaged in many places, and before the soil removal it was impossible to evaluate the current state of the inside walls preservation. It was also impossible to determine precisely the building foundation depths and the technical state of the foundation walls.

Fig. 1. Northern façade of the facility before commencement of works

The design allows for using the space between the curtain walls for commercial purposes by creating the Tadeusz Kościuszko Conference and Exhibition Centre (Fig. 2) [6]. As a result of space development between the curtains and making a flat roof restoring original curtain topping form, functional space will be created on three storeys (cellar, ground floor and first floor) connected by two stairways, with mezzanine above first floor. Designed flat roof will have the form of an observation deck, which will be available through the restored ramp (Fig. 3).

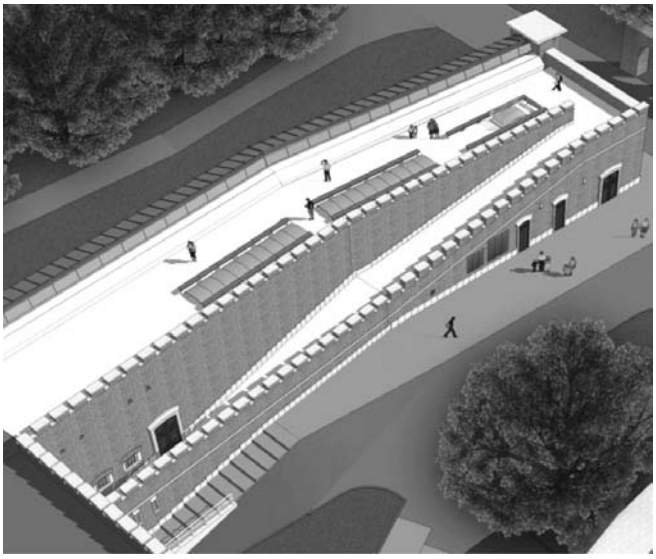

Fig. 2. Facility visualisation

Fig. 3. Northern façade – May 2013

Additionally, it is planned to develop the area adjacent to the fort. In the courtyard between the curtain and rotunda there will be a pedestrian and vehicular traffic route with a parking lot and station with bicycle stands. From the northern façade side, there will be a green area with a playground for children.

Kościuszko Mound Committee is the investor and future user of the curtain. The Committee finances this project, supported by the European Union and National Fund for the Restoration of Krakow's Historic Monuments. Gross investment value is 7,920,501.19 PLN. The project preparation is carried out by Pracownia Konserwacji Zabytków "Arkona" ["Arkona" Historic Buildings Conservation Office], while Skanska S.A. [a joint-stock company] is responsible for its implementation. The works are planned from July 2011 until December 2013.

4. Analysis and evaluation of design solutions

The scope of analysis includes two proposals for the design of a flat roof in the renovated building [7], which will be subject to multi-criteria assessment carried out using the AHP method [2, 10].

Flat roof design suggestions

The first of the analysed structures is a design solution for a flat roof made as an observation deck (Fig. 4) [11]. For the purposes of the performed analysis, this solution will be marked A.

The second variant is an intensive green flat roof with vegetation including sedums, grasses and herbs, which is made in a reversed layout (Fig. 5) [12]. Layer structure for selected green roof type has been designed on the basis of system solutions from Optigrün International AG [9]. This solution will be marked B.

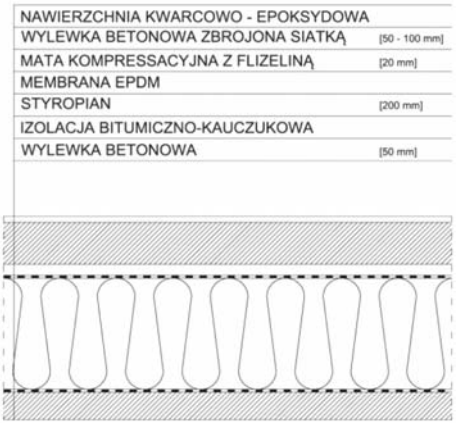

Fig. 4. Flat roof layer structure

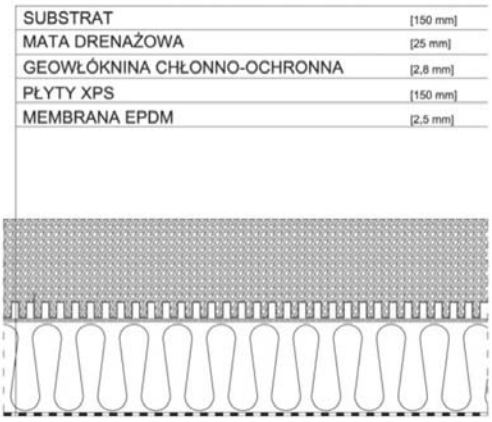

Fig. 5. Green flat roof layer structure

Multi-criteria analysis

Completed multi-criteria analysis involves the assessment of presented solutions considering specific factors. We distinguish several stages in it:

1. Preparing the list of criteria to be applied to assess presented solutions.
2. Assessing criteria significance using the AHP method:
   - creating matrix of comparisons in pairs,
   - calculating local priorities – determining largest own value of matrix and own vector corresponding to it,
   - checking evaluation compliance by determining compliance index and ratio,
   - computing global priorities.
3. Evaluation of decision-making options.
4. Presentation of results in form of a GSM matrix.

Comparative criteria. The first stage involved preparing a list of factors, which would be used to consider two decision-making options. These factors were divided into two groups – internal (Table 1) and external (Table 2).

Evaluation of criteria and decision-making options. It involves creating proper matrixes of comparisons in pairs – external and internal factors assessed according to general purpose of the analysis, that is selection of the best constructional solution in given conditions, and analysed solutions compared as regards individual factors.

When comparing individual elements, we use the relative preference scale created by Saaty, in which we distinguish five basic situations, matched by a numerical scale [2]. These are: equivalence (numerical equivalent 1); weak preference (3); significant preference (5); distinct preference (7); absolute preference (9). Among these, there are also indirect preferences – 2, 4, 6, 8. This allows us to prepare the following matrixes.

$$A^w = \begin{bmatrix} 1 & 5 & 5 & 5 & 3 & 5 \\ \frac{1}{5} & 1 & 1 & 1 & \frac{1}{3} & 3 \\ \frac{1}{5} & 1 & 1 & 1 & \frac{1}{3} & 3 \\ \frac{1}{5} & 1 & 1 & 1 & \frac{1}{5} & 3 \\ \frac{1}{3} & 3 & 3 & 5 & 1 & 5 \\ \frac{1}{2} & \frac{1}{3} & \frac{1}{3} & \frac{1}{3} & \frac{1}{5} & 1 \end{bmatrix} \qquad A^z = \begin{bmatrix} 1 & 1 & \frac{1}{3} & \frac{1}{3} & \frac{1}{5} & \frac{1}{3} \\ 1 & 1 & \frac{1}{3} & \frac{1}{3} & \frac{1}{5} & \frac{1}{3} \\ 3 & 3 & 1 & 3 & \frac{1}{3} & 3 \\ 3 & 3 & \frac{1}{3} & 1 & \frac{1}{3} & \frac{1}{3} \\ 5 & 5 & 3 & 1 & 1 & 3 \\ 3 & 3 & \frac{1}{3} & 3 & \frac{1}{3} & 1 \end{bmatrix}$$

$$A^1 = \begin{bmatrix} 1 & 9 \\ \frac{1}{9} & 1 \end{bmatrix} \quad A^5 = \begin{bmatrix} 1 & \frac{1}{3} \\ 3 & 1 \end{bmatrix} \quad A^{3'} = \begin{bmatrix} 1 & \frac{1}{3} \\ 3 & 1 \end{bmatrix}$$

$$A^2 = \begin{bmatrix} 1 & \frac{1}{7} \\ 7 & 1 \end{bmatrix} \quad A^6 = \begin{bmatrix} 1 & \frac{1}{7} \\ 7 & 1 \end{bmatrix} \quad A^{4'} = \begin{bmatrix} 1 & 5 \\ \frac{1}{5} & 1 \end{bmatrix}$$

$$A^3 = \begin{bmatrix} 1 & 3 \\ \frac{1}{3} & 1 \end{bmatrix} \quad A^{1'} = \begin{bmatrix} 1 & 3 \\ \frac{1}{3} & 1 \end{bmatrix} \quad A^{5'} = \begin{bmatrix} 1 & \frac{1}{9} \\ 9 & 1 \end{bmatrix}$$

$$A^4 = \begin{bmatrix} 1 & \frac{1}{3} \\ 3 & 1 \end{bmatrix} \quad A^{2'} = \begin{bmatrix} 1 & 5 \\ \frac{1}{5} & 1 \end{bmatrix} \quad A^{6'} = \begin{bmatrix} 1 & \frac{1}{5} \\ 5 & 1 \end{bmatrix}$$

where:

A^w – evaluation of internal factors,
A^z – evaluation of external factors,
$A^1, \ldots, A^6$ – assessment of solutions as regards internal factors,
$A^{1'}, \ldots, A^{6'}$ – assessment of solutions as regards external factors.

Local and global priorities. Local priorities are determined for all obtained matrixes by way of determining highest own values for matrixes λ_{max} (5) and corresponding to them own vectors w (4). Values obtained in this way are used to determine global priorities, which are the basis for choosing the best solution. Individual values are determined using methods developed by Saaty [e.g. 2,10]:

$$A = \begin{pmatrix} a_{11} & \dots & a_{1j} & \dots & a_{1n} \\ \vdots & \ddots & \vdots & & \vdots \\ a_{i1} & \cdots & a_{ij} & \dots & a_{in} \\ \vdots & & \vdots & \ddots & \vdots \\ a_{n1} & \dots & a_{nj} & \dots & a_{nn} \end{pmatrix}$$

$$a_i^* = \sqrt[n]{\Pi_{j=1}^{n} a_{ij}}, \quad i = \overline{1,n} \tag{1}$$

$$a_i^* = \sqrt[n]{\Pi_{j=1}^{n} a_{ij}}, \quad i = \overline{1,n} \tag{2}$$

$$a^* = \sum\nolimits_{i=1}^{n} a_i^* \tag{3}$$

$$w_1 = \frac{a_i^*}{a^*}, \quad i = \overline{1,n} \tag{4}$$

$$\lambda_{\max} = \sum\nolimits_{j=1}^{n} a_j^* w_j \tag{5}$$

Using the obtained matrix own values, we check if the received results are correct. In order to do that, we determine compliance index C.I. (6) and compliance ratio C.R. (7) – if they are less than 0.1, the completed assessment may be deemed correct (method details are available e.g. in literature items [2, 10]). In case of higher values, the decision-making problem should be rethought and the evaluation should be repeated.

$$\text{C.I.} = \frac{\lambda_{\max} - n}{n-1} \tag{6}$$

$$\text{C.R.} = \frac{\text{C.I.}}{\text{R.I.}} \tag{7}$$

where:

n – matrix dimension,

R.I. = 1.24 for $n = 6$.

In this case, we received C.I. 0.6, C.R. 0.05 for matrix of internal factors and C.I. 0.09, C.R. 0.08 of matrix of external factors.

The last stage of computations is to determine global priorities, meaning the sum of products of priorities for each branch of considered decision-making options for the purposes of the pondered general problem. In the case of the issue analysed by us, cumulative tables are prepared which contain evaluation of both variants regarding internal (Table 1) and external (Table 2) factors.

GSM matrix. The obtained results are shown in a four-field GSM matrix (Fig. 6), in which both flat roof solutions are shown in the form of points in two-dimensional space. The horizontal axis is the evaluation of internal factors, and the vertical axis is the evaluation of external factors. A is the symbol of the flat roof made according to the original design, and B is the green flat roof proposed by the author.

Table 1

Evaluation of internal factors

Internal factors		Criterion priority	Evaluation of variant A	Modified* evaluation factors A	Evaluation of variant B	Modified* evaluation factors B
1	Structure construction cost	0.44	0.90	0.396	0.10	0.044
2	Structure construction time	0.09	0.13	0.012	0.87	0.078
3	Requirements regarding employee qualifications	0.09	0.75	0.068	0.25	0.023
4	Requirements regarding construction site layout	0.09	0.25	0.023	0.75	0.068
5	Structure stability	0.25	0.25	0.063	0.75	0.188
6	Structure aesthetics	0.04	0.13	0.005	0.87	0.035
SYNTHETIC EVALUATION			∑	0.567	∑	0.436

* Product of criterion priority and evaluation of variant

Table 2

Evaluation of external factors

External factors		Criterion priority	Evaluation of variant A	Modified* evaluation factors A	Evaluation of variant B	Modified* evaluation factors B
1’	Availability of constructional materials	0.06	0.75	0.045	0.25	0.015
2’	Availability of qualified staff	0.06	0.83	0.050	0.17	0.010
3’	Requirements regarding the structure use and making	0.24	0.25	0.060	0.75	0.180
4’	Users’ interest and evaluation	0.12	0.83	0.100	0.83	0.020
5’	Conservator’s guidelines	0.35	0.1	0.035	0.83	0.315
6’	Situation in construction industry	0.17	0.17	0.029	0.75	0.142
SYNTHETIC EVALUATION			∑	0.319	∑	0.682

* Product of criterion priority and evaluation of variant.

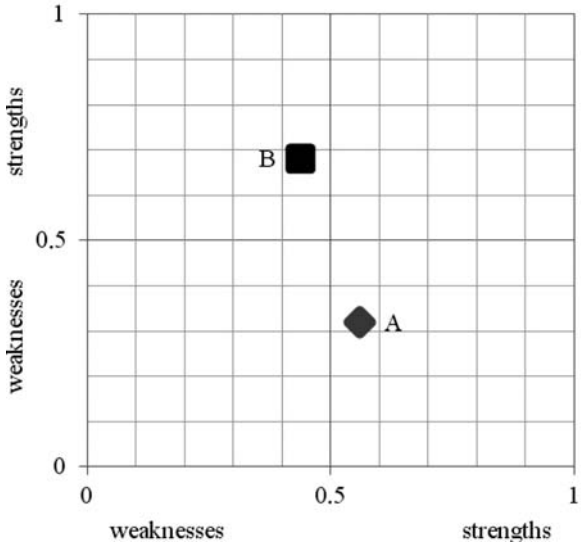

Fig. 6. GSM matrix

5. Conclusions

Results obtained from an analysis carried out using the AHP method are not unequivocal. Analysis of the decision-making options regarding internal factors gives results in favour of solution A, that is the flat roof made according to the prepared building permit design. However, the difference between evaluations of both projects is insignificant. In the case of analysis for external factors, difference in evaluations is much more considerable. Evidently, solution B prevails, that is the reversed intensive green roof.

The following have greatest impact on the obtained results: for internal factors – the structure construction cost (criterion weight 0.44) and its stability (criterion weight 0.25), and for external factors – conservator's guidelines (criterion weight 0.35) and requirements regarding the structure use and keeping (criterion weight 0.24). It's worth observing that in the case of prevailing internal factors, we receive certain divergence – the design solution is predominant as regards costs, however the green solution has been deemed more durable. There are no such differences in the case of external factors – most important factors have been assessed to be in favour of the green roof. The obtained results agree with the general analysis of both solutions [5], which has taken into account weight, cost and time of making individual structures, and also historical study of the building.

In situations like the selection of the flat roof solution demonstrated in this study, the investor faces difficult choices with regard to economic aspects, aesthetic values and striving for preserving historical conformity of the facility with its original state. Curtain subject to renovation is expected to serve commercial purposes as potential location for conferences and meetings, therefore, according to the author, external factors should play a greater role in the selection of a constructional solution. Although uncommon in Poland, a green roof may increase the building's attraction, which should translate into greater interest in using

this new commercial space. This sort of operation is observed in the case of the construction of the University Library building in Warsaw for example, where a decision has been made to incur much higher expenses, which are expected to translate into an increase of investors' interest and profits from using the space for commercial purposes. One of the elements aimed at increasing the building value is a grand-scale design of the garden on the building roof.

References

[1] Brzoskwinia W., Janczykowski J., *Atlas Twierdzy Kraków. Zabytki fortyfikacji Twierdzy Kraków. Ochrona i konserwacja w latach 1991–1998*, BitArt, Kraków 1998.

[2] Duzinkiewicz K., *Struktury i algorytmy wspomagania decyzji 2012/2013, Wieloatrybutowe problemy decyzyjne – metody rozwiązywania* (http://www.ely.pg.gda.pl/kiss/dydaktyka/siawd/wyklad/1093-w14w15 – 12.03.2013).

[3] Górski M., *Konserwatorskie zasady adaptacji dzieł obronnych fortyfikacji nowszej w kontekście funkcji dydaktycznej*, [In:] *Adaptacja obiektów zabytkowych do współczesnych funkcji użytkowych*, Edit. B. Szmygin, Politechnika Lubelska, Warszawa–Lublin 2009.

[4] Janczykowski J., *The Krakow Atlas Twierdzy Kraków. Fort 2 „Kościuszko"*, BitArt, Kraków 1994.

[5] Marina V., Tamosaitiene J., Turskis Z., Zavadskas E.K., *Multicriteria selection of project managers by applying grey criteria*, [In:] Technical and economic development of economy, Baltic Journal of Sustainability, 14 (4). Edit. E.K. Zavadskas, Vilnum Technika, 2008.

[6] *Projekt wykonawczy przebudowy*, PKZ Arkona, Krakow 2010.

[7] Pukowiec A., *Projekt dachu w remontowanym obiekcie zabytkowym – Centrum Konferencyjno-Wystawiennicze im. Tadeusza Kościuszki w Krakowie*, Engineer's graduation design under direction of A. Sobotka, AGH University of Science and Technology, Faculty of Mining and Geoengineering, Krakow 2011.

[8] Nahid Rezaeiniyaa, Sarfaraz Hashemkhani Zolfanib & Edmundas Kazimieras Zavadskas Greenhouse locating based on ANP-COPRAS-G methods – an empirical study based on Iran. International Journal of Strategic Property Management, vol. 16, 2, 2012, 188-200.

[9] *Optigrün – Green Roofs* (www.optigruen.pl – 11.03.2013).

[10] Sobotka A., *Logistyka przedsiębiorstw i przedsięwzięć budowlanych*, Wydawnictwa AGH, Kraków 2010.

[11] Sokołowska B., Krajczyński M., *Stropodachy. Projektowanie i wykonawstwo*, Wydawnictwo Uczelniane Politechniki Koszalińskiej, Koszalin 2004.

[12] Ślusarek J., *Rozwiązania strukturalno-materiałowe balkonów, tarasów i dachów zielonych*, Politechnika Śląska, Gliwice 2006.

[13] Zavadskas E.K., Turskis Z., Vilutiene T., *Multiple criteria analysis of foundation instalment alternatives by applying Additive Ratio Assessment (ARAS) method*, Archives of Civil and Mechanical Engineering , vol. 10 (3), 2010, 123-141.

[14] Zavadskas E.K., Vilutiene T., Turskis Z., Tamosaitiene J., *Contractor selection for construction works by applying SAW-G and TOPSIS grey techniques*, Journal of Business Economics and Management, vol. 11 (1), 2010, 34-55.

TECHNICAL TRANSACTIONS | CZASOPISMO TECHNICZNE
CIVIL ENGINEERING | BUDOWNICTWO
2-B/2013

IGA REWERS, TERESA SERUGA, MAGDA KIJANIA*

$M_{Rd} – N_{Rd}$ INTERACTION CURVES WITH ANALYSIS OF SECOND ORDER EFFECTS FOR REINFORCED CONCRETE COLUMNS

KRZYWE INTERAKCJI $M_{Rd} – N_{Rd}$ Z ANALIZĄ EFEKTÓW II RZĘDU DLA SŁUPÓW ŻELBETOWYCH

Abstract

The paper presents regulations for evaluating $M_{Rd} – N_{Rd}$ interaction curves for reinforced concrete members subjected to axial force and bending moments in one plane, comparing two simplified methods. An example for application of interaction curves in designing columns was presented. The latter part of the paper consists of two simplified methods of designating second order effects according to EC2 – nominal curvature method, nominal stiffness method. The comparison of them was made with $M_{Rd} – N_{Rd}$ interaction curves.

Keywords: reinforced concrete column, interaction curve, second order, nominal stiffness, nominal curvature

Streszczenie

W artykule przedstawiono zasady wykonywania krzywych interakcji $M_{Rd} – N_{Rd}$ dla przekrojów elementów żelbetowych, obciążonych siłą osiową i momentem zginającym w jednej płaszczyźnie, porównując dwie metody uproszczone ich opracowywania. Zaprezentowano również przykład zastosowania krzywych interakcji do doboru zbrojenia słupów krępych. W dalszej części pracy zawarto porównanie dwóch uproszczonych metod wyznaczania efektów II rzędu wg EC2 – metody nominalnej krzywizny i metody nominalnej sztywności, wykonane przy pomocy krzywych interakcji $M_{Rd} – N_{Rd}$.

Słowa kluczowe: słupy żelbetowe, krzywa interakcji, efekty II rzędu, nominalna sztywność, nominalna krzywizna

* M.Sc. Eng. Iga Rewers, Ph.D. Eng. Teresa Seruga, M.Sc. Eng. Magda Kijania, Institute of Building Materials and Structures, Faculty of Civil Engineering, Cracow University of Technology.

1. Introduction

1.1. The purpose and scope of the article

The following paper presents regulations of determining $M_{Rd} – N_{Rd}$ interaction curves, comparing two different methods [5, 16] (including an easy method suitable for creating spreadsheets). In the latter part of the article, two simplified methods of evaluating second order effects according to EC2 [17] were compared – nominal stiffness method (MNS) and nominal curvature method (MNC).

The article is not intended to assess the accuracy of methods of MNS and MNC, because such an assessment can be credible only on the basis of experimental results. The aim of the paper is to indicate the need for comments to EC2 [17], which could be followed when choosing the method of calculating the second order effects.

The following comparison was made by placing values of second order moments on the interaction curves. In the analysis column, the slenderness λ, λ/λ_{lim} ratio, the reinforcement ratio and an effective creep coefficient were variable.

The article also presents an example of using interaction curves in designing reinforced concrete columns.

1.2. Interaction curves

The load-bearing capacity of a cross-section subjected to an axial force and a bending moment in one plane can be illustrated by an $M_{Rd} – N_{Rd}$ interaction curve. An area created by the curve presents permissible values of pairs of generalised forces. A point (M_{Ed}, N_{Ed}) beyond the interaction curve means an exceeding of the ultimate limit state.

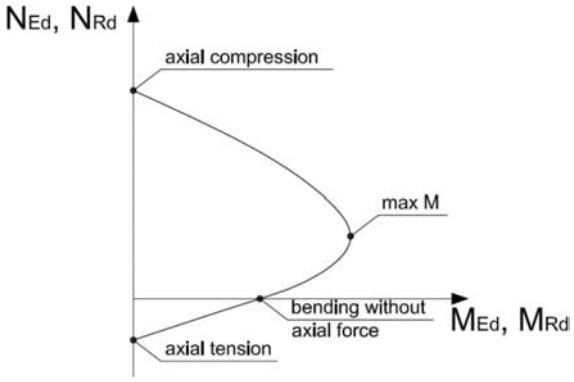

Fig. 1. $M_{Rd} – N_{Rd}$ interaction curve with designated cases of concrete cross-section work

Interaction curves for assumed steel and concrete grades, reinforcement ratios and dimensions ratios, presented as nomograms suitable for designers are published in books and resources for designers. A set of such nomograms for different shapes of cross-sections is included for example in [1], and in CEB/FIP Manual on Bending and Compression Design

of Sections under Axial Action Effects at the Ultimate Limit State [2]. In paper [3] there is a graph presenting a possible simplification of the $M_{Rd} – N_{Rd}$ interaction curve (Fig. 2).

Basic information and examples of nomograms were also included in M. Knauff's recently published book [4]. A detailed description of this issue can be found in R. Kliszczewicz paper [5].

$M_{Rd} – N_{Rd}$ interaction curves used and presented in papers and in specialist software [6, 7, 8, 9, 10, 11, 12, 13] are not commonly used in engineering projects. Not much attention is paid to this issue also in students books and teaching resources. However, interaction curves and nomograms based on them are popular in other countries [14, 15], for instance, they are found in a large part of an academic book for designing concrete structures, published by ČVUT in Prague [16].

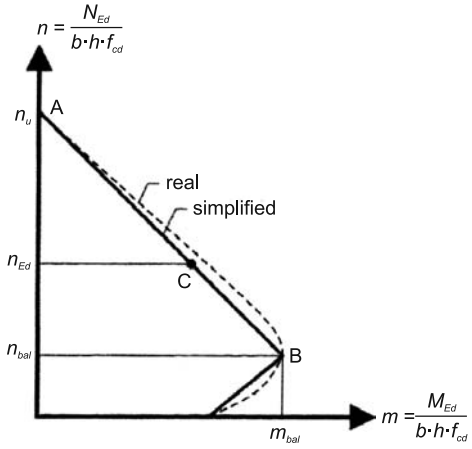

Fig. 2. Possible simplification of an $M_{Rd} – N_{Rd}$ interaction curve (according to [3])

2. Creating interaction curves with simplified methods

Drawing an interaction curve for reinforced concrete cross-sections is possible not only with a general method, but also with a so-called partly-simplified method [5]. This one is significantly easier in calculations, whilst simultaneously maintaining proper accuracy. Simplification is based on assumptions such as rectangular stress distribution in concrete, with a compressed zone depth λx and a value of ηf_{cd} ($\lambda = 0.8$; $\eta = 1.0$ – values for concrete grades from C12/15 up to C50/60) or a horizontal line at level f_{yd} on stress-strain graph for reinforcing steel. Due to such assumptions, stresses in steel are taken as proportional to strains, which can be presented in the following way:

- $\sigma_{si} = \varepsilon_{si} \cdot E_s$ if $|\varepsilon_{si}| \leq \varepsilon_{yd}$
- $\sigma_{si} = f_{yd}$ if $\varepsilon_{yd} < |\varepsilon_{si}| \leq 10‰$

In the current version of EC2 [17], there is no limitation of tensile reinforcement strains to 10‰ assuming a horizontal top branch of $\sigma_s – \varepsilon_s$ diagram. Such a restriction can be applied, however, in the design procedures. Justification of such limitation can be found in [9] for example.

To draw an interaction curve, a system of two equations of forces equilibrium in the cross-section is used (equations for rectangular cross-sections are presented below):

- sum of longitudinal forces:

$$N_{Rd} = 0.8 \cdot f_{cd} \cdot b \cdot x + \sum_{1}^{n} \sigma_{si} \cdot A_{si} \tag{1}$$

- sum of moments on the axis parallel to the neutral axis, crossing the centre of concrete cross-section:

$$M_{Rd} = 0.8 \cdot f_{cd} \cdot b \cdot x \cdot (0.5 \cdot h - 0.4 \cdot x) + \sum_{1}^{n} \sigma_{si} \cdot A_{si} \cdot (0.5 \cdot h - a_i) \tag{2}$$

2.1. Method presented by R. Kliszczewicz [5]

According to this method (marked in the following part of an article as RK) five ranges of possible column's strains should be taken into consideration. The parameters of equations for the $M_{Rd} - N_{Rd}$ interaction curves are:

- ε_{c1} in the I range,
- x in ranges II–IV,
- ε_{s2} in the V range.

These ranges are given in Table 1 and presented in Fig. 3 and 4. Turns of forces in Fig. 4 were assumed in accordance to turns of acting forces. Attention should be paid to three issues. Firstly, the RK method allows to consider the reinforcement in the varied location of the section's height. Secondly, the effective depth of a cross-section d is treated here as a distance between the most compressed concrete fibre and the axis of the most distant reinforcement. Finally, values a_i are given as distances from the most compressed concrete fibre, as well.

Table 1

Design ranges of partly-simplified method, according to [3]

Range	x	Parameters of equilibrium equations	Reinforcing steel strains
I	$x = \frac{h}{0.8}$	$\frac{14}{23}‰ \leqslant \varepsilon_{c1} \leqslant 2‰$	$\frac{(0.002 - \varepsilon_{c1}) \cdot (3h - 7a_i)}{4h} \boxplus 0.002$
II	$h \leq x \leq \frac{h}{0.8}$	x	$0.002 \frac{7x - 7a_i}{7x - 3h}$
III	$\frac{7d}{27} \leq x \leq h$	x	$0.0035 \frac{x - a_i}{x}$

Table 1 – continued

IV	$0 \le x \le \frac{7d}{27}$	x	$-0.010\frac{x-a_i}{x-d}$
V	$x = 0$	$-10‰ \le \varepsilon_{s2} \le -10‰\frac{a_2}{d}$	$\varepsilon_{s2} - (0.010 + \varepsilon_{s2})\frac{a_i - a_2}{d - a_2}$

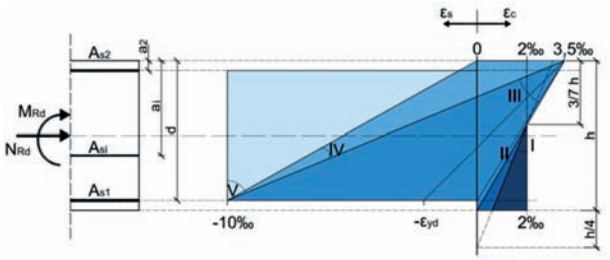

Fig. 3. Design ranges of partly-simplified method, according to [5]

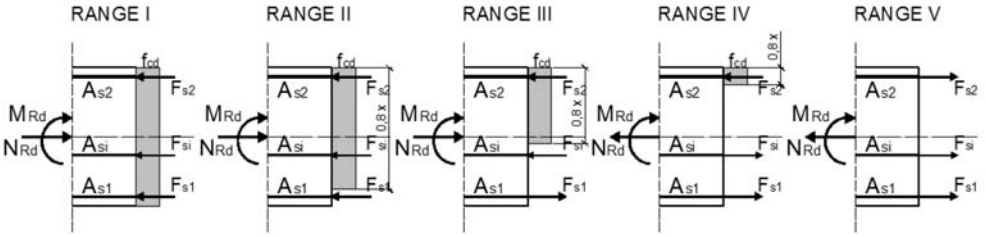

Fig. 4. Schemes for calculating load-bearing capacity for each range in RK method [5]

In ranges from I to IV, stress-strain distribution in compressed concrete zone is rectangular. In V range there is no compressed zone at all.

In all ranges, M_{Rd} and N_{Rd} values are calculated from equations (1) and (2); in the fifth range, an influence of concrete is omitted due to lack of compressed zone.

Ranges I and II apply to compression with very small eccentricity, when the neutral axis is placed beyond the cross-section. Stresses in concrete are equal to f_{cd}. Reinforcement in ranges I and II is compressed on the whole depth and stresses in steel can access value of f_{yd}.

Range I: $x = \frac{h}{0.8}$ i $\frac{14}{23}‰ \leqslant \varepsilon_{c1} \leqslant 2‰$

In range I, the whole cross-section is compressed. We assume that strains in reinforcement are proportional to ε_{c1} strains of the less compressed edge of concrete and that they are equal to:

$$\varepsilon_{si} = \frac{(0.002 - \varepsilon_{c1}) \cdot (3h - 7a_i)}{4h} + 0.002.$$

Range II: $h \le x \le \dfrac{h}{0.8}$

Stress distribution in the compressed zone (of depth 0.8x) does not cover the whole cross-section. An assumption is made that strains for each reinforcing bar are proportional to strains ε_c = 2‰ of concrete in the distance of from the more compressed edge of concrete cross-section and are equal to: $\varepsilon_{si} = 0.002\dfrac{7x - 7a_i}{7x - 3h}$.

Range III: $\dfrac{7d}{27} \le x \le h$

Stress distribution in the compressed concrete zone of depth equal to 0.8x does not cover the whole cross-section; there are three possibilities of neutral axis location:

– neutral axis located between d and $\dfrac{3}{7}h$ ($d \le x < h$) – reinforcement in the cross-section is not subjected to tension (the tension zone reaches no further than to the bottom reinforcement axis);
– compression zone depth is lower than effective depth of the cross-section $\left(\dfrac{700d}{700 + f_{yd}} \le x \le d\right)$ – bottom reinforcement is subjected to tension, but its strains are lower than ε_{yd} and stresses do not reach the value of f_{yd}
– neutral axis located from $\dfrac{7d}{27} \le x < \dfrac{700d}{700 + f_{yd}}$; reinforcement in the tensile zone can reach limit value of ε_s = –10‰;

In whole range III, for each of neutral axis locations, we assume $\varepsilon_{si} = 0.0035\dfrac{x - a_i}{x}$.

Range IV: $0 \le x \le \dfrac{7d}{27}$

A_{s1} reinforcement reaches limit strains ε_s = –10‰, while strains of the most compressed concrete fibre range from 0 to 3.5‰;

Strains in steel ε_{si} are calculated as proportional to limit values: $\varepsilon_{si} = -0.010\dfrac{x - a_i}{x - d}$.

Range V: $x = 0$ and $-10‰ \le \varepsilon_{s2} \le -10‰\dfrac{a_2}{d}$

This range applies to tension with a small eccentricity, when there is no compression zone in concrete. Strains in steel are then calculated according to the equation:

$$\varepsilon_{si} = \varepsilon_{s2} - (0.010 + \varepsilon_{s2})\frac{a_i - a_2}{d - a_2}.$$

R. Kliszczewicz [5] presents two ways of evaluating interaction curves using these ranges and equations mentioned above.

First method:

In the aim of creating the right branch of the graph, an optimal number of parameters from described ranges is assumed, then stresses and strains in the reinforcement are calculated.

It allows for the determining of pairs of N_{Rd} and M_{Rd} using equations (1) and (2). The left side of the graph is obtained in case of symmetrical cross-section by reflecting the right branch of the graph towards the vertical axis of a coordinate system. In the case of non-symmetrical reinforcement, a theoretical 180 degrees rotation of the cross-section should be made and calculations have to be repeated.

Second method:

The right branch of the interaction curve is built by calculating the maximal and minimal values of longitudinal force N_{Rd}, for I range assuming $\varepsilon_{c1} = 2‰$, for V $\varepsilon_{s2} = -10‰$ and dividing the obtained range into parts (depending on necessary accuracy). In this way, a set of coordinates of the graph is created.

Furthermore, N_{Rd} values are calculated for extremes of ranges and for designated N_{Rd} calculation of respective M_{Rd} values is made using iteration. This is how pairs of (M_{Rd}, N_{Rd}) forces creating the right branch of the graph can be obtained. The left part is created as in the first method.

According to the authors of this article, while setting parameter values for which $M_{Rd} - N_{Rd}$ pairs are calculated (especially when the division of range $N_{Rdmax} - N_{Rdmin}$ is not very dense), a special point should not be omitted – the point relating to maximal moment ($x = \xi_{eff.lim} \cdot d$, $\varepsilon_{s1} = f_{yd} \cdot E_s$).

2.2. Method presented by J. Procházka, A. Kohoutkova, J. Vaškowa [16]

In the paper of J. Procházka, A. Kohoutkova, J. Vaškowa [16], which is an academic book, a simpler method of creating interaction curves is presented. For the purposes of simplification, in the following part of this article, this method is described as PKV, from surnames of authors of the book [16]. Several specific strains are taken into consideration instead of ranges of strains – therefore, it is enough to calculate only 10 pairs of $M_{Rd} - N_{Rd}$ values. Accuracy of this method is satisfactory in accordance with its simplicity and quickness. In the PKV method, a rectangular cross-section of stresses in concrete is assumed, with the compression zone depth equal to 0.8x, constant value of stresses equal to f_{cd}, and a horizontal top branch of stress-strain distribution on reinforcing steel equal to f_{yd}. The PKV method only takes into account the reinforcement arranged at the top and bottom edge of the cross section. An example of the interaction curve obtained with the PKV method is shown in Fig. 5.

In Fig. 5, point A represents the load-bearing capacity of a cross-section subjected to axial compression with strains equal to 2‰. It is respective to extreme value of the first range in RK method. This way the maximal N_{Rd} capacity for compression is designated.

Point B corresponds to a situation in which the depth of compression zone x is equal to an effective depth of the cross-section, d, which implicates zero strains in steel reinforcement A_{s1}. Strains in reinforcement A_{s2} are assumed as 3,5‰. This case responds to the third range from the RK method.

Point C represents capacity of a cross-section in which the depth of the compression zone is equal to $x_{lim} = \xi_{lim} \cdot d$, which for the rectangular stress distribution in compressed concrete gives $x_{eff.lim} = \xi_{eff.lim} \cdot d$. Checks should be made as to whether $x_{bal.1} = \xi_{bal.1} \cdot d \geq x_{bal.2} = \xi_{bal.2} \cdot a_2$, where $\xi_{bal.1}$ is equivalent for $\xi_{lim} = \dfrac{\varepsilon_{cu.3}}{\varepsilon_{cu.3} + \varepsilon_{yd}}$, and $\xi_{bal.1} = \dfrac{\varepsilon_{cu.3}}{\varepsilon_{cu.3} - \varepsilon_{yd}} \cdot$ If so, it can be assumed that both A_{s1} and A_{s2} reinforcement is completely used, which means that $\sigma_{s1} = \sigma_{s2} = f_{yd}$. With

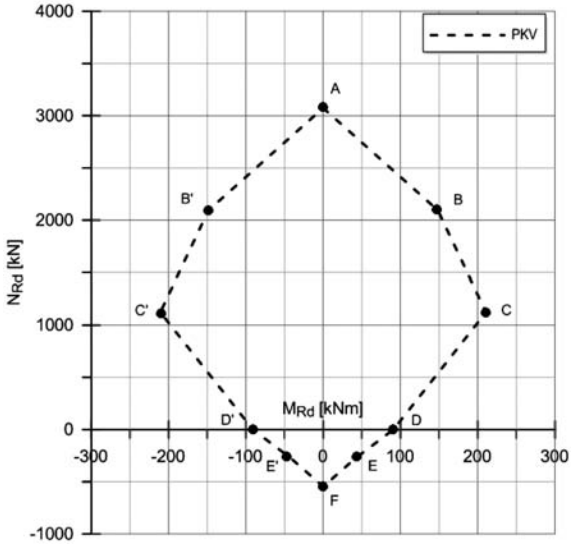

Fig. 5. An example of interaction curve according to PKV method [16]

such assumption, a maximum value of M_{Rd} is obtained. This case responds to the third range from the RK method.

Point D shows the capacity of a bended cross-section without axial force, it is a case which belongs to the fourth range. In the PKV method, an influence of compressed A_{s2} reinforcement is omitted.

Point E represents the capacity of a cross-section subjected to eccentric tension with a small eccentricity, the compression zone is omitted.

Point F shows the capacity of a cross-section subjected to axial tension. The bending moment is equal to zero. Reinforcements A_{s1} and A_{s2} are completely exploited. It is an example corresponding to an extreme value of a fifth range, from which we obtain maximal value of N_{Rd} for tension.

Points B`, C`, D`, E` in case of symmetrical reinforcement can be designated by reflection towards the vertical axis. In cases when the reinforcement is not symmetrical, the cross-section should be theoretically rotated by 180 degrees and these points should be calculated with similar assumptions, treating reinforcement A_{s2} as A_{s1} and so on.

3. The comparison of $M_{Rd} – N_{Rd}$ interaction curves (according to RK and PKV methods)

The following part of the article consists of a comparison of interaction curves obtained from two described methods, RK and PKV, with assumptions:

– rectangular column cross-section with dimensions 30 × 40 cm,
– C30/37 concrete grade
– RB500W steel,

– 3.0 cm cover,
– main reinforcement diameter: ϕ 20 mm,
– stirrups diameter: ϕ_s 6 mm,
– reinforcement ratio: 1.0% i 3.1%,
– symmetrical reinforcement, placed only at the top and bottom edge of the section.

Comparing these graphs (Fig. 6), it can be noted that the differences in results obtained from PKV methods in relation to those from the RK method are on the safe side. The advantages of the PKV method are its simplicity and the ability to perform calculations efficiently, such as in a spreadsheet.

If input data change and the reinforcement ratio is higher, e.g. ρ = 3.1% ($A_{s1} = A_{s2} = 18{,}85$ cm^2), then point D of the PKV curve will not cover the curve from the RK method (Fig. 7). It is due to the fact that in the PKV method, compressed reinforcement is omitted while designating point D. The differences between these two methods in point D (moment value for zero axial force) will increase with an increasing reinforcement ratio or steel grade and with decreasing concrete strength.

Calculations for the PKV method can be simplified by omitting point E, because the curve for tension is close to linear.

$M_{Rd} – N_{Rd}$ interaction curves presented in the above figures were verified with curves obtained from computer software [10].

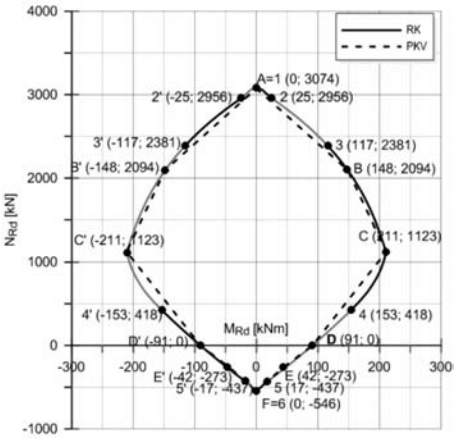

Fig. 6. $M_{Rd} – N_{Rd}$ interaction curves according to RK [5] and PKV [16] methods, with ρ = 1.0%

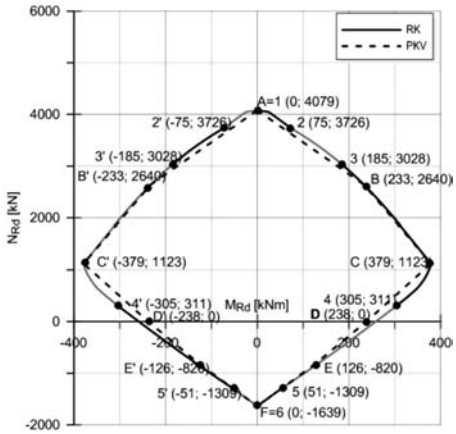

Fig. 7. $M_{Rd} – N_{Rd}$ interaction curves according to RK [5] and PKV [16] methods, with ρ = 3.1%

4. An example of using interaction curves to design thick reinforced concrete columns

To choice reinforcement for 47 columns of a vessel support structure interaction curves created with RK method were used. Dimensions of the cross-sections of the designed columns were equal to 50 × 50 cm and could be analysed without considering second order effects. Columns were subjected to longitudinal forces and bending moments in both directions (skew

bending). The assumptions were made that there would be only four types of reinforcement (table 2) and that each type of reinforcement would be symmetrical and equivalent in both planes.

$M_{Rd} - N_{Rd}$ interaction curves were evaluated for these types of reinforcement. They take into account the whole reinforcement (not only concentrated on opposite sides, but also a part of it which is distributed parallel to the plane of bending).

Table 2

Assumed types of vessel support structure reinforcement

Column reinforcement	Reinforcement in both planes	Description in Fig. 8.
12 ϕ16	$A_{s1} = A_{s2} = 4\phi16$	4 ϕ16
12 ϕ25	$A_{s1} = A_{s2} = 4\phi25$	4 ϕ25
16 ϕ25	$A_{s1} = A_{s2} = 5\phi25$	5 ϕ25
16 ϕ28	$A_{s1} = A_{s2} = 5\phi28$	5 ϕ28

$M_{Rd} - N_{Rd}$ interaction curves for planes *xy*; *xz*; with points corresponding to pairs of $M_{Ed} - N_{Ed}$ forces (representing the results of static calculations) are presented in Fig. 8. A preliminary increase of forces and moments by 50 percent has been made while putting $M_{Ed} - N_{Ed}$ points onto interaction curves. Due to such an attitude, a designed reinforcement fulfils the EC2 [17] simplified criteria for skew bending:

$$\left(\frac{M_{Edz}}{M_{Rdz}}\right)^a + \left(\frac{M_{Edy}}{M_{Rdy}}\right)^a \le 1.0 \tag{3}$$

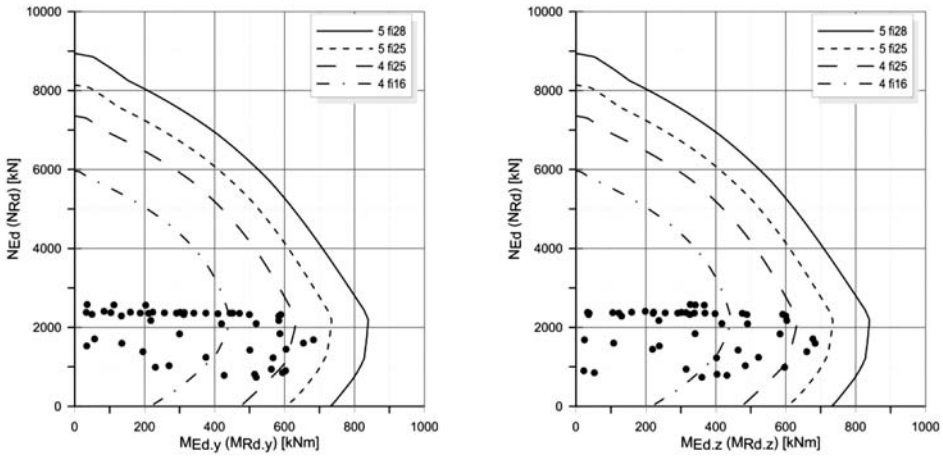

Fig. 8. $M_{Rd} - N_{Rd}$ interaction curves in *xy*, *xz* planes. Preliminary choice of reinforcement for vessel support structure

The power a has been assumed according to EC2 depending on the relation N_{Ed} /N_{Rd}.

After preliminary choice of reinforcement for skew bending according to interaction curves, the capacity of columns was checked. As a result, values fulfilling the normative conditions were obtained for all analysed columns.

It is important to include the reinforcement located along the section's height. A comparison of interaction curves which take into account only bars on opposite sides of the cross-section (dashed lines) with those taking into account all bars along the height of the section (solid lines) is shown in Fig. 9.

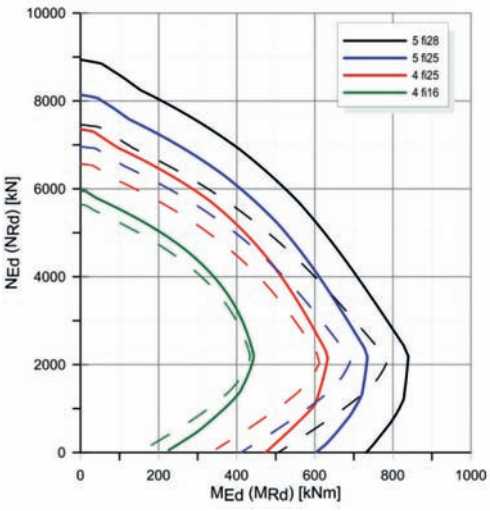

Fig. 9. The $M_{Rd} – N_{Rd}$ interaction curves in *xy* and *xz* planes which take into account only the reinforcement located by the top and bottom edges (dashed line) and which take the whole reinforcement in the cross-section into account (solid line)

5. Second order effects on $M_{Rd} – N_{Rd}$ interaction curves

The following part of the article presents $M_{Rd} – N_{Rd}$ interaction curves which take into consideration the reduction of capacity of columns due to second order effects. A comparison of an influence of chosen factors on the values of second order effects calculated with two simplified methods given by EC2 – nominal stiffness method (MNS) and nominal curvature method (MNC) was made.

5.1. Assumptions for analysis

Three cross-sections were analysed (as in Fig. 10), with the following data:

- rectangular column cross-section with dimensions 40 × 50 cm,
- C30/37 concrete grade
- RB500W steel,
- γc = 1.4,

- γ_s = 1.15,
- 3.0 cm cover,
- main reinforcement diameter: ϕ = 20 mm,
- stirrups diameter: ϕ_s = 6 mm,
- symmetrical reinforcement as in Fig. 12.

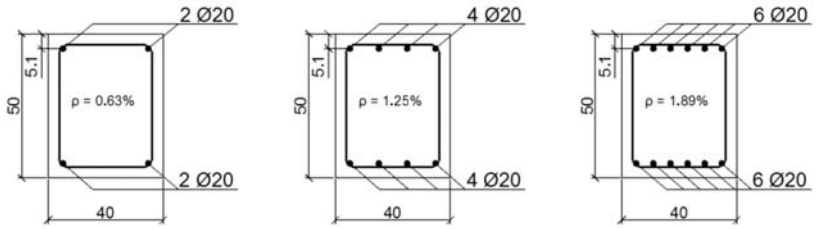

Fig. 10. Analysed cross-sections of columns

In the analysis, the following variable parameters were assumed, with values as follows:

- column slenderness: λ = 21; 35; 49,
- λ/λ_{lim} ratio= 0.5; 1.0; 2.0,
- reinforcement ratio ρ = 0.63%; 1.25%; 1.89%,
- effective creep coefficient φ_{eff} = 0; 1.5.

In the MNS method, two assumptions were made – coefficient depending on first order moments distribution c_0 = 8 (first order moment is constant, r_m = 1), and coefficient depending on reinforcement ratio K_s = 1.0. K_c was calculated according to the formula 5.22 from EC2 [17]. In the MNC method, a distribution of total curvature was assumed to be sinusoidal, similarly for the second order effects. This approximation is on the safe side. For such curvature, a distribution of a coefficient c is equal to $\pi^2 \approx 10$. The n value for which the maximum limit value of a moment is achieved, was assumed as n_{bal} = 0.4.

5.2. Second order effects on $M_{Rd} - N_{Rd}$ interaction curves. Variable slenderness λ

Fig. 11a and b (below) present interaction curves with second order effects for columns with different slenderness. Second order effects were calculated with MNS and MNC for three different λ values, with assumed first order eccentricity e_0 = 0.07 m (thus, for the values of moments m_I resultant from this eccentricity and from values of longitudinal forces).

The values of second order effects, obtained from the MNC method are presented in the whole range of loadings (similar to results considered in the engineer design of columns according to EC2), assuming stresses in steel equal to f_{yd}.

The following graphs (Fig. 11) present m_I values for first order impacts with imperfections and m_{II} values relevant for second order effects for n = 0.6. There is an increase of m_{II} with an increase of slenderness λ. For the analysed columns, values of second order effects from MNS and MNC differ significantly and this difference depends on the n level.

Fig. 12a and b present second order effects obtained from MNS and MNC for three different values of slenderness and corresponding imperfections measured from relevant lines. For the chosen value of n = 0.6, values of m_{imp} (moments from imperfections),

m_{II} (second order moments), m_{static} (moments caused by loadings) were shown. Values of m_{II} were calculated not for assumed first order eccentricity as in the previous example, but for the highest possible values of m_{static} in relevance to capacity on a level of n.

The area between the interaction curve and a second order effects line for exact λ value is an area of possible values of m_{static}. By comparing the interaction curves for two methods, it can be concluded that this area is significantly smaller for MNS than from MNC.

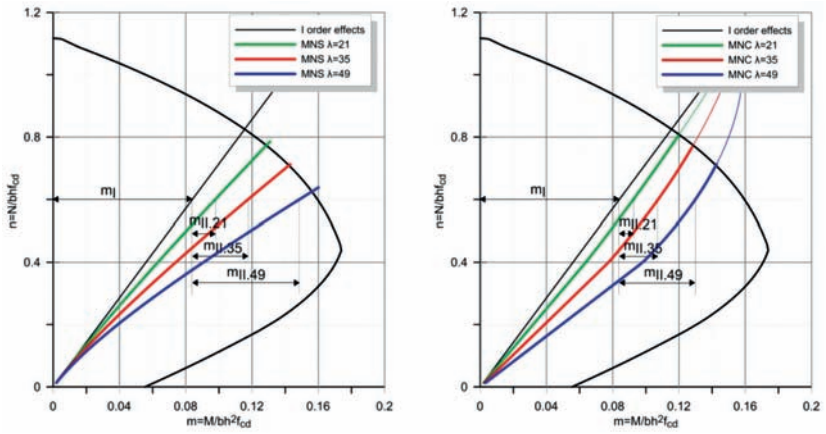

Fig. 11a, b. $M_{Rd} – N_{Rd}$ interaction curves with second order effects for columns with different slenderness. Comparison of second order effects from MNS and MNC. Reinforcement ratio ρ = 0,63%, effective creep coefficient $\varphi_{eff} = 0$

Discontinuity of the graph obtained for λ = 49 (Fig. 12a) with use of MNS, is caused by normative restriction of the value of k_2 coefficient, which is used to consider the cracking and creep influence on the nominal stiffness of slender compressed concrete members.

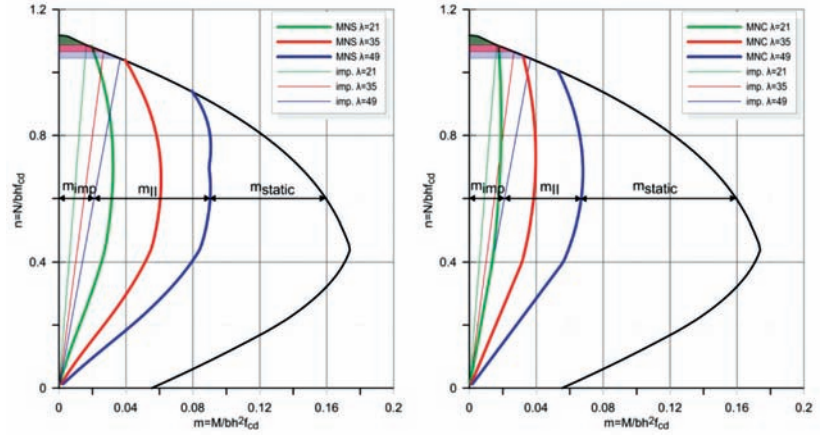

Fig. 12a, b. $M_{Rd} – N_{Rd}$ interaction curves with second order effects (measured from imperfection line) for columns with different slenderness. Possible areas of m_{static} values calculated with MNS and MNC. Reinforcement ratio ρ = 0.63%, effective creep coefficient $\varphi_{eff} = 0$

To simplify using interaction curves with areas of possible values of m_{static}, second order effects can be measured from interaction curves as in Fig. 13a and b. The shadowed area represents possible first order moments for different forces n and slenderness λ; $m_I = m_{static} + m_{imp}$.

Similar to former graphs, m_{II} moments were calculated for the biggest possible values of m_I due to capacity on the exact level of n.

Values of m_I and m_{II} designated for $n = 0.6$ apply to slenderness $\lambda = 49$.

Comparing Fig. 13a and b, it can be noticed that an area of possible m_I values for the MNS method is significantly smaller than for MNC, this rule applies for each slenderness value.

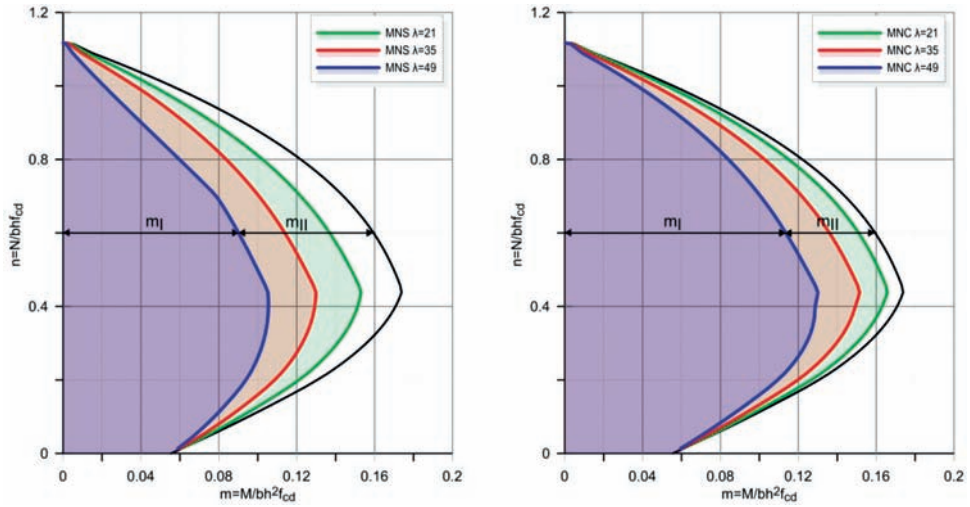

Fig. 13a, b. $M_{Rd} – N_{Rd}$ interaction curves with second order effects (measured from interaction curves) for columns with different slenderness. Comparison of areas of possible m_I values according to MNS and MNC methods. Reinforcement ratio $\rho = 0.63\%$, effective creep coefficient $\varphi_{eff} = 0$

5.3. Second order effects on $M_{Rd} – N_{Rd}$ interaction curves – variable ratio of λ/λ_{lim}

$M_{Rd} – N_{Rd}$ interaction curves below (Fig. 14a, b) present second order effects calculated with MNS and MNC for a variable value of λ and for three different slenderness ratios λ/λ_{lim}, which equal 0.5; 1.0; 2.0, (with an assumed I order eccentricity $e_0 = 0.07$ m). For chosen value of $n = 0.6$ values of m_I and m_{II} were shown; for slenderness ratio $\lambda/\lambda_{lim} = 2$.

We can distinguish slight impact of slenderness lower than λ_{lim} and a significant influence of slenderness exceeding the limit value λ_{lim} on second order effects m_{II}.

For bigger values of λ/λ_{lim}, differences between second order effects calculated with MNS and MNC are more distinct.

Furthermore, for values of $n < n_{bal}$ second order effects from MNS are lower than from MNC, whereas for $n > n_{bal}$ the situation is opposite

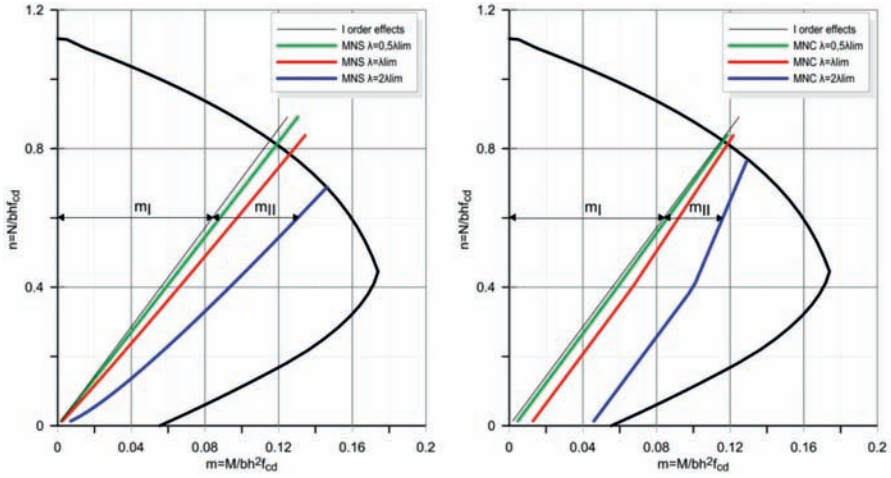

Fig. 14a, b. $M_{Rd} – N_{Rd}$ interaction curves with second order effects calculated with MNS and MNC for columns with different slenderness λ/λ_{lim} ratios. Reinforcement ratio $\rho = 0.63\%$, effective creep coefficient $\varphi_{eff} = 0$

5.4. Second order effects on $M_{Rd} – N_{Rd}$ interaction curves – variable reinforcement ratio ρ

The following $M_{Rd} – N_{Rd}$ interaction curves (Fig. 15a, b) present second order effects calculated with MNS and MNC for three different reinforcement ratios $\rho = 0.63; 1.25; 1.89$ (with an assumed first order eccentricity equal to $e_0 = 0.07$ m).

For the chosen value of $n = 0.8$, values of m_I and m_{II} relevant for reinforcement ratio $\rho = 1.89\%$ were presented.

In graphs considering MNS an influence of reinforcement ratio on second order effects m_{II} is clear; however graph for MNC claims that values of second order effects m_{II} are not dependent on reinforcement ratio.

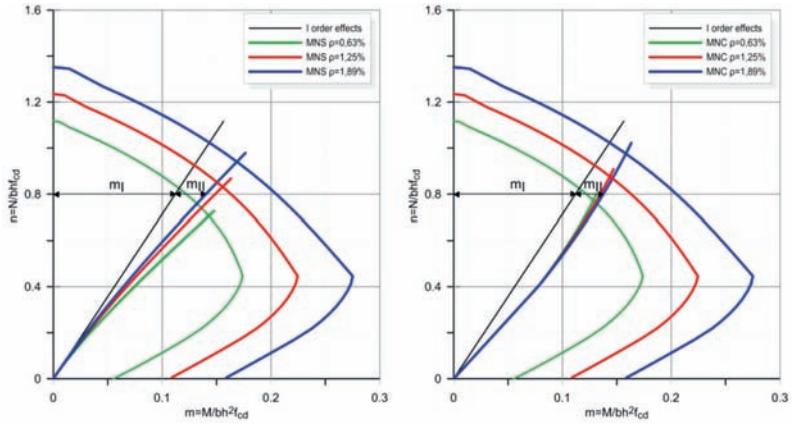

Fig. 15a, b. $M_{Rd} – N_{Rd}$ interaction curves with second order effects calculated with MNS and MNC for various reinforcement ratio. Column slenderness $\lambda = 35$, effective creep coefficient $\varphi_{eff} = 0$

5.5. Second order effects on $M_{Rd} - N_{Rd}$ interaction curves – variable creep coefficient

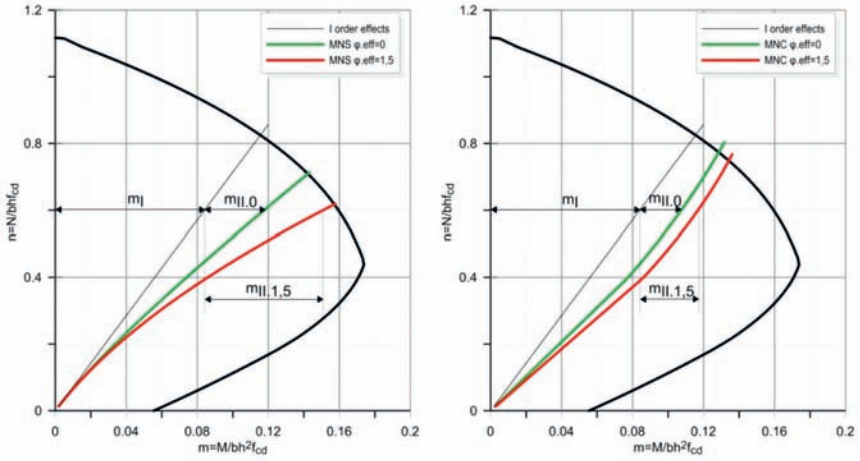

Fig. 16a, b. $M_{Rd} - N_{Rd}$ interaction curves with second order effects calculated with MNS and MNC for various creep coefficient φ_{eff}. Column slenderness $\lambda = 35$, reinforcement ratio $\rho = 0.63\%$

Fig. 16a and b, present second order effects calculated with MNS and MNC on $M_{Rd} - N_{Rd}$ interaction curves for creep coefficients equal to $\varphi_{eff} = 0$ and $\varphi_{eff} = 1.5$ (with an assumed first order eccentricity equal to $e_0 = 0.07$ m). For the chosen value of $n = 0.6$, values of m_I and m_{II} relevant for creep coefficient $\varphi_{eff} = 0$ were presented. In analysed cases for $n > n_{bal}$ the impact of creep on second order effects m_{II} calculated with MNS is higher than on second order effects from MNC.

6. Conclusions

The first part of the paper presents two methods of evaluating $M_{Rd} - N_{Rd}$ interaction curves for members subjected to axial force and bending moment in one plane (partly-simplified RK and PKV methods) [5, 16]. It was proven that despite the different assumptions in methods PKV and RK, results obtained from both methods are similar. There was also an example of applying the interaction curves to the choice of the reinforcement in vessel support structure.

The second part of the paper considers the reduction in $M_{Rd} - N_{Rd}$ interaction curves due to second order effects. Interaction curves were designated with RK method. Second order effects were calculated with methods of nominal stiffness and nominal curvature, according to EC2, for various values of slenderness, λ/λ_{lim} ratio, reinforcement ratio ρ and creep coefficient φ_{eff}.

The usefulness of $M_{Rd} - N_{Rd}$ interaction curves not only for designing and checking the capacity of columns, but also for analysis, such as the one carried out in this article – comparing second order effects evaluated with different methods, was indicated in the article.

On the basis of the conducted analysis:

- it was proved that second order effects calculated with MNS and MNC differ significantly, their comparison was presented on $M_{Rd} - N_{Rd}$ interaction curves
- it was claimed that differences between second order effects from MNS and MNC depend on the value of $n = N_{Ed}/bhf_{cd}$,
- it was noticed that for the analysed column, the area of possible m_{static} values for second order effects from MNS is considerably lower than from MNC
- an increase of m_{II} value with an increase of ratio of slenderness to its limit value λ/λ_{lim} in MNS and MNC and its dependence on n/n_{bal} ratio was presented
- the differences between an impact of reinforcement ratio on second order effects were shown; this influence is distinct in MNS and inconsiderable in MNC *confusing sentence – we usually expect to see differences between something and something else.*
- it was presented that the influence of creep on second order effects in MNC is lower than in MNS.

The comparisons of second order effects calculated by MNS and MNC methods presented in the paper, are aimed at depicting the situation encountered by the designer applying the rules of Eurocode 2 [17] and to indicate the need for comments to this standard (standard czy code? Tu sama nie jestem pewna, raczej code – od Eurocode chociażby), which could help to choose the right method.

References

[1] *Podstawy projektowania konstrukcji betonowych i żelbetowych według Eurokodu 2*, praca zbiorowa pod redakcją M. Knauffa, Dolnośląskie Wydawnictwo Edukacyjne, Wrocław 2006.

[2] *CEB/FIP Manual on Bending and Compression Design of Sections under Axial Action Effects at the Ultimate Limit State*, Bulletin d'Information, No. 141, 1982.

[3] *Model Code 2010. Final draft*, April 2012.

[4] Knauff M., *Obliczanie konstrukcji żelbetowych wg Eurokodu 2. Zasady ogólne i zasady dotyczące budynków*, Wydawnictwo Naukowe PWN, Warszawa 2012.

[5] Kliszczewicz R., *Konstrukcje betonowe. Obliczanie elementów żelbetowych w stanach granicznych nośności i użytkowania wg PN-B-03264:2002*, Wydawnictwo Politechniki Śląskiej, Gliwice 2008.

[6] Bažant Z.P., Cedolin L., Tabbara M.R., *New method of analysis for slender columns*, ACI Structural Journal; July–August 1991, 391-401.

[7] Kamińska M.E., *High–strength concrete and steel interaction in RC members*, Cement & Concrete Composites 24, 2002, 281-295.

[8] Westerberg B., *Second order effects in slender concrete structures. Background to the rules in EC2*, Betongbyggnad, 2004.

[9] Czkwianianc A., Kamińska M., *Nośność przekrojów obciążonych momentem zginającym i siłą podłużną,* w: *Podstawy projektowania konstrukcji betonowych i żelbetowych według Eurokodu 2*, praca zbiorowa pod redakcją M. Knauffa, Dolnośląskie Wydawnictwo Edukacyjne, Wrocław 2006.

[10] Program KBB udostępniony przez Politechnikę Łódzką.

[11] Pallarés L., Bonet J.L., Fernandez M.A., Miguel P.F., C_m *factor for non-uniform moment diagram in RC columns*; Engineering Structures 31, 2009, 1589-1599.
[12] Cortés-Moreno E., Bonet J.L., Romero M.I., Miguel P.F., *Slenderness limit of the weak axis in the design of rectangular reinforced concrete non-sway columns*, Engineering Structures 33, 2011, 1157-1165.
[13] Csuka B., Kollár L., *Design of reinforced concrete columns under centric load according to Eurocode 2*, Concrete Structures, 2011.
[14] Feix J., Walkner R., *Betonbau. Grundlagen der Bemessung nach EC2*, Studia Universitätsverlag, 2012.
[15] Fingerloos F., Hegger J., Zilch K., *Eurocode 2 für Deutschland: DIN EN 1992-1-1 Bemessung und Konstruction von Stahlbeton- und Spannbetontragwerken. Tiel 1-1, Kommentierte Fassung;* Berlin, Wien, Zürich, 2012.
[16] Procházka J., Kohoutkova A., Vaškowa J.: *Příklady navrhování betonowých konstrukcí 1*, ČVUT, Praga 2007.
[17] PN-EN 1992-1-1:2008 – Eurokod 2. Projektowanie konstrukcji z betonu. Część 1-1: Reguły ogólne i reguły dla budynków.
[18] Lechman M., *Wymiarowanie przekrojów elementów z betonu zginanych z udziałem siły osiowej według Eurokodu 2. Przykłady obliczeń*, Instytut Techniki Budowlanej, Warszawa 2011.

TECHNICAL TRANSACTIONS | CZASOPISMO TECHNICZNE
CIVIL ENGINEERING | BUDOWNICTWO
2-B/2013

KATARZYNA RYNGIER, WIT DERKOWSKI*

STRENGTHENING OF BENT REINFORCED CONCRETE BEAMS WITH FRP COMPOSITES – COMPARISON OF ULS DESIGN GUIDELINES

WZMACNIANIE ZGINANYCH BELEK ŻELBETOWYCH MATERIAŁAMI KOMPOZYTOWYMI FRP – PORÓWNANIE PROCEDUR PROJEKTOWANIA Z UWAGI NA NOŚNOŚĆ

Abstract

The paper raises an issue of designing flexural strengthening of reinforced concrete beams with FRP composite materials. Three different design approaches are presented. The conducted analysis consists of the determination of the load-bearing capacity of a beam, the assumption of loading and the evaluation of a capacity increase after strengthening the beam with a CFRP strip. Results are compared and justified and some conclusions are drawn. Furthermore, an author's computer software for simple verification of ultimate limit state is briefly presented.

Keywords: FRP composite materials, CFRP strips, flexural strengthening, RC beams

Streszczenie

Artykuł porusza kwestię projektowania wzmocnień belek żelbetowych na zginanie przy pomocy materiałów kompozytowych FRP. Opisano procedury projektowania i porównano wyniki obliczeń przykładowej belki według trzech różnych norm, ponadto przedstawiono autorski program komputerowy pozwalający na obliczenie wzmocnienia belki o przekroju prostokątnym taśmami CFRP.

Słowa kluczowe: materiały kompozytowe FRP, taśmy CFRP, wzmacnianie na zginanie, żelbet

* B. Eng. Katarzyna Ryngier, Ph.D. Eng. Wit Derkowski, Institute for Building Materials and Structures, Civil Engineering Faculty, Cracow University of Technology.

1. Introduction

For more than 20 years, widely known fibre reinforced composite materials have become much more frequently used for strengthening reinforced concrete structures. Their mechanical properties, such as exceptionally high tensile strength, perfect corrosion resistance and low mass make a contribution to the constantly increasing popularity of FRP materials. A considerable advantage is also the lack of influence on not only self-weight of the strengthened construction, but also on the dimensions of the cross-section of elements, which is sometimes a decisive factor during the choice of strengthening method.

The tensile strength of FRP composite strips is within the range of 2000 – over 3000 MPa, while their elasticity modulus is also relatively high, – approximately 160–200 GPa for standard strips and above 300 GPa for high-modulus strips.

FRP composite materials can contribute to an increase of the load-bearing capacity of various construction members, such as columns, beams or slabs. Strips with non-metallic, continuous fibres, arranged in one direction, are used for flexural strengthening, whereas for shear strengthening, a preferable material is FRP sheets with fibres organised orthogonally in the composite matrix. Strengthening reinforced concrete beams subjected to bending is realised by bonding the strip to the tensile, usually bottom, surface of the strengthened member using proper adhesive. The most widely used adhesives are based on epoxy resins. Optionally, there is a possibility to anchor ends of the strip using steel blocks or FRP composite elements (Fig. 1).

Fig. 1. Examples for strengthening concrete beams and slab with anchoring elements [7]

The first European guidelines considering FRP strengthening were published by *fib* (The International Federation for Structural Concrete) in 2001 [1]. Nowadays, there is a variety of design guidelines, among which there are: American *'Guide for the Design and Construction of Externally Bonded FRP Systems for Strengthening Concrete Structures'* (ACI440, 2R-08, 2008 (first version in 2000), Italian National Research Council (CNR) publication (CNR-DT 200/2004, 2004), Swiss guidelines (SIA166, 2004), Canadian (CAN/CSA-S806-02, 2002) and British Concrete Society document (TR55, 2004) [3]. But on the other hand, in many countries, such as Poland, any formal guidelines for the design of such strengthening have still not been developed. Also, the EC-2 is beyond the scope of modern composite materials used

for concrete reinforcement. Model Code 2010 [N5] takes on a non-metallic reinforcement for concrete, determining the material properties and the problem of bonding such a reinforcement for concrete, but does not provide specific design rules for ULS and SLS.

The following paper presents a short description of design procedures for strengthening reinforced concrete beams for flexure and the most important differences between three of the above-mentioned documents: *fib* Bulletin no. 14 [N4], ACI 440, 2R-08 [N2] and the Italian CNR-DT 200/2004 [N3]. Results obtained from these calculations were compared and justified. Furthermore, an author's computer program, written in Delphi environment, is briefly described. It allows for the checking of the ultimate limit state of the strengthened bent RC element, according to *fib* [N4] and the results from the program are also presented.

2. Design guidelines for FRP strengthening

2.1. American ACI 440, 2R-08

The *Guide for the Design and Construction of Externally Bonded FRP Systems for Strengthening Concrete Structures*, which was developed in the United States, widely describes the strengthening and retrofitting of concrete structures with FRP materials. Procedures given in this document start from calculating existing strains in extreme concrete fibres of the strengthened member and then continue to the estimation of the neutral axis depth. The β_1 coefficient for rectangular shape of stress distribution varies from 0.65 to 0.85, depending on concrete compressive strength.

Nominal capacity is decreased by two coefficients, the first of which is a strength reduction factor Φ [cf. N1 p. 9.3.1], dependent on the character of cross-section work (flexure, compression, shear etc.). A value of Φ proper for flexure (tension-controlled sections) is assumed as 0.9 and hence such a value was used during calculations. The second one is an additional strength reduction factor, ψ_f, which is equal to 0.85 and its aim is to decrease the FRP contribution to total flexural capacity.

2.2. *fib* Bulletin no. 14

The technical report, Bulletin no. 14 of *fib*, entitled '*Externally bonded FRP reinforcement for RC structures'*, published in 2001, presents FRP strengthening materials and techniques, design assumptions and description of strengthening for various actions (flexure, shear and torsion, confinement). The guidelines present a set of criteria essential to fulfilling the aim of ensuring a proper bond between composite materials and the strengthened member concrete surface.

The document also highlights the importance of the relevant requirements for the structure to be strengthened. Firstly, the element should be of a good quality – all wide cracks should be formerly injected to protect the member from problems caused by the penetration of water, such as steel reinforcement corrosion, and to avoid weakening of bond strength in places of horizontal cracking. The injection should be made with a low-viscosity resin, which allows for the connection of composite material with the concrete surface properly. Furthermore, the minimum concrete tensile strength should exceed 1.5 MPa and the recommended minimal concrete grade is C15/20 [N4].

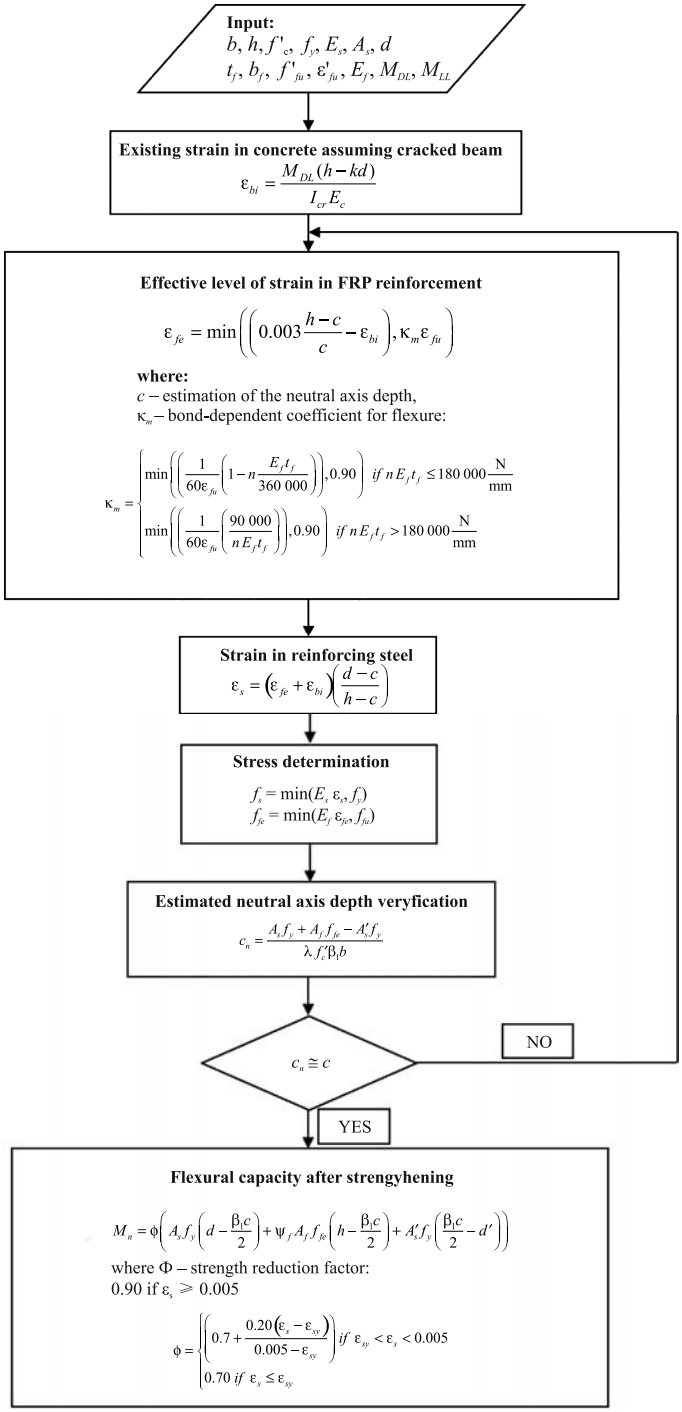

Fig. 2. ACI 440.2R-08 design procedure flowchart

The *fib* guidelines distinguish two groups of failure modes – assuming full composite action or loss of composite action. The former is divided into two cases – concrete crushing in compressed section due to exceeding maximum strains and FRP rupture caused by failure in tension. The latter group consist of various types of debonding, which means that the local deformation of the FRP strip in the critical cross-section is greater than can be carried by the bond between the strip (or laminate) and concrete substrate. There are two possible modes of failure: debonding of the laminate from its end and mid-span shear debonding.

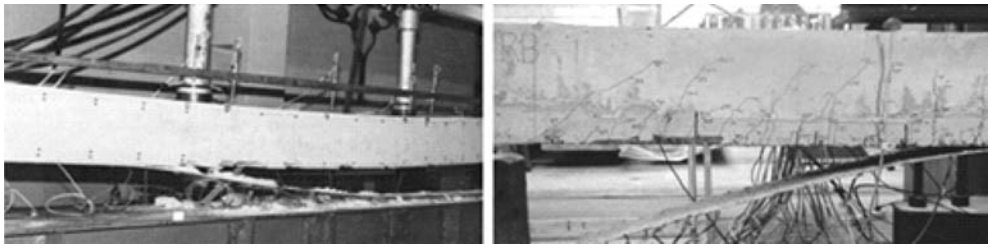

Fig. 3. Failure examples of concrete beams strengthened with EBR FRP [3]

The most probable failure model should be analysed checking ultimate limit state. Considering the strain distribution in the strengthened cross-section a verification whether the limit strain values are exceeded in FRP ($\varepsilon_f = \varepsilon_{flim}$, but $\varepsilon_c < \varepsilon_{cu}$) or in concrete ($\varepsilon_c = \varepsilon_{cu}$, but $\varepsilon_f < \varepsilon_{flim}$) is possible.

If failure is due to FRP rupture real strains in the most compressed concrete fibre should be determined and, furthermore, the constant values of ψ and δ_G coefficients are replaced by equations dependent on previously calculated concrete strains:

$$\psi = \begin{cases} 1000\,\varepsilon_c \left(0.5 - \dfrac{1000}{12}\varepsilon_c\right) & \text{for} \quad \varepsilon_c \le 0.002 \\ 1 - \dfrac{2}{3000\,\varepsilon_c} & \text{for} \quad 0.002 \le \varepsilon_c \le 0.0035 \end{cases}$$

$$\delta_G = \begin{cases} \dfrac{8 - 1000\,\varepsilon_c}{4\,(6 - 1000\,\varepsilon_c)} & \text{for} \quad \varepsilon_c \le 0.002 \\ \dfrac{1000\,\varepsilon_c\,(3000\,\varepsilon_c - 4) + 2}{2000\,\varepsilon_c (3000\varepsilon_c - 2)} & \text{for} \quad 0.002 \le \varepsilon_c \le 0.0035 \end{cases}$$

FRP material safety factors (Table 1), which are necessary for ULS calculations, are assumed depending on the type of application and on-site working conditions (type A – normal quality control conditions, prefab systems, type B – difficult conditions, wet lay-up conditions).

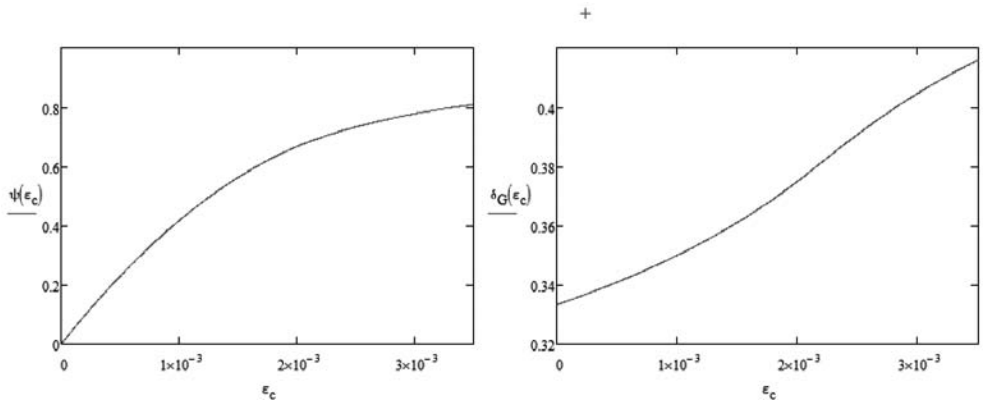

Fig. 4. Coefficients ψ and δ_G in dependence on ε_c

Table 1

Partial safety material coefficients for FRP [N4]

FRP type	Application type A	Application type B
CFRP	1.2	1.35
AFRP	1.25	1.45
GFRP	1.3	1.5

According to statements included in the *fib* guidelines, there is a necessity to check not only the Ultimate Limit State, but also the Serviceability Limit State conditions, for instance to prevent the strip from peeling-off phenomena, described above. Verification whether bond failure at the end anchorage and along the FRP occurs is essential for complete design and a good assessment of reliability. Broadly conceived research considering this problem was conducted in Poland by R. Kotynia [6]. SLS conditions not rarely govern the design, hence maximum acceptable strains in FRP should be reduced to a certain limit, for example as identified in the research [6]. However, in this paper authors focused only on the procedure given for ULS verification. Finally, after determining the failure mode, a calculation of the neutral axis depth of strengthened members can be evaluated based on the balance of forces equation, and therefore a value of increased flexural capacity is obtained from the equilibrium of bending moments. The *fib* Bulletin No. 14 design procedure flowchart is presented in Fig. 5.

2.3. CNR-DT 200/2004 Italian code

The procedure of strengthening design according to Italian code is quite different than the two previously mentioned examples. At the beginning, a calculation of maximum allowable strains in CFRP must be made, and the obtained value is later used in following calculations. This strain is determined to prevent the structure from debonding failure mode – the maximum

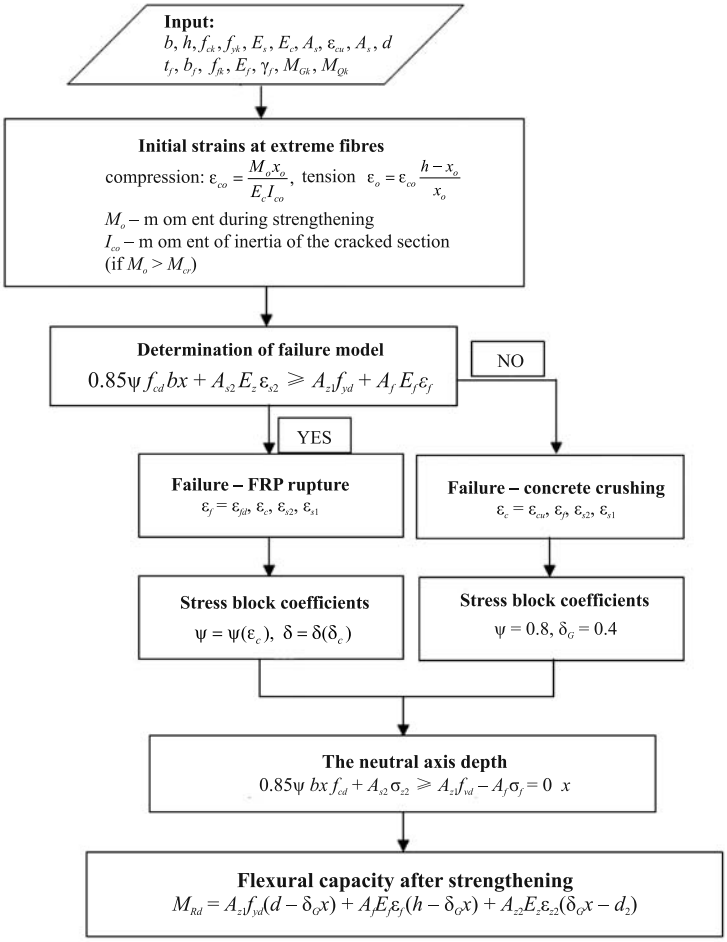

Fig. 5. *fib* Bulletin No. 14 design procedure flowchart

force that may be transferred from concrete to FRP material is evaluated with the specific fracture energy of the FRP-concrete interface is taken into account.

Then the determination of the failure mode is made, similar to the *fib* approach, however in Italian design codes, it is determined by comparing mechanical ratios: μ_s and μ_f – related to tension steel reinforcement and FRP system, respectively, with the balanced mechanical ratio μ_{f12}, calculated as follows (u is the ratio between compression and tension reinforcement area):

$$\mu_{f12} = \frac{0.8\,\varepsilon_{cu}\,\dfrac{h}{d}}{\varepsilon_{cu} + \varepsilon_{fd} + \varepsilon_0} - \mu_s (1 - u)$$

Once the failure mode is known, it is possible to evaluate the existing strains in concrete, FRP and steel reinforcement, determine the neutral axis depth and then calculate the flexural capacity (Fig. 6).

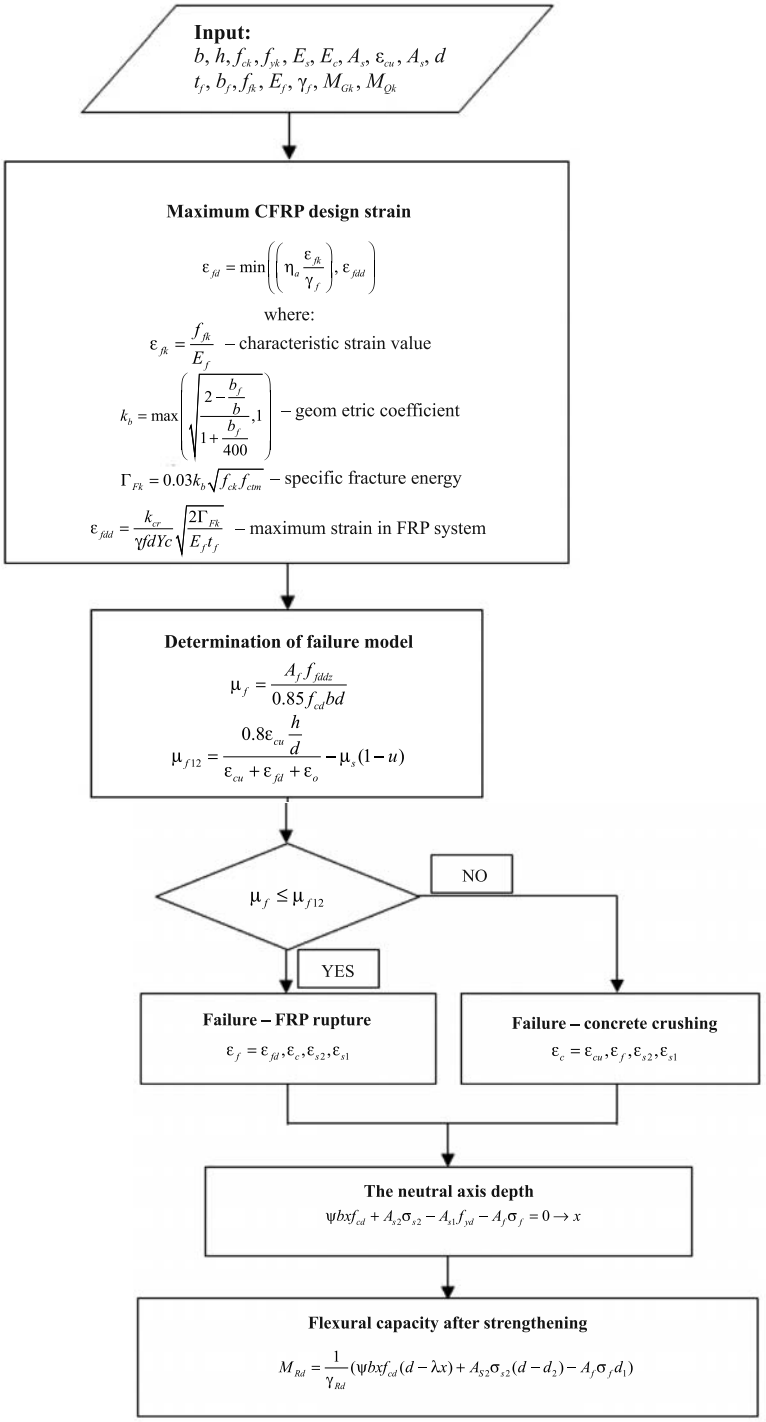

Fig. 6. CNR-DT 200/2004 design procedure flowchart

During the flexural capacity evaluation, the partial safety factor γ_{Rd} for resistance models is assumed as 1.0 (for bending), so there is no reduction of the final moment value, as it will be in case of shear, torsion strengthening or confinement (values of γ_{Rd} equal to 1.20 and 1.10, respectively) [N3].

3. Design example

3.1. Assumptions and the subject of analysis

A rectangular RC beam of height equal to 50 cm and width of 30 cm, with tensile reinforcement of 4 bars Φ = 16 mm was subjected to a simple comparative analysis. The assumed material parameters are as follows: concrete grade C30/37 and steel of tensile strength equal to 500 MPa. The beam was analysed as one, simple-supported, 5-metre long span.

The analysis was conducted in two steps. The first step was based on the determination of the load-bearing capacity of the beam according to each guideline, then loading was assumed to exceed the capacity in the middle cross-section of the beam span. The second step of the analysis was to determine an increase of capacity after strengthening the beam with the same CFRP strip.

3.2. Capacity and loading

Loading was the same for each case in the analysis, nevertheless there are differences in moment values. This issue is mainly due to various load partial safety factors for each of the considered guidelines (cf. Table 2).

Table 2

Total loading and maximum moment values for different guidelines

Guidelines & Combination scheme		Load safety factor	Loading (characteristic)	Loading (design)	Total loading (design)	Total moment (design)
		[–]	[kN/m]	[kN/m]	[kN/m]	[kNm]
ACI (1.4DL + 1.7LL)	DL	1.4	28.75	40.25	61.50	192.19
	LL	1.7	12.50	21.25		
FIB (1.35Gk + 1.5Qk)	Gk	1.35	28.75	38.81	57.56	179.88
	Qk	1.5	12.50	18.75		
CNR (1.4Gk + 1.5Qk)	Gk	1.4	28.75	40.25	59.00	184.38
	Qk	1.5	12.50	18.75		

The values of bending moment capacities were different in dependence on the guidelines, which is a result of various factors.

ACI318 [N1] defines no partial safety material coefficients as do FIB [N4] and CNR [N3], instead, a global strength reduction factor is determined dependent upon the character of cross-section work (flexure, compression, shear etc.). A slight difference also occurs in coefficients for rectangular shapes with regard to stress distribution – in ACI β_1 vary from 0.65 to 0.85, depending similarly on the concrete compressive strength. Furthermore, there is a difference in defining the modulus of elasticity of concrete E_c, which, according to ACI, is calculated in relation to concrete compressive strength and is distinctly lower.

Differences between the fib guidelines and CNR code are not major and they are mainly as a result of different partial safety material factors for concrete – γc = 1.6 for CNR and 1.5 for FIB.

All of these issues have an impact on the calculated capacities and caused the value for this beam according to ACI to be higher in comparison to FIB or CNR (cf. Table 3).

However, a set-up of calculated design capacities and the required capacity (due to the loading assumed above) proves that the deficiency of the bending moment capacity is approximately 20 per cent in each case, and the value for ACI is placed between those for FIB and CNR despite higher values of capacities calculated formerly.

Table 3

Total flexural capacities for different guidelines and values required due to loading

Guidelines	Capacity	Required capacity	Deficiency
	[kNm]	[kNm]	[%]
ACI	157.69	192.19	21.9
FIB	151.36	179.88	18.8
CNR	150.68	184.38	22.4

The second step of the conducted analysis was to determine the increase in capacity after strengthening the beam with a non-stressed, single CFRP strip.

- Assumed CFRP strip properties are: width – 80 mm,
- thickness – 1.2 mm (cross-section area – 96 mm^2),
- tensile strength – 3100 MPa,
- modulus of elasticity – 165 GPa.

The results of these calculations are presented in Table 4 and show that the value of capacity after strengthening was the highest according to FIB guidelines and caused an increase of 69.5% in comparison to ACI (25.3%) and CNR (16.5%).

The large difference between *fib* and the other guidelines is mainly due to not taking into account the assumptions of serviceability limit state (SLS) and verification of possible bond failure, which restrict maximum allowable FRP strains because of debonding failure mode (cf. p. 2.2). In ACI and CNR, this phenomenon is considered by various limiting factors included in the design procedures: κ_m (bond-dependent coefficient for flexure) in ACI and ε_{fdd} (maximum allowable strain in FRP system) in CNR.

Table 4

Flexural capacities after strengthening for different guidelines

Guidelines	Initial capacity	Capacity after strengthening	Strengthening ratio	Required capacity	*Is* strengthening sufficient?
	[kNm]	[kNm]	[%]	[kNm]	
ACI	157.69	197.62	25.3	192.19	YES
FIB	151.36	256.54 (210.38*)	69.5 (38.9%*)	179.88	YES
CNR	150.68	175.53	16.5	184.38	NO

Assuming that characteristic FRP strain limit value preventing from debonding is 0.85% instead of 1.7% alternative calculations were conducted and their results are presented in brackets in Table 4. A capacity of 210.38 kNm is obtained and a strengthening ratio is decreased to 38.9%.

Considering CNR results, strengthening was not sufficient for loadings assumed before, as obtained capacity does not exceed the required one. One of the possibilities for achieving the necessary capacity according to CNR is by using a wider strip – verification shows that a strip of width equal to 150 mm is sufficient (capacity raises to 186.31 kNm and strengthening ratio up to 24%).

4. Author's computer software

The author's program, which was written in the Delphi environment, allows for easy and fast checking of the conditions of the ultimate limit state for reinforced concrete elements with rectangular cross-section, strengthened with FRP strips for flexure (Fig. 7).

There is a possibility for the user to choose concrete grade from the list as well as to define material parameters manually; a similar situation occurs for FRP material characteristics. After determining the geometry of the element, reinforcement and materials calculations are made according to the *fib* procedure (as described in p. 2.2, of this article). The initial capacity and capacity after strengthening is evaluated.

A failure model is determined and illustrated with an appropriate graph of strains – real strains are calculated both in FRP strip and in concrete most compressed fibre and therefore ψ i δ coefficients are determined. It is necessary to give information about the bending moment during strengthening (for instance, in the case of possible partial unloading).

Finally, a strengthening ratio (defined as a ratio of the bending moment capacity after strengthening to the initial capacity) is calculated and presented (Fig. 8).

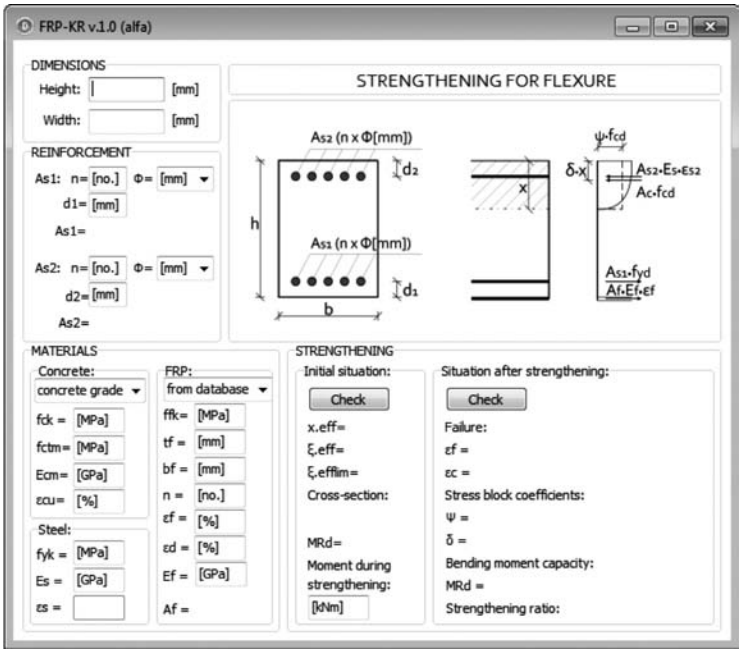

Fig. 7. Layout of the described program

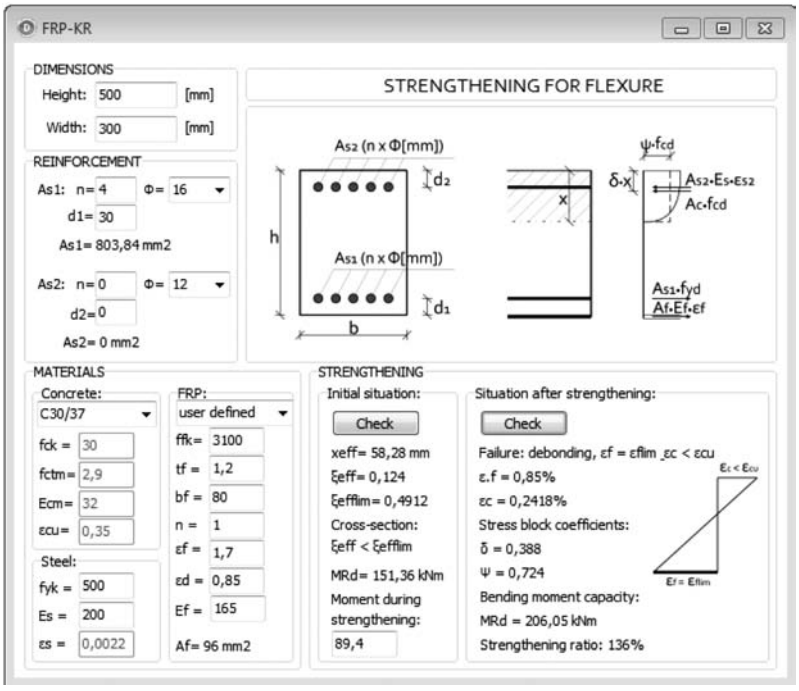

Fig. 8. Calculations and the way of presenting results

5. Conclusions

In Poland, there is no standard dedicated to strengthening reinforced concrete structures with FRP materials but, on the other hand, there are many different guidelines on this subject in the world, so it was necessary to perform a comparative analysis that will identify the most important differences between them.

This paper describes different design procedures for the flexural strengthening of reinforced concrete beams with FRP composite materials, however, only the ultimate limit state was taken into consideration. We analyzed the American and Italian standards as well as fib guidelines which, although are the oldest, are considered to be the basic document in many countries. It should be noted that in the analyzed strengthening technology, the issue of the debonding of the FRP laminate is essential. All the analyzed guidelines address this issue, but in different ways.

Comparing the results of performed calculations is not easy, because the final results are affected by a number of small differences in many factors. The highest initial bending moment capacity was obtained from the ACI318 [N1] design model. The main difference is due to a lack of partial material safety factors, which appear in Eurocodes, and an existence of the global strength reduction factor which decreases the value of the nominal bending moment.

Load partial safety factors are different in each set of guidelines, what contributes to different values of required strength although the same load values were assumed. The bending moment required by ACI is the highest, and values of moments obtained for CNR and FIB do not differ significantly.

The most conservative values of strengthened cross-section capacity were obtained for the CNR code, and the least from the fib recommendations.

Finally, the strengthening ratio (calculated as the ratio of the capacity increase to the initial capacity) differs significantly between three analysed approaches. It is mainly due to the lack of straight verification of debonding failure mode in the ULS fib procedure. In ACI and CNR, factors which aim is to prevent debonding, are included in the design ULS procedures, whereas in fib, these calculations are separate.

The article also presents the concept of the author's program for quick verification of bearing capacity for the bent RC cross-section strengthened with FRP laminates. For now, this is the start of work on a program for engineering use – it needs to be significantly expanded.

References

[N1] ACI 318-08, *Building Code Requirements for Structural Concrete and Commentary*, American Concrete Institute, USA 2008.

[N2] ACI 440, 2R-08, *Guide for the Design and Construction of Externally Bonded FRP Systems for Strengthening Concrete Structures*, American Concrete Institute, USA 2008.

[N3] CNR-DT 200/2004, *Guide for the Design and Construction of Externally Bonded FRP Systems for Strengthening Existing Structures*, National Research Council, Rome, Italy 2004.

[N4] fib Bulletin No. 14, Externally bonded FRP reinforcement for RC structures, Lausanne, Switzerland 2001.

[N5] Model Code 2010, Final Draft, March 2010, Lausanne, Switzerland.

[1] Balaguru P., Nanni A., Giancaspro J., *FRP Composites for Reinforced and Prestressed Concrete Structures*, Taylor&Francis, New York 2009.

[2] Bencardino F., Rizzuti L., Spadea G., *Strengthening/retrofitting of an RC structure with bonded CFRP laminates: reliability evaluation using different guidelines*, FRPRCS-8 Conference Materials, Patras 2007.

[3] Czaderski Ch., *Fibre Composite Materials in Structural Engineering – Flexural strengthening of reinforced concrete – Swiss Code 166 and other codes/guidelines*, ETH Lecture 101-0167-01L, EMPA, Switzerland 2012.

[4] Derkowski W., *Ultimate Limit State of the bent RC beams strengthened with FRP composites under static and fatigue load*, 4th International Conference "Analytical Models and New Concepts in Concrete and Masonry Structures", Kraków 2002.

[5] Hollaway L.C., Teng J.G., *Strengthening and Rehabilitation of Civil Infrastructures Using Fibre-Reinforced Polymer (FRP) Composites*, *CRC Press*, 2008.

[6] [6] Kotynia R., Kamińska M.E., *Ductility and failure mode of RC Beams Strengthened for Flexure with CFRP*, Experimental Researches of Concrete Members and Structures, Vol. 13, Wydawnictwo Katedry Budownictwa Betonowego Politechniki Łódzkiej, Łódz 2003 [in Polish].

[7] S&P Reinforcements *Technical Papers.*

TECHNICAL TRANSACTIONS | CZASOPISMO TECHNICZNE
CIVIL ENGINEERING | BUDOWNICTWO
2-B/2013

RAFAŁ SIEŃKO, TOMASZ HOWIACKI, SEBASTIAN JEDLIŃSKI*

DESIGN ERRORS RESULTING FROM THE ADOPTION OF AN INCORRECT MODEL OF A STRUCTURE

BŁĘDY PROJEKTOWE WYNIKAJĄCE Z PRZYJĘCIA NIEWŁAŚCIWEGO MODELU KONSTRUKCJI

Abstract

The paper presents the design errors resulting from the adoption of an incorrect model of a structure as an example of real tanks. In addition, based on our own numerical analysis of a football stadium, the paper shows the differences between results obtained from the three--dimensional model – and other, more simplified schemes.

Keywords: 3D model, tank, football stadium

Streszczenie

W artykule zaprezentowano błędy projektowe wynikające z niewłaściwego przyjęcia modelu konstrukcji na przykładzie rzeczywistych zbiorników. Ponadto w oparciu o własną analizę numeryczną stadionu piłkarskiego pokazano różnice w wynikach uzyskanych z modelu trójwymiarowego – oraz innych, bardziej uproszczonych schematów.

Słowa kluczowe: model 3D, zbiornik, stadion piłkarski

* Ph.D. Eng. Rafał Sieńko, Eng. Tomasz Howiacki, Eng. Sebastian Jedliński, Institute of Building Materials and Structures, The Civil Engineering Faculty, Cracow University of Technology.

1. Introduction – contemporary design tools

Construction is one of the oldest expressions of human rational activities. Since man gave up his nomadic way of life, he began to erect buildings using various materials. The art of construction has evolved over the years from simple mud huts to enormous, engineering facilities.

The development of sciences such as mathematics, strength of materials and last, but not least, the information technology revolution, have resulted in the creating of computer programs that use different types of numerical methods. This has created completely new possibilities for designers and made it possible to exceed barriers not even thought of in the past.

This software is commonly used today in the design process of complex facilities whose operation is typically spatial. It allows creation of three dimensional models where all components are involved in the load carrying process. Simplified 2D analysis can lead to significant over-dimensioning or, even worse, to inappropriate assessments of a structure's response.

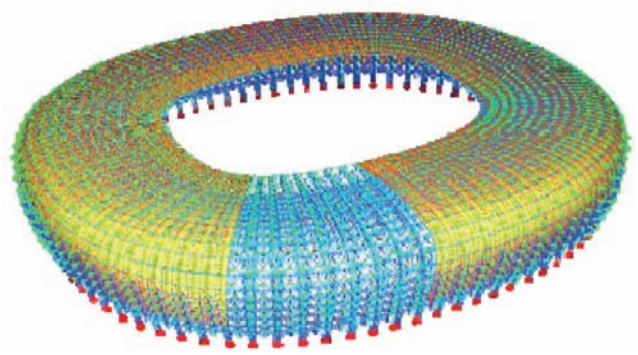

Fig. 1. Model of the structure of the stadium in Gdańsk – SOFiSTiK (5)

The contemporary, three-dimensional models (and 4D, used increasingly, which includes the time factor), in conjunction with the virtual reality technology, form a very important tool used not only in engineering practice, but also in the teaching process. They display in an intelligible manner, the features of the response of a structure. In the 21st century, access to specialised software is widespread, however, it should always be remembered that the use of software requires "the skills and knowledge to create economic and viable solutions"[1].

In the past, the massive character of a structure was a protection buffer for inaccurate models. The modern design has changed these relationships – advanced numerical models allow the design of light, simple and cost-effective facilities, consistent with Antoine de Saint-Exupéry's quotation: "The engineer knows that he has reached perfection not when there is nothing left to add, but when there is nothing left to remove".

[1] For more information, see (1).

2. Errors in the conical model of a reinforced concrete fermentation chamber ZKF roofing [2]

The structure and size of the tank is shown in Fig. 2. The roofing is in the form of a truncated cone, which consists of 44 prefabricated, reinforced concrete hollow-core rib plates, connected to each other with spandrel beams. The continuity of the circumferential reinforcement is provided by welded rods connection in the spandrels, while the L-shaped Ø6 reinforcement every 20 cm, connects the spandrel beam with the prefabricated element ribs (Fig. 3). At the top of the cone, there is a cross-reinforced concrete monolithic slab with a 50 cm thickness and a diameter of 6 m. The roofing is connected with the cylindrical shell by means of a circumferential ring.

As a result of biogas explosion, the tank suffered much damage and was out of operation. The damage observed included disruption of the connection between the prefabricated element ribs and the concrete topping. Moreover, the connection between the roofing and the cylindrical shell at the height of the ring was torn. Also, the ring was locally torn and displaced outwards along the plane of the connection with cylindrical shell (Fig. 4), the top plate was cracked along the perimeter and the cylindrical shell was cracked vertically beneath the ring.

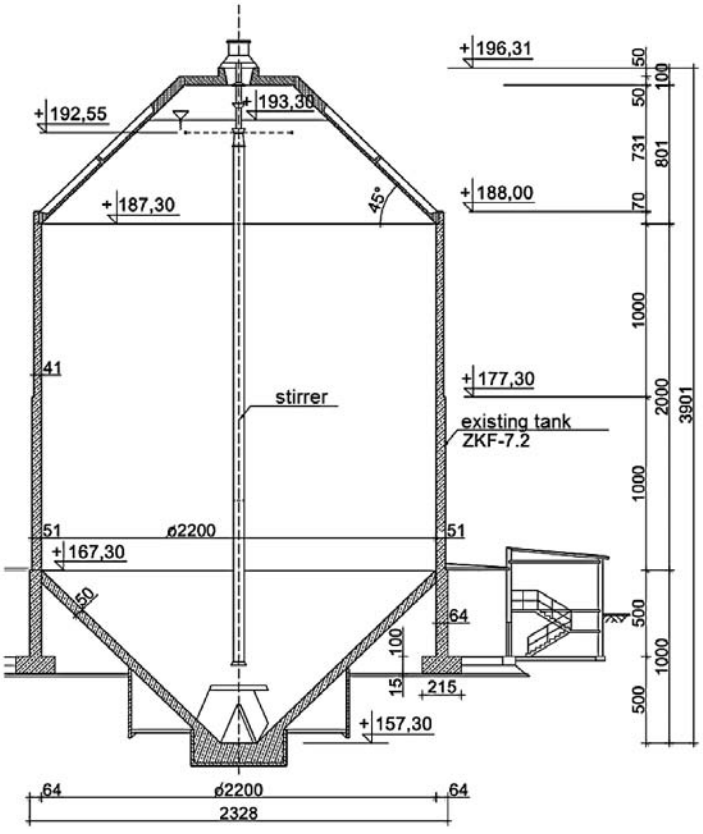

Fig. 2. Cross-sectional view of the tank (2)

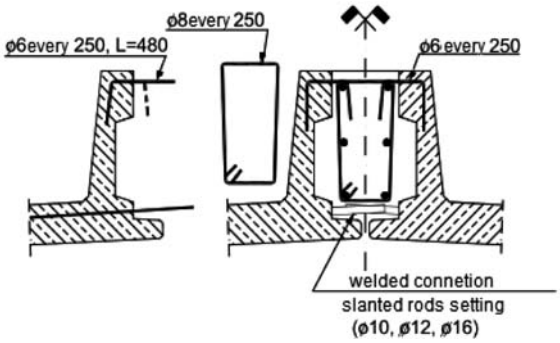

Fig. 3. Detail of the prefabricated elements connection (2)

One of the main causes of the extensive damages was the errors at the design stage – in creating the calculation model, to be more precise. After the roofing elements were made monolithic, a radial-wise ribbed coating with a thickness of 12 cm (rib height 55 cm) was created. Probably such a shape of the structure made the designers render the operation of the cone with vertical frames loaded with wastewater pressure. The consequence of this assumption was considering the shell spatial work only in the meridional direction, while disregarding completely the direction of the parallel.

In this direction, the reinforcement was determined for a scheme of a unidirectional slab supported on ribs and loaded with wastewater pressure at a variable level. The circumferential connections, as shown in Fig. 3, were the weakest link of the roofing structure. The effect was that they were damaged already in the initial phase of use, with a minimum overload (3% of the working load).

Fig. 4. Morphology of damages on the top of the tank (2)

The example discussed above shows how a lack of understanding of the work of a structure and the resulting adoption of its simplified model (two-dimensional frames), may lead to a structural disaster.

3. Errors in the model of a double-chamber reinforced concrete phosphorus tank (3)

Another example of a structure whose failure was caused by errors at the design stage is an underground double-chamber phosphorus storage tank, insulated with a 10-cm Styrofoam layer. Its geometry is shown in Fig. 5.

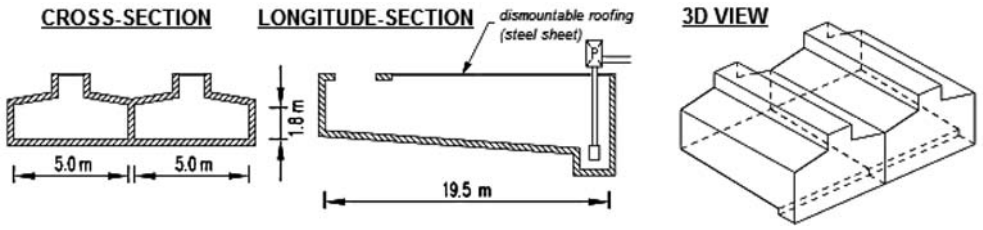

Fig. 5. Geometry of the analysed tank (3)

The phosphorus storage technology requires a water seal, with a water temperature of approx. 90°. The diagram of such a water seal has been shown in Fig. 6. Disregarding the thermal load was a fundamental error in the design documentation. In addition, certain technological loads were not taken into account, subsoil was not examined, and an incorrect structural model was adopted, which did not represent the actual spatial work of the tank.

The individual walls of the structure were treated as separate, bent beams, with no axial forces. The adopted model is shown below.

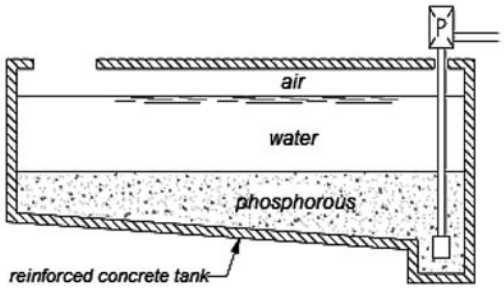

Fig. 6. Water seal diagram (3)

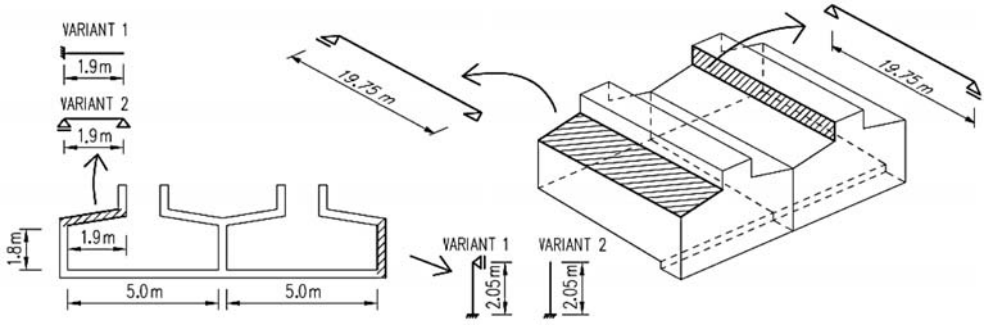

Fig. 7. Static diagrams included in the tank design (3)

4. Errors in the model of a three-chamber reinforced concrete tank in a wastewater treatment plant (4)

The reinforced concrete sewage tank consists of three chambers: one main and two smaller ones, the dimensions of which are presented in the diagram of tank structure (Fig. 8). The tank height is 4.15 m (calculated from the top surface of the bottom slab). The thickness of the foundation slab is 40 cm, and the thickness of the external walls is 30 cm. Tank walls were reinforced with Ø14 mm mesh every 30 cm in the parallel and meridional directions, which in combination with the foundation slab, was condensed (Ø14 mm every 15 cm).

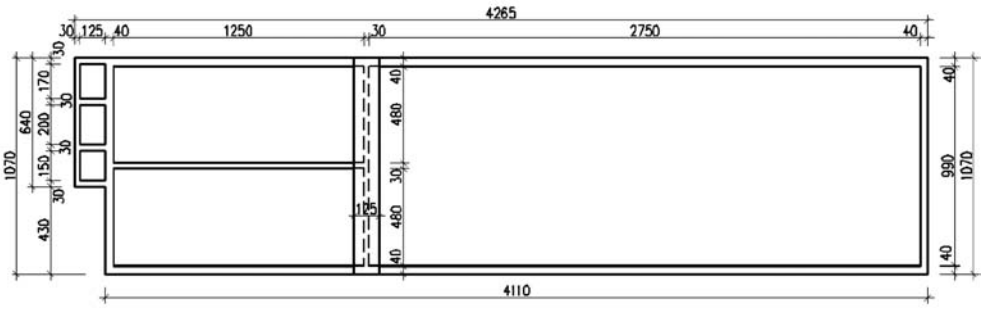

Fig. 8. Tank diagram – tank projection from the top (4)

The main reason for the tank to fail was the adoption of simplified static diagrams, the omission of the axial forces occurring in the walls, and the omission of temperature effects. The cumulative effect of the errors was that the actual work of the tank structure was not modelled.

5. Differences in the results of two- and three-dimensional analyses based on the example of the football stadium model

The examples given in the section below clearly show what errors can result from oversimplifications of a model. The results of the two-dimensional analysis were compared with those obtained from a three-dimensional model. The discussed object is a football stadium, the numerical analysis of which was performed in the SOFiSTiK environment.

5.1. The boundary conditions adopted

For simple structures, a virtual cut-out of an individual structural element (e.g. a beam) and assignment of boundary conditions consistent with the classical mechanics, i.e. fixed or hinged, in general, does not lead to significant errors.

For complex spatial structures, however, verification of the actual support conditions plays a very important role since the nature of the element's work is no longer so obvious.

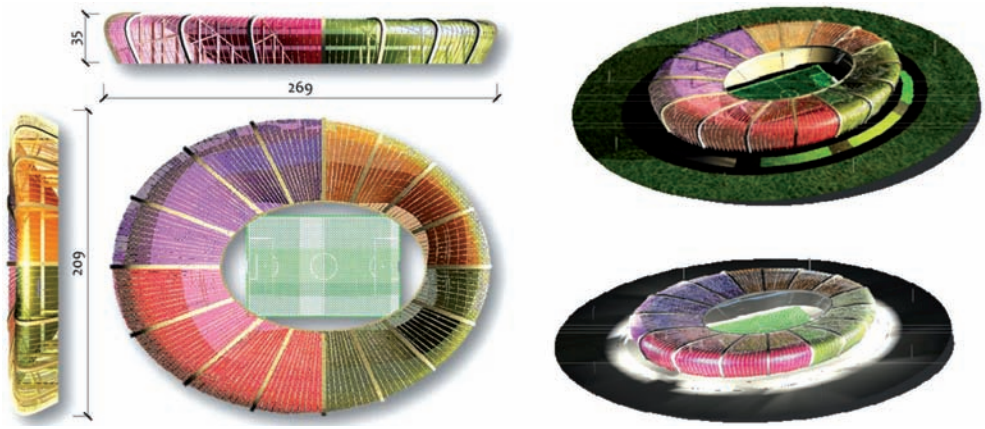

Fig. 9. Size of football stadium and its visualisation (done by the authors)

Below an example of a two-span beam as a binding joist of the third floor of the stadium is given.

In different models, the functions of bending moments, resulting solely from the dead weight of the entire structural system, were analysed. For one-dimensional models, it is impossible to determine the impact of the remaining part of the structure on the beam. This is because spans are not directly loaded, and the interaction between components is transmitted through the nodes. Numerical analysis of the question leads to interesting conclusions.

Fig. 10. Models of the beam support: hinged, fixed, monolithic in 2D frame, monolithic in 3D skeleton arrangement

The 2D frame model changed the nature of the supports at the beam-ends due to different levels of stiffness of the elements connected in the node. The first support behaves in a similar way to the hinge; the second one is similar to the fixed support. However, the respective moment is over 30% greater than the fixing moment of the one-dimensional analysis. Such a result, without taking into account the impact of deformation, would not be possible. In the 3D model, the moments changed not only quantitatively, but also qualitatively – stretching of lower fibres occurred in the first node. The omission of this fact in the calculation is, of course, unacceptable. In addition, over the centre support the value of the bending moment increased by over 35% compared with the 2D analysis and up to 70% compared with the 1D analysis with the supports.

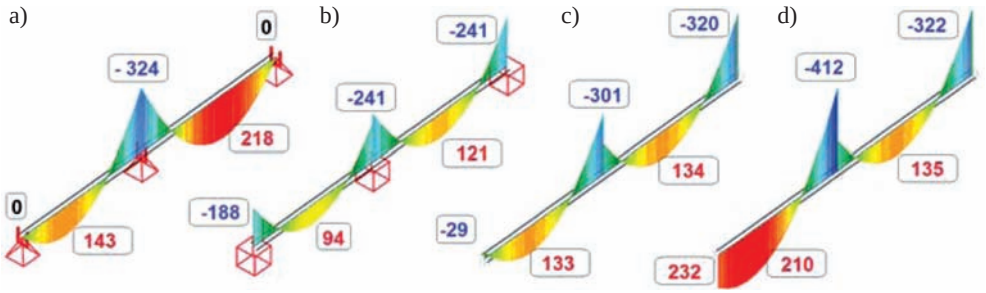

Fig. 11. Bending moments (kNm) for different support conditions: (a) hinged (b) fixed (c) monolithic in the 2D frame (d) monolithic in the 3D skeleton arrangement

This brief analysis leads to a simple conclusion – classic simplifications for complex engineering systems may lead to a qualitatively incorrect assessment of the structural response.

5.2. Work of a structure as a shell

The next issue is the bending analysis of the structure of the stadium with respect to the nature of roofing work as a shell. In the presented object, the elements can have spans of several dozen metres only when the interactions between the spatial girders, ring, and shell have been taken into account.

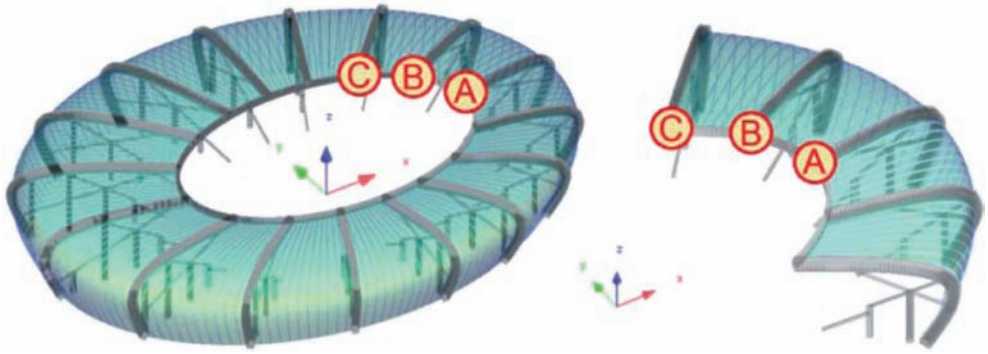

Fig. 12. Three-dimensional model of the total shell and of a part of it

Of course, it is possible to cut out a single 2D frame from the structure, or even an entire section of the structure (as in the figure above) and calculate the displacements using the program. However, such an approach wrongly assumes that girders are operating as cantilevers. In fact, the structure under dead load and other loads, works as a shell ribbed in two directions. The deflections are affected by the stiffness of the roofing structure in the longitudinal direction (perpendicular to the girders axis). To render this phenomenon as close as possible to the actual response of the structure, a three-dimensional model needs to

be used. In our case, even a simplified model (peripheral stiffness ensured only by the shell) showed that the actual deflections are reduced by about 20% from those obtained with the support model.

Table 1

Deflections for the discussed models calculated using the SOFiSTiK (mm) program

point	direction	deflections in the complete configuration	deflections in the fragmentary configuration	change %
A	z	–87	–102	17.2
B	z	–102	–118	15.7
C	z	–92	–114	23.9

5.3. Two- or the three-dimensional space

To perform a 2D analysis, the engineer must have greater experience and intuition because it is essential to adopt certain assumptions. When discussing the frame, the question of the connection of the girder with the compressed circumferential ring arises. From among many possibilities, partial fixing was adopted, which allows a vertical displacement, but at the same time induces bending moments. Loading with a shell (the steel truss) was assumed to be as evenly distributed over the girder length, and the weight of the ring was modelled by a concentrated force. In case of the 3D model, simplifying assumptions described above were not made.

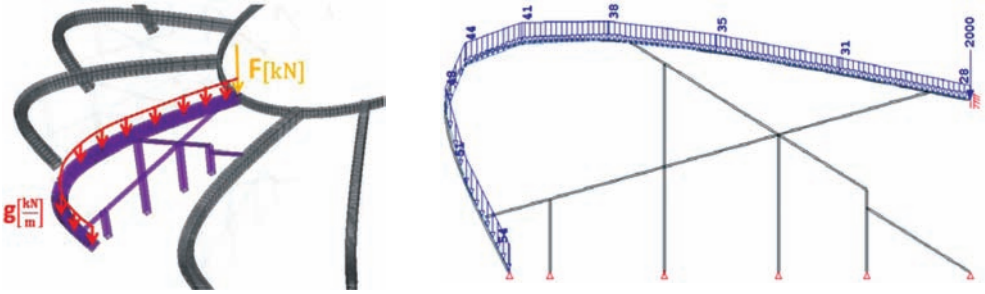

Fig. 13. Static 2D frame diagram

Numerical analysis results showed over-dimensioning of the structure's elements in 2D analysis, i.e. the values obtained for the cross-sectional forces of the presented example are on average 20% higher in the 2D than in the 3D model. This is due to the fact that the three-dimensional object has a spatial stiffness, which is not available when 2D frames are chosen for modelling.

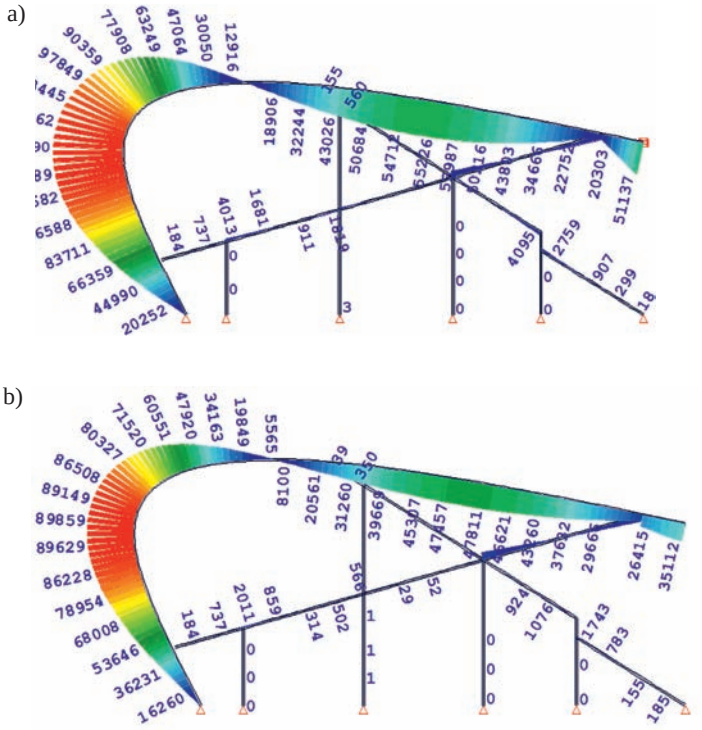

Fig. 14. Bending moments (kNm): a) from 2D analysis; b) from 3D analysis

5.4. The rod or shell model

The awareness of the need for the 3D design of building facilities has become increasingly common, which is proved by an increasing number of programs to model structures in such environments. In some cases, applying models that involve only spatial features of the geometry of objects is not enough. It is often necessary to replace rod models with the solid or shell models. Such analyses are most frequently performed for nodes and points of application of major concentrated loads. To illustrate the problem, simple diagrams present the results obtained from the solution of two models – rod and shell models. The effects of the two models as deformations are shown in the same scale.

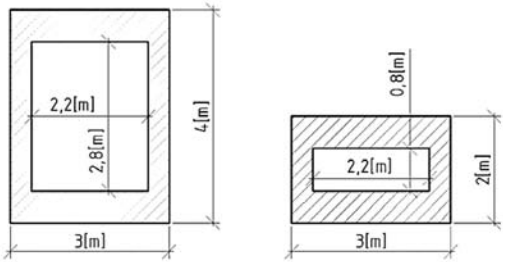

Fig. 15. Cross-section of the girders at the base and at the top

The analysis of the shell model showed that in the connection area, there is a stress state in the girder which cannot be determined on the rod model.

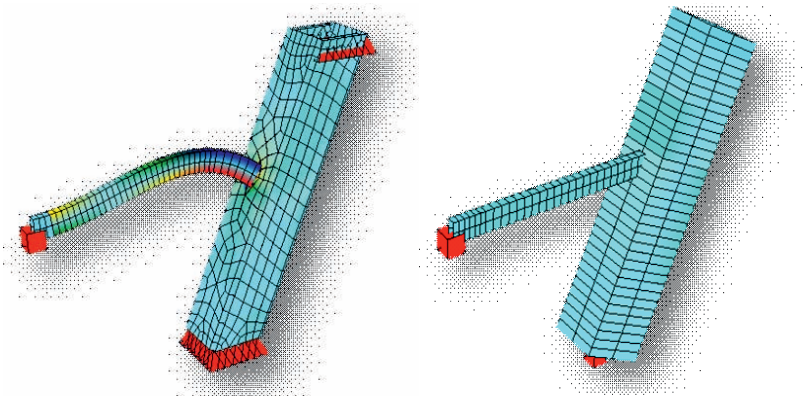

Fig. 15. On the left: the shell model of the girder; on the right: the rod model of the girder

6. Conclusions

The article presents examples of errors made in the assessment of a structure's work. These errors, resulting from the adoption of an incorrect model, show how important it is to realistically model the actual behaviour of structures. The complexity of the facilities designed nowadays very often makes the adoption of simple models that involve a number of simplifying assumptions which are inadequate. This may effect in incorrect quantitatively, and sometimes also qualitatively, assessment of the structure's work. Creating structural models requires the designer's significant experience and a proper understanding of the performance of a structure. Unfortunately, even the most complex three-dimensional model, if based on incorrect assumptions, will result in an incorrect structural solution.

In the article, only elastic models of structures were analysed, models taking into account other physical laws, crack formation in reinforced concrete structures, or concrete creep omitted deliberately. Taking into account these material properties would render an unambiguous assessment of the errors resulting from specific models difficult.

References

[1] Sampaio l.Z.,. Cruz C.O., Martins O.P., *Didactic Models in Civil Engineering Education: Virtual Simulation of Construction Works*, Technical University of Lisbon, Dep. Civil Engineering and Architecture, Lisbon.

[2] Dyduch K., Płachecki M., Sieńko R., *Odbudowa zniszczonego wybuchem biogazu stożkowego przekrycia żelbetowej komory fermentacyjnej ZKF*, XXIV Konferencja Naukowa „Awarie Budowlane", Szczecin–Międzyzdroje 2009.

[3] Łukacz M., Płachecki M., *Awaria dwukomorowego żelbetowego zbiornika spowodowana oddziaływaniami termicznymi*, XXV Konferencja Naukowa „Awarie Budowlane", Szczecin–Międzyzdroje 2011.
[4] Płachecki M., Koziński K., *Błędy projektowe i wady wykonawcze oraz projekt i realizacja wzmocnienia trójkomorowego żelbetowego zbiornika w oczyszczalni ścieków*, XXV Konferencja Naukowa „Awarie Budowlane", Szczecin–Międzyzdroje 2011.
[5] *Stadion PGE Arena – BURSZTYN Z GDAŃSKA*, Świat Architektury 8(15)/2011.

TECHNICAL TRANSACTIONS | CZASOPISMO TECHNICZNE
CIVIL ENGINEERING | BUDOWNICTWO
2-B/2013

BOGUMIŁ WRANA, WOJCIECH KALISZ, MIKOŁAJ WAWRZONEK*

NONLINEAR ANALYSIS OF PILE DISPLACEMENT USING THE FINITE ELEMENT METHOD

NIELINIOWA ANALIZA OBCIĄŻENIE–PRZEMIESZCZENIE PALA W UJĘCIU MES

Abstract

The objective of this paper is a nonlinear analysis of the displacement pile using the finite element method. The results of computer simulation are compared with the *in-situ* test of static load. The authors made an attempt to check this process in order to verify applied computer models in terms of consistency of results. In FEM simulation there are used: actual models of constitutive relations; forming an appropriate geometry; initial and boundary conditions and area discretization of finite elements mesh. The paper is of theoretical character with the results of numerical analysis of pile displacement. Numerical calculations carried out by the authors in this study were conducted using ABAQUS package, which is used for solving problems in soil mechanics.

Keywords: Soil mechanics, computer modelling, finite element method, constitutive soil models

Streszczenie

Artykuł poświęcony jest zagadnieniu nieliniowej analizy osiadania pala w gruncie uwarstwionym pod obciążeniem charakterystycznym od budowli. Przedstawiono problemy odpowiedniego doboru modeli konstytutywnych gruntu, posługując się systemem metody elementów skończonych ABAQUS. Parametry warstw gruntu zostały pomierzone *in-situ* przy zastosowaniu sondy statycznej CPTU i na tej podstawie przyjęto stałe materiałowe modeli teorii plastyczności zastosowanych do opisu równań konstytutywnych. Geometrię warstw gruntu wprowadzono na podstawie przekrojów geotechnicznych. Artykuł ma charakter zarówno teoretyczny (przez dyskusję równań konstytutywnych), jak i praktyczny (przez porównanie wyników symulacji z wynikami testu statycznej nośności pala).

Słowa kluczowe: Mechanika gruntów, metoda elementów skończonych, równania konstytutywne gruntu

* Ph.D. Eng. Bogumił Wrana, prof. PK; Eng. Wojciech Kalisz; Eng. Mikołaj Wawrzonek, Institute of Structural Mechanics, Faculty of Civil Engineering, Cracow University of Technology.

1. Introduction

Pile foundations are widely used in engineering practice. In the traditional approach, the designing of pile foundations consists in checking the limit states. It is fundamental to recognize a soil structure and gain knowledge of a real interaction of the pile that transfers the load with the surrounding soil. Eurocode 7 and the PN-83/B-02482 standard recommend to apply test static load to assess bearing capacity of piles and pile foundations. Currently, an alternative way to discover and understand complex processes in the soil environment are computer simulations. However, this requires a precise description of the area geometry and the adoption of advanced models of materials and load. It is important here to compare a numerical solution with the results obtained in in-situ tests.

In the object analysed in the paper the pile foundations made in the CFA technology were used. It is one of the most popular technologies in Poland.

2. Constitutive models

Constitutive soil models are sets of equations representing the relationship between the stress and strain tensor. Constitutive relations should reproduce the complexity of the soil environment, which consists of three-phase soil property, strong nonlinearity, anisotropy, plastic strengthening and weakening, dilatancy, variable compressibility factor and many more. In this paper, the authors present constitutive models available in the ABAQUS software.

2.1. The Mohr-Coulomb model

The Mohr-Coulomb model (MC) represents the linear envelope of the dependence of normal stress σ from shear stress σ, determining the shear strength. The Mohr Coulomb plasticity condition can be written as an equation describing the six planes forming a distinctive pyramid in the principal stresses space.

$$F = \frac{1}{2}(\sigma_{max} - \sigma_{min}) + \frac{1}{2}(\sigma_{max} + \sigma_{min})\sin(\phi) - c \cdot \cos(\phi) \tag{2.1}$$

where:

σ_{max} – maximum compressive stresses,
σ_{min} – minimum compressive stresses.

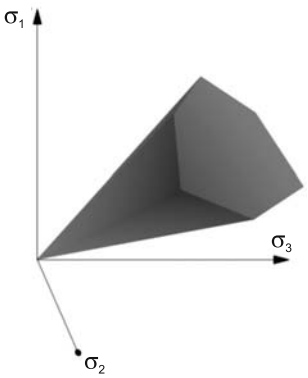

Fig. 1. The MC criterion in the space of stress principal components

2.2. The Drucker–Prager model

The Drucker–Prager model (DP) surface is a cone in the space of the principal stresses, it has a smooth shape on the octahedral plane.

The linear equation of plasticity function:

$$F = t - p \cdot \mathrm{tg}(\beta) - d = 0 \tag{2.2}$$

where:

β – an angle indirectly related to the angle of internal friction – it can be determined experimentally or by the equation relating it to φ:

$$\mathrm{tg}(\beta) = \frac{3 \cdot \sqrt{3} \cdot \mathrm{tg}(\phi)}{\sqrt{9 + 12 \cdot \mathrm{tg}^2(\phi)}} \tag{2.3}$$

d – parameter includes the cohesion c and internal friction φ given by

$$d = \frac{3 \cdot \sqrt{3} \cdot c}{\sqrt{9 + 12 \cdot \mathrm{tg}^2(\varphi)}} \tag{2.4}$$

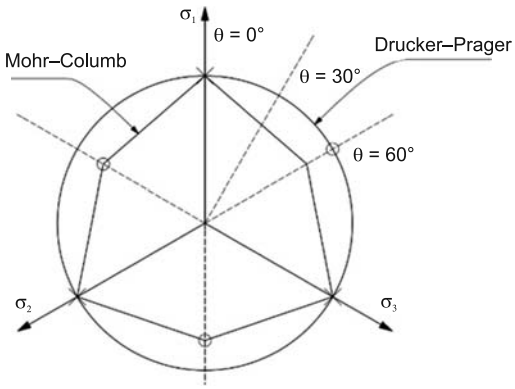

Fig. 2. The Lode angle Θ on the deviatoric plane (p = const) and directions of triaxial compression and tension

3. Soil modelling – FEM formulation

Soil is a porous material with a complex structure – a skeleton (for mineral grains or organic particles) and a space filled with air and/or water (or other liquid). Soils are modelled as a single-, two- or three-phase materials depending on the volume ratio of the skeleton, air or water in the pores. The single phase model maps the soil as a mixture with mechanical and physical parameters at each point of the area. The two-phase model is used for solving problems related to fully saturated soils or the case of dry soils. To analyse the issues presented in this paper, the authors took into account the two-phase property of the soil environment.

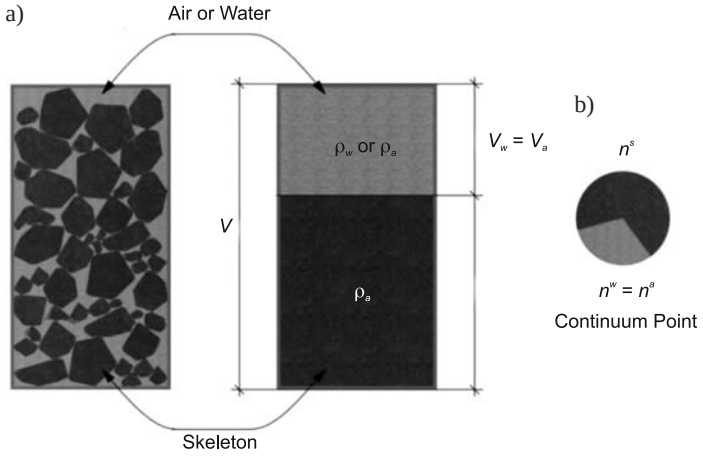

Fig. 3a) The two-phase model of soil, $n^s + n^w = 1$ (air or water and skeleton), b) Continuum point

Using the finite element simulation of displacement pile requires application of appropriate modelling of pile elements interactions with the surrounding soil. In computer simulation one can use: the case without a contact (the soil elements and adjacent pile elements are forced to move together) or the case with a contact. The main advantages of using the contact are: 1) frictional behaviour of a pile with soil is fully represented in the model; 2) different movements of the pile elements and soil (slip) are possible. It should be noted that pile elements are relatively rigid to the surrounding soil deformations. The surface of pile elements that are in contact with the soil elements is referred to as the main surface (*master*). The surface of the soil elements in contact is set as the secondary surface (*slave*). In the ABAQUS program these surfaces are called *contact pairs*. The contact pair representing the interaction of a pile with the soil is shown in Fig. 3.

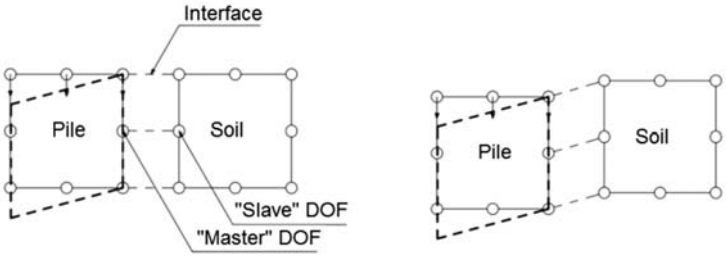

Fig. 4. The contact pair scheme in ABAQUS

The contact behaviour of the two surfaces is determined by the Coulomb law of sliding friction. The Coulomb model of friction applies to the maximum allowable friction (shear), including the normal stress at the interface between the two surfaces.

The force of sliding friction between two bodies is proportional to the normal component of the force, keeping bodies in contact as given by the formula:

$$\tau_{crit} = \mu\, p \tag{3.1}$$

where:

τ_{crit} – the critical shear stress on the interface,
μ – the friction coefficient,
p – normal component of the stress between the two surfaces.

If the frictional stress balances the tangential stress, it is a condition called “gluing”.

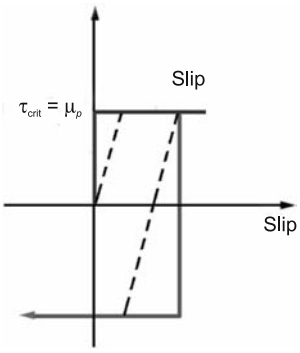

Fig. 5. The Coulomb model of friction

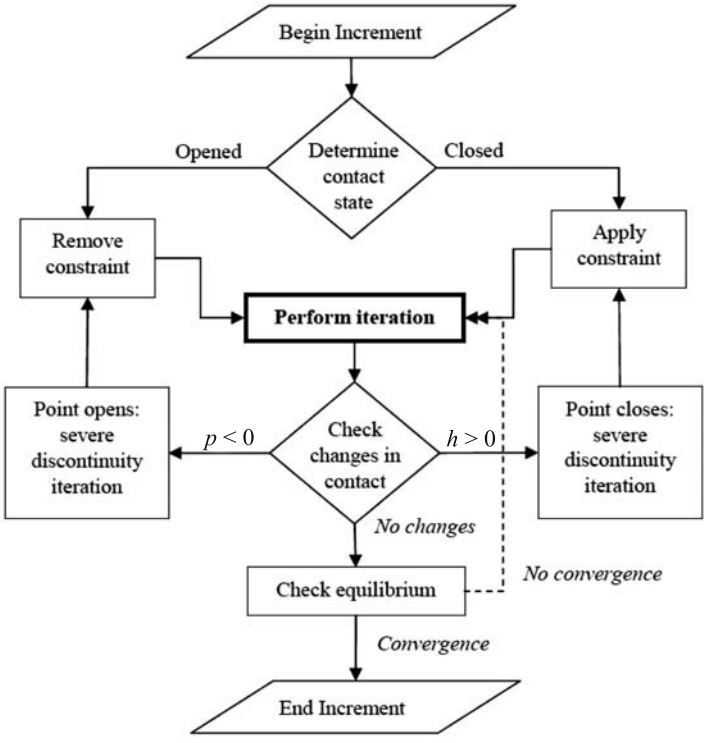

Fig. 6. The master-slave contact algorithm in ABAQUS

The contact algorithm implemented in the ABAQUS program can be summarized as follows:

1. Determination of the condition of all contact interactions by checking whether each slave node (slave) is "open" (the distance from the master node is greater than zero) or "close" (the distance is equal to zero) at the beginning of each increment.
2. The imposition of a restriction for each closed slave node, while it is still closed or removing the restriction, if the contact status of the node changes from closed to opened; determination whether a closed node is glued or slipping.
3. Contact calculating conditions are provided by iteration in each slave node up to limits control. Having updated the condition of contacts, a check of forces and/or moments balance for this increase is made.
4. Checking the pressure p and distance h in each slave node. If the pressure is negative after the iteration, the status of the contact in this slave node is changed from "closed" to "opened". On the other hand, if the pressure is negative and the distance from the master node after the iteration is zero, the contact of each node is changed from "opened" to "closed". In both cases, the condition is specified as a "severe discontinuity iteration" and the balance is not checked.
5. Updating a contact reduction after the first iteration – repeating the iteration procedure until there are changes in the contact condition.

4. The geometry model

Modelling of soil environment in terms of FEM includes mapping the actual state by adopting selected constitutive relations, creation of the appropriate geometry, boundary conditions. The theoretical soil area is unlimited half-space. The authors decided to apply the standard approach – the model with finite dimensions.

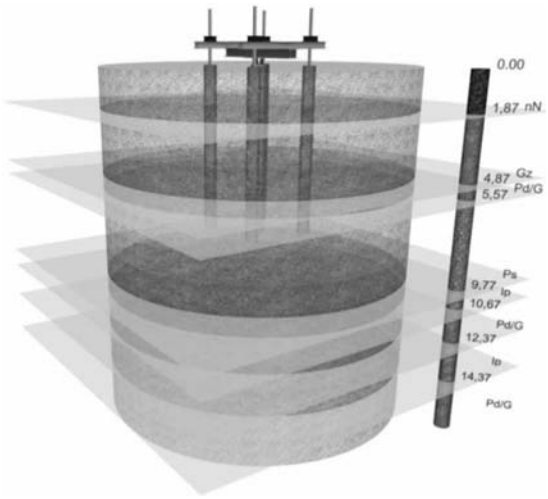

Fig. 7. The physical model of a pile

Due to the location of anchor piles at a distance of 2.75 m from the axis of the loaded pile, the authors ignored their impact in the numerical model. ABAQUS computing system was applied as an axisymmetric model of a cylindrical pile with a diameter of 0.75 m and a length of 8 m. The radius of the soil area was adopted as 8 m (length of the pile) and the model height was 16.83 m (two times greater than the length of the pile) on the basis of a test borehole. Symmetry conditions allowed modelling of a half section of the pile and surrounding soil.

The finite element grid was formed with 1025 elements. The pile was modelled using axisymmetric CAX4R type elements (4-*nodal bilinear axisymmetric quadrilateral*) while the soil by CAX4P type elements (4-*nodal axisymmetric quadrilateral, bilinear displacement*, *bilinear pore pressure*). These elements are available in the library of ABAQUS/Standard elements. The contact between the pile and the soil was modelled using the *master-slave* contact. The coefficient of friction $\mu = tg\phi = 0.39$ was adopted for an average value of the angle ϕ of soil layers.

5. The material model

The elastic coefficients were chosen on the basis of the PN-81/B03020 standard and geotechnical tests.

Table 1

Elastic parameters of soils

Soil	Oedometric modulus of elasticity, *M* [MPa]	Modulus of elasticity, *E* [MPa]	Poisson's ratio *v*
Ne (non-building fill)	33.5	25.1	0.3
Cc (compact clay)	34	23.7	0.32
Fs/Cl (fine sand/clay)	60	44.5	0.3
Ms (medium sand)	130	104	0.27
Sl (sand loam)	18	10.2	0.37
Fs/Cl (fine sand/clay)	60	44.5	0.3
Sl (sand loam)	18	10.2	0.37
Fs/Cl (fine sand/clay)	60	44.5	0.3

The values of oedometric modulus of elasticity were chosen from PN-81/B03020 standard on the basis of geotechnical tests. Due to the nature of the applied load, the authors decided to use the initial value. The Poisson's ratio has been chosen on the basis of Table 3 of the PN-81/B03020 standard. The modulus of elasticity was calculated using the formula:

$$E = M\frac{(1+\nu)\cdot(1-2\nu)}{(1-\nu)} \tag{5.1}$$

Volume weights of individual soil layers have been adopted on the basis of the PN-81/B03020.

Using the Mohr–Coulomb model, the authors selected the coefficients listed in Table 2.

Table 2

Plastic coefficients of the Mohr-Coulomb model

Soil	ϕ [°]	*c* [kPa]	ψ [°]
Ne (non-building fill)	15	0	0
Cc (compact clay)	10	11.3	0
Fs/Cl (fine sand/clay)	30.3	0	0.3
Ms (medium sand)	34.2	0	4.2
Sl (sand loam)	12.4	50	0
Fs/Cl (fine sand/clay)	30.3	0	0.3
Sl (sand loam)	12.4	50	0
Fs/Cl (fine sand/clay)	30.3	0	0.3

The angle of internal friction and cohesion were selected on the basis of the PN-81/B03020. The angle of dilatancy has been chosen according to literature. For the application of the Drucker–Prager model, the coefficients given in Table 3 were used.

Table 3

Plastic coefficients of the Drucker–Prager model

Soil	β [°]	*d* [kPa]	ψ [°]
Ne (non-building embankment)	24	0	0
Cc (compact clay)	17	19	0
Fs/C (fine sand/clay)	40	0	0.3
Ms (medium sand)	43	0	4.2
Sl (sand loam)	20	84	0
Fs/C (fine sand/clay)	40	0	0.3
Sl (sand loam)	20	84	0
Fs/C (fine sand/clay)	40	0	0.3

6. The load model

The analysis was divided into five steps. The GEOSTATIC step, CONSOLIDATION steps, mapping the process of loading and unloading of the pile during the test. In the GEOSTATIC step, for all elements in the model, the dead load was applied by the gravitational acceleration equal to $g = 9.81\frac{\mathrm{m}}{\mathrm{s}^2}$ using an automatic scheme of time increment under small deformation conditions. The first time step (initial time) was: $t_i = 1 \cdot 10^{-1}$ with the total duration of $t = 1$. Automatic increment was used in the analysis for time steps from the range: $\Delta t_{min} = 1 \cdot 10^{-5}$and $\Delta t_{max} = 1$. Water pressure changes in the pores at any increment are set using the UTOL option. If the maximum change in the pore water pressure at any node is greater than the predetermined tolerance, the increment is repeated with the proportional reduction of the time step. Otherwise, the time step increases. The total time of steps (2–5) SOILS, CONSOLIDATION is $t = 770$ min according to the actual time of sample testing of the pile. The pile was loaded with the concentrated force of a value1085 kN applied to the pile head, scaled in the following steps of the analysis according to the diagram.

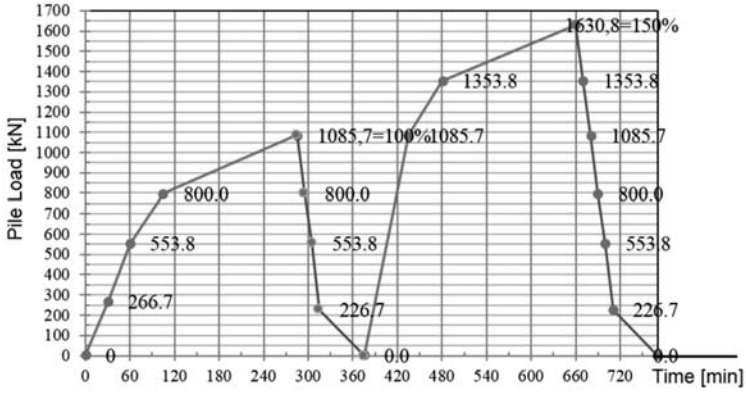

Fig. 8. The load range in the following steps of the analysis

In step 2 the pile is loaded to 100% of its bearing capacity of ULS. In step 3 the pile is unloaded from 100% to 0% of a value at the time $t = 90$ min. The total duration of step 3 is $t = 375$ min.

In the next step, the pile is re-loaded to 150% at the time $t = 285$ min The total duration after step 3 is $t = 660$ min

In the last step, the force value drops to 0% at the time $t = 770$ min.

7. Results of the analysis

The results of the numerical analysis of two constitutive models (MC and DP) are presented with the field tests results.

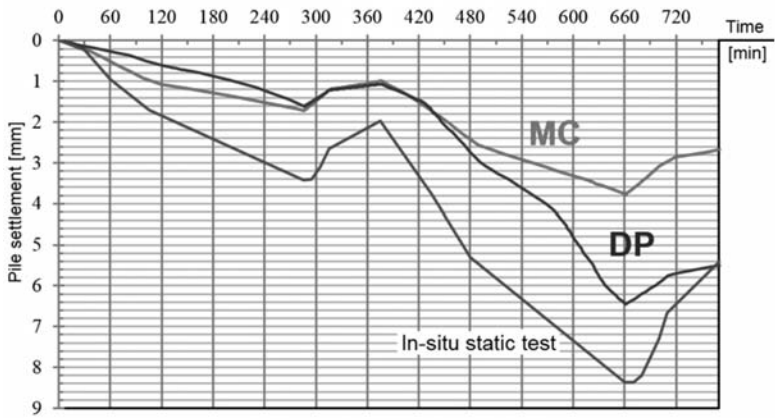

Fig. 9. Comparison of displacements

Fig. 9. presents the results of the two computer models and the in-situ static test results. It should be noted that the shape of the graph for the MC model is similar to the shape of actual displacements. The differences result from:

– the application of constitutive models,
– incorrect selection of soil parameters resulting from errors and inaccuracies in geological studies – these parameters should be calibrated using e.g. an inverse method,
– approximate description of geological strata due to a certain distance of the test pile from a geological surveys borehole,
– adopted average value $\mu = tg\phi$ over the length of the pile.

The plot shown in Fig. 10. representing the comparison of the results for the DP model shows displacements very similar to the real values – in step 4 (150%) for the DP model the displacements reach a maximum value of 6.45 mm compared to 8.37 mm found in the in-situ tests. After the last step of the analysis, the permanent displacements are equal to 5.49 mm for DP, while they are 5.41 mm in the in-situ tests. However, the shape of the graph shows different behaviour in comparison to the actual tests.

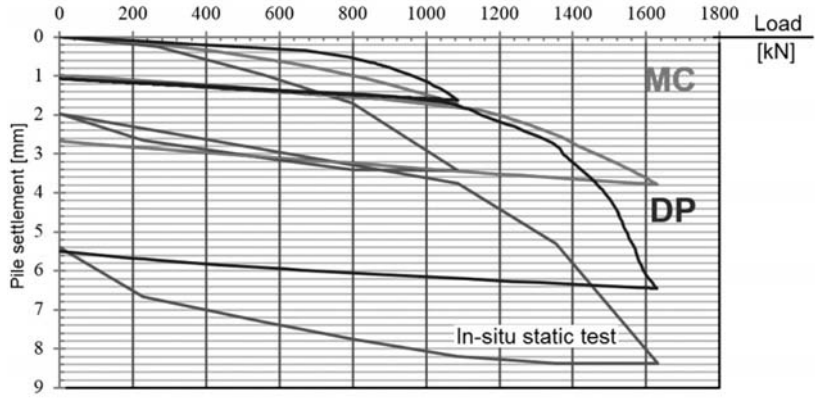

Fig. 10. The comparison of graphs showing the displacement-load dependence

Analysing Fig. 10, it should be noted that in the first phase of the in-situ load application – the 2nd step of the analysis – their shapes are similar. In step 4, the applied force increases from 0 to 150% NP within the same time interval as in step 2. At this stage of the analysis, the MC and DP soil response models are divergent.

In the DP model the displacements are greater, resulting in larger permanent (plastic) deformation that can be noticed after completing the analysis. The authors concluded that the Drucker-Prager constitutive equation applied as a model of soil gives a solution more similar to the static load field tests.

References

[1] *Analysis of Geotechnical Problems with Abaqus*, ABAQUS, Inc., 2006.

[2] *ABAQUS User's Manual*, 2011.

[3] Cichoń C., *Computer Methods in the Linear Structural Mechanics*, Wydawnictwo Politechniki Krakowskiej, Kraków 2002.

[4] Gryczmański M., *Load Path Methods in the Analyses of Soil Mechanics Problems*, 2002.

[5] Helwany S., *Applied Soil Mechanics: with ABAQUS Applications*, John Wiley & Sons, Inc., 2007.

[6] Gwizdała K., *Piles and Pile Foundations Settlement. Seminar – Pile Foundations Issues*, Gdańsk 2004.

[7] Han L.H., *A Modified Drucker-Prager Cap Model for the Compaction Simulation of Pharmaceutical Powders*, International Journal of Solids and Structure, 45 (10), 2008, 3088-3106

[8] Cudny M., Binder K., *Criteria of Soil Shear Strength in Geotechnology*, Inżynieria Morska i Geotechnika 6, 2005, 456-465.

[9] Ivorra S., *Drucker–Prager yield criterion application to study the behaviour, of CFRP confined concrete under compression*, XXXVII IAHSWorld Congress on Housing, October 26–29, Santander, Spain 2010.

[10] Schümann B., *Modelling of soils as multiphase-materials with Abaqus*, SIMULIA Customer Conference, 2010.

[11] Torben Pichler T.P., *High-Performance Abaqus Simulations in Soil Mechanics*, SIMULIA Community Conference, 2011.

[12] Wiłun Z., *Introduction to Geotechnology*, WKŁ, 2005.

[13] Wrana B., *Soil Dynamics. Computational Models*, Wydawnictwo Politechniki Krakowskiej, Kraków 2012.

[14] Zienkiewicz O.C., Taylor R.T., *The Finite Element Method*, Butterworth-Heineman, 2000.

TECHNICAL TRANSACTIONS | CZASOPISMO TECHNICZNE
CIVIL ENGINEERING | BUDOWNICTWO
2-B/2013

ŁUKASZ ZDANOWICZ*, PIOTR NOAKOWSKI**

STIFFNESS NONLINEAR ANALYSIS OF SECTIONS FOR REINFORCED CONCRETE MEMBERS

SZTYWNOŚCIOWA NIELINIOWA ANALIZA PRZEKROJÓW ŻELBETOWYCH

Abstract

An example of nonlinear mechanics of reinforced concrete based on stiffness of the analysed elements (*stiffness oriented design*) is presented in the paper. To define internal forces in reinforced concrete members, usually a linear relation is used. There is lack of considering an effect of stiffness variation after the first cracking. It often leads to underestimation of cross-sectional forces, which may give incorrect calculation results. The stiffness oriented nonlinear analysis allows for the description of work and behaviour of the structure much more precisely, which leads to an increase of safety and economy of the designed object.

Keywords: stiffness, curvature, nonlinear analysis, cracking, reinforced concrete elements

Streszczenie

W artykule zaprezentowano przykład nieliniowej mechaniki żelbetu opartej na sztywności analizowanych elementów (*stiffness oriented design*). Określenie sił wewnętrznych w elementach żelbetowych zwykle oparte jest na związkach liniowych. Nie uwzględnia się zjawiska zmiany sztywności po pojawieniu się zarysowania. Prowadzi to często do niedoszacowanych wielkości sił przekrojowych, co może skutkować niemiarodajnym wynikiem obliczeń. Nieliniowa analiza zorientowana sztywnościowo pozwala poznać dokładniej pracę i zachowanie się konstrukcji, co prowadzi do podwyższenia bezpieczeństwa i ekonomii projektowanego obiektu.

Słowa kluczowe: sztywność, krzywizna, analiza nieliniowa, zarysowanie, elementy żelbetowe

* M.Sc. Eng. Łukasz Zdanowicz, Institute of Building Materials and Structures, Faculty of Civil Engineering, Cracow University of Technology.
** Prof. Piotr Noakowski, Exponent Düsseldorf, TU Dortmund University.

1. Introduction

The criterion of adequate similarity between the real object and its design model is a condition for the proper designing of building structures. The methods and tools for analysis should be so selected as to fulfil the criterion for the required level of reliability.

The most popular assumption used in the designing of reinforced concrete elements is linear stress-strain (σ-ε) distribution. The classic linear theory [6, 12] takes into consideration the work of reinforced a concrete element in three phases: (1) phase 1 for uncracked element; (2) phase 2 for cracked section; (3) phase 3 treated as exceeding the limit state of this section. However, the possibility of redistribution of static values caused by cracking is omitted. It causes that a change of the element stiffness (local decreases of stiffness in cracked sections) is not taken into account, which is usually a significant value [4]. As a result, it can lead to underestimation of internal forces values that most often occurs in the response of a structure to temperature changes, forced displacements or abrupt changes of stresses. Usually in these cases, using a more precise and proper approach is required, such as, for instance, a nonlinear analysis [1, 11, 13].

Nonlinear analysis allows for the defining of distributions of internal forces and displacements of the structure closer to reality [15], what influences directly its level of reliability. *Meaning unclear, consider rephrasing* The Nonlinear method embraces two aspects here: physical and geometrical. Physical nonlinearity of reinforced concrete is connected with the law of behaviour of this material under current action, whereas geometrical nonlinearity is connected with the geometry and strains of the structure.

This paper focuses on the nonlinear analysis of reinforced concrete in the stiffness aspect (*stiffness oriented design*) [9, 10]. The article is restricted to physical nonlinear problem and omits the effects of geometric nonlinearity of the structure (LNR method, where L – geometric linearity, N – physical nonlinearity, R – real stiffness of the element) [6].

2. Nonlinear analysis

2.1. Assumptions

Current national standard [N2] concerning the design of the concrete structures allows for the use of nonlinear idealisation of the structure response. The regulation in [N2] states: "5.1.1(4)P Analysis shall be carried out using idealisations of […] the behaviour of the structure. The idealisations selected shall be appropriate to the problem being considered". Therefore a proper method should be applied depending on the problem.

In the statically determinate systems, cross-sectional forces are not dependent on their material and geometric attributes (except for the loads implicated from the self-weight). In the statically indeterminate systems, these attributes already become significant. Differences in stiffness of members caused by cracking and nonlinear behaviour of concrete influence the distribution of internal forces in the element [3, 4]. Therefore, values of cross-sectional forces are, among other things, a function of the physical and geometrical attributes.

The advantage of nonlinear approach, as distinct from other advanced methods, e.g. plastic analysis [8], is a possibility of its application for defining both the ultimate limit states (ULS) and serviceability limit states (SLS) [16].

2.2. Relation of bending moment to curvature (M-κ)

The basic assumption of the stiffness nonlinear analysis of reinforced concrete members is the relationship of bending moment to curvature of the member. This relationship, which is based on experimental results, is strongly nonlinear (Fig. 1). The initial, linear character of the M-κ function (phase 1, concrete in cooperation with reinforcement works on its whole height) is saved until achieving the value of the cracking moment M_{cr} in section. First cracks are created after obtaining this value, and as a result, an abrupt variation of the curvature of the element occurs (from this moment, concrete in the cracked section is bearing only compression stresses – the reduction of local stiffness can be observed). The stiffness of the section is represented here by the function of an angle α (tg(α_I)) for phase 1, tg(α_{II}) and for phase 2, tg(α_i) – the stiffness of element after i-th crack. In this area, cracking will occur without any increment of the bending moment. The stiffness of the bent element is considerably reduced until it achieves a stabilized cracking [6]. After the pattern of cracks in the element stabilises, an increment of bending moment will cause an increase in the width of these cracks (the number of cracked sections will remain approximately constant) until it achieves the value of the maximum moment M_y. Then, a breakage of tensile steel reinforcement occurs (the stress in reinforcement is equal to f_y).

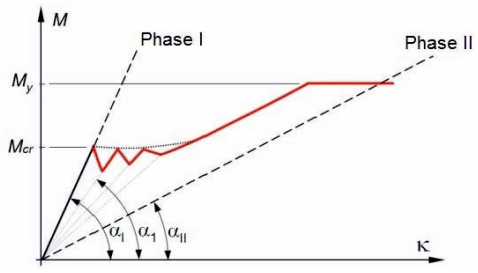

Fig. 1. Relation bending moment – curvature of the cross-section (M-κ) [6, 7, 17]

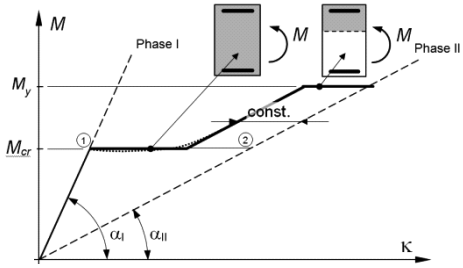

Fig. 2. Simplified relation M-κ [10]

A simplification of the M(κ) function is presented [9, 10]. It is based on replacing the abrupt changes of the curvature in the sections of unstabilised cracking by a horizontal line at the level of value of the cracking moment M_{cr} (Fig. 2). It is assumed here, in agreement with experimental data [5], that occurrence and development of cracks happen without an increase of the bending moment ($M = M_{cr}$). Concrete between the cracked sections cooperates with reinforcement bars by carrying tension stresses and causes strengthening of the areas between cracks (*tension stiffening*). The value of this strengthening (dk) in section is constant (it is assumed as 40% of the length 1–2 [10] – confer Fig. 2) and independent from the increment of bending moment (cracks spacing in elements is approximately constant) – confer [2, 5, 14] too.

2.3. Iterative evaluation of the cross-section stiffness

To define the proper values for the element (crack width, deflection), its stiffness shall be defined. It requires using iteration in the nonlinear stiffness method (confer Fig. 3).

The iteration here is done by assuming such value of the element curvature (κ_i) that the value of bending moment for this curvature (M_i) lays on the nonlinear function $M(\kappa)$. The number of iterations (n, on Fig. 3. $n = 4$) depends on the assumed length of the iteration step and accuracy (%) of a ratio of iterative moment M_i to the value of moment readout from the M-κ function, i.e. $\Delta M = M_i / [M_i - M(\kappa)]$).

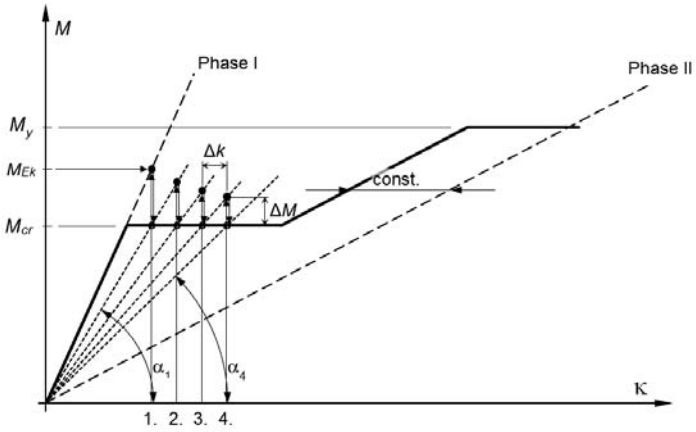

Fig. 3. Relation M-κ – iterative evaluation of stiffness of the cross-section

A block diagram illustrating an iterative procedure is presented below.

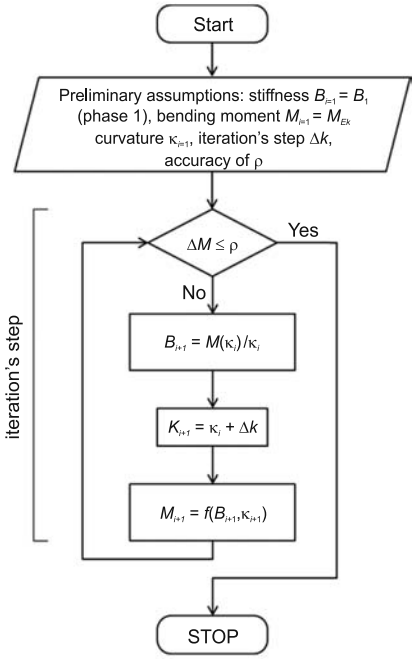

Fig. 4. Block diagram for iteration

3. Design example

As an example, a reinforced concrete two-span beam with a continuous load (cf. Fig. 5) was analyzed, where:

– geometry: L_{eff} = 10.0 m, b = 0.5 m, h = 1.0 m,
– material: concrete C30/37, reinforcement B500St: A_{s1} = 30 cm^2, A_{s2} = 20 cm^2,
– bending moment in the "B" support $M_{Ek.B}$ = 500 kNm.

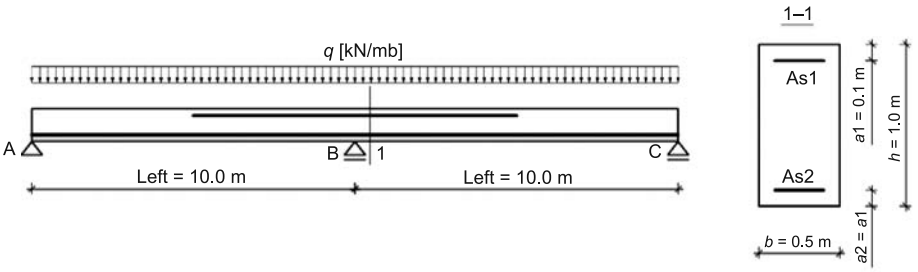

Fig. 5. Two-span beam – geometry and design scheme

It is assumed that:

– step of iteration $\Delta k = 20 \cdot 10^{-4}$%/m,
– relative error of iteration ρ = 5% (12.1 kNm),
– the cracking moment M_{cr} = 242 kNm,
– stiffness of the cross-section $B_{I} = 1.522 \cdot 10^6$ kNm^2 (phase I) and $B_{II} = 0.331 \cdot 10^6$ kNm^2 (phase II).

After execution of n = 7 steps of iteration (Fig. 6), the relative error of iteration is equal to ρ = 4.8%, which gives values of bending moment $M_{i=7}$ = 253.6 kNm, curvature $\kappa_{i=7} = 436.12 \cdot 10^{-4}$%/m and revised stiffness of the analysed section $B_{i=7} = 0.485$ kNm^2 (30.18°). The results of the subsequent iteration steps are presented in Table 1. For comparison – stiffness of the same cross-section defined according to EC2 procedure [N2] is equal to $B_{EC2} = 0.405 \cdot 10^6$ kNm^2, where relative error of stiffness $B_{i=7}$ and B_{EC2} is equal to 19.8%.

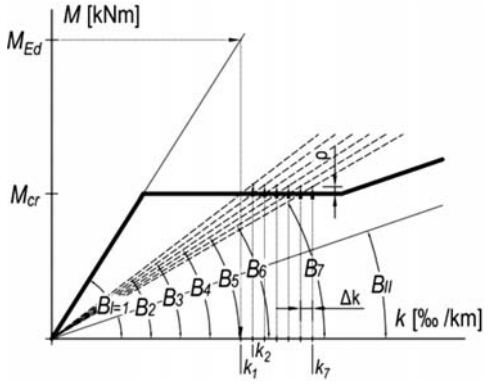

Fig. 6. M-κ diagram according to specific data

Table 1

Results of subsequent iteration steps

Iteration's step (i)	B_i [10^6 kNm^2]	κ_i [10^{-4}%/m]	M_i [kNm]	ρ_i
1.	1.484	316.12	500.0	106.9%
2.	0.579	336.12	257.4	6.5%
3.	0.558	356.12	256.4	6.1%
4.	0.539	376.12	255.6	5.8%
5.	0.519	396.12	254.9	5.5%
6.	0.502	416.12	254.2	5.2%
7.	**0.485**	**436.12**	**253.6**	**4.8%**

The results in Table 1 present speed of iterative convergence in the subsequent steps. This example shows that just after the first step of iteration, the value of an iteration error is approximately $\rho_{i=1} = 7\%$, which should be acknowledged as a satisfactory result. The next iterative steps ($i \geq 2$) reveal moderate convergence. This convergence however is not linear, but decreasing.

4. Conclusions

Nonlinear analysis in the stiffness aspect allows for the defining of the values of internal forces much more precisely in relevance to classical linear theory (here almost 20%). Their scope can be used to analyse problems which significantly exceed the scope of a linear approach (for example: the redistribution of internal forces, design for exciting forces). Additionally, such an aspect of nonlinear analysis might be used – opposite to plastic analysis – to define serviceability limit states (SLS) for the structure.

The presented nonlinear design model based on stiffness oriented design method gives an opportunity to assume any accuracy of values (controllable parameters: numbers of iterations and relative difference of cross-sectional forces). Just after the first step of iteration, the founded values allow for the forecasting of the final result. It is a legible and algorithmic method, suitable for common application in practice and for implementation in design software. Designing according to the nonlinear stiffness method increases reliability of the structures and rationality in forming their geometry.

References

[N1] PN-EN 1990:2002/A1:2008/NA:2010 Eurocode – Basis of structural design (in Polish).

[N2] PN-EN 1992-1-1:2008/Ap1:2010/NA:2010/AC:2011 Eurocode 2: Design of concrete structures – Part 1-1: General rules and rules for buildings (in Polish).

[1] Bathe K.-J. et al., *Nonlinear analysis of concrete structures*, Computers & Structures, Vol. 32, No. 3/4, 1989, 563-590.

[2] Bischoff P.H., *Effects of shrinkage on tension stiffening and cracking in reinforced concrete*, Canadian Journal of Civil Engineering, 28, 2001, 363-374.

[3] Czkwianianc A., Kamińska M., *Analysis of structure*[in:] Plain, reinforced and prestressed concrete structures. Scientific commentary for PN-B-03264:2002, t. 1, Building Research Institute, Warsaw 2005.

[4] Czkwianianc A., Kamińska M., *Method of nonlinear analysis of one-dimensional reinforced concrete memebers*, PAN – IPPT, No. 36, Warsaw 1993.

[5] Lee G.-Y., Kim W., *Cracking and Tension Stiffening Behavior of High-Strength Concrete Tension Members Subjected to Axial* Load, Advanced in Structural Engineering, Vol. 12, No. 2, 2009, 127-137

[6] Knauff M., *Calculation of reinforced concrete structures according to Eurocode 2*, PWN, Warsaw 2013.

[7] Koeberl B., Willam K., *Question of Tension Softening versus Tension Stiffeinig in Plain and Reinforced Concrete*, Journal of Engineering Mechanics, 2008, 804-808,

[8] Nielsen M.P., Hoang L.C., *Limit Analysis and Concrete Plasticity*, CRC Press – Taylor & Francis Group, 2011.

[9] Noakowski P., *Nachweisverfahren für Verankerung, Verformung, Zwangbeanspruchung und Rißbreite*, DAfStb, Heft 394, Beuth Verlag, Berlin 1988.

[10] Noakowski P., Schäfer H.G., *Steifigkeitsorientierte Statik im Stahlbetonbau*, Ernst&Sohn, Berlin 2003.

[11] Polak M.A., Vecchio F.J., *Nonlinear Analysis of Reinforced Concrete Shells*, Publication 93-03, University of Toronto, Department of Civil Engineering, Toronto 1993.

[12] Rombach G.A., *Finite element design of concrete structures*, Thomas Telford, London 2004.

[13] Vecchio F.J., *Non-linear finite element analysis of reinforced concrete at the crossroads?*, Structural Concrete, 2, No. 4, 2001, 201-212,

[14] Whittle R., Jones T., *Technical Report No. 59: Influence of tension stiffeinig on deflection of reinforced concrete structures*, The Concrete Society, Camberley, 2004, http://www.docin.com/p-282876679.html – dostęp: 21.06.2013.

[15] Winnicki A., Cichoń Cz., Waszczyszyn Z., *Nonlinear analysis of reinforced concrete bar members using FEM*, Archiwum Inżynierii Lądowej, 36, z. 1-2, 1990, 29-61.

[16] Wołowicki W., Garstecki A., *Static analysis of structure* [in:] *Basics of structural design of reinforced and prestressed concrete structures according to Eurocode 2*, DWE, Wroclaw 2006 (in Polish),

[17] Wu H. Q., Gilbert R. I., *Modeling short-term tension stiffening in reinforced concrete prisms using a continuum-based finite element model*, Engineering Structures 31, 2009, 2380-2391.

TECHNICAL TRANSACTIONS | CZASOPISMO TECHNICZNE
CIVIL ENGINEERING | BUDOWNICTWO
2-B/2013

ŁUKASZ ZDANOWICZ*, RYSZARD WOJDAK**

STRUCTURAL ANALYSIS OF A FAILURED RC BEAM WITH OPENINGS IN A BUILDING UNDER CONSTRUCTION

ANALIZA STANU AWARYJNEGO BELKI ŻELBETOWEJ Z OTWORAMI W NOWO WZNOSZONYM BUDYNKU

Abstract

Examples of defectively constructed-designed and constructed openings in RC beams in a building under construction were presented in the paper. As a result of errors in the design and construction-construction phases, the beams could not fulfil their function. The state of the considered beam with openings was defined as critical (a failure). The results of an analysis of the designed and constructed-constructed state showed differences in the static performance of the structure. However, the redistribution of internal forces is not significant because of the relatively stiff floor slab which takes over the loads from beams. This paper can also provide a background for a more general discussion about the present quality of coordination between design and construction of building structures.

Keywords: beam openings, failure, construction-construction errors, RC structures

Streszczenie

W artykule przestawiono przykłady błędnie wykonanych otworów w belkach żelbetowych nowo wznoszonego budynku. Na skutek błędów projektowo-wykonawczych belki nie mogły spełniać swojej funkcji. Stan analizowanej belki z otworami określono jako awaryjny. Wyniki obliczeń stanu projektowanego i istniejącego wykazały różnice w pracy statycznej konstrukcji. Redystrybucja sił wewnętrznych nie jest jednak znacząca z powodu zastosowanej względnie sztywnej płyty stropowej, która przejmuje na siebie obciążenia z belek.

Słowa kluczowe: otwory w belce, awaria, błędy wykonawcze, konstrukcje żelbetowe

* M.Sc. Łukasz Zdanowicz, Institute of Building Materials and Structures, Faculty of Civil Engineering, Cracow University of Technology.

** Ph.D. Ryszard Wojdak, Chair of Concrete Structures and Concrete Technology, Faculty of Civil and Environmental Engineering, Gdansk University of Technology.

1. Introduction

Reinforced concrete floor beams are often an element of monolithic structures of buildings. Openings are made due to a necessity of equipping objects in various ceiling installations through these beams (and also floor slabs, walls etc.). The location and size of these openings should not influence the capacity and stability of the load-bearing element.

The subject of the analysis is a structure in which openings in load-bearing elements were defectively designed and constructed. The author of this paper has the design documentation and his own documentation in the form of photographs. Examples of incorrectly designed and constructed openings in reinforced concrete beams and other load-bearing elements (floor slabs, walls) in the public building under construction were presented in the paper. As a result of significant defects of construction, a question appeared as to whether load-bearing elements (mostly beams) can perform their function during new, changed static conditions of a structure. The aim of this analysis is an attempt to answer such a question based on the performed analysis. The condition of reinforced concrete beams was described as critical (i.e. a failure).

2. The building specification

2.1. Geometry and materials

The described building is a monolithic reinforced concrete structure of mixed type – flat slab dominates and slab-beam floor appears in several rooms, in addition, there are some columns and load-bearing walls. In considered part of the building, there are five above-ground stores (the height at the attic: +22.60 m) without basement; main dimensions in plane 54 × 16 m (Fig. 1). The building is dilated at G-G' (44 m/10 m), which is why two separate parts can be considered.

Full, flat floor slabs of 22 cm thickness made of concrete C25/30 (the same concrete grade as for floor slabs and beams), supported on columns (dimensions of cross-sections were diversified, concrete grade C25/30), were designed and constructed. In the considered area,

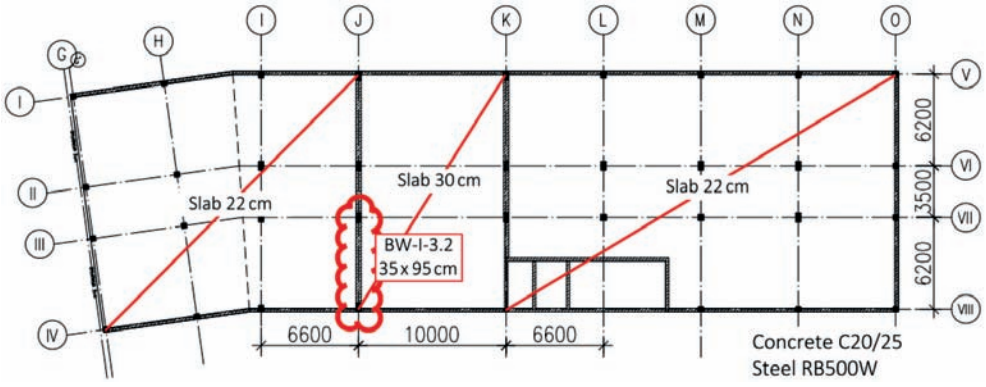

Fig. 1. The considered Floor Plan (defective beam marked)

a slab-beam floor with increased thickness (to 30 cm) occurs between axes J-K/V-VIII on level +9.35 m. The main beams supporting floor slab in this area have dimensions of cross-section 35 × 95 m, concrete C20/25, steel tensile reinforcement 3ϕ25 mm A-IIIN (RB500W), a concrete cover of main reinforcement equal to 6 cm.

2.2. Actions on the structure

Designer [1] predicted typical actions on the load-bearing elements (only the loads affecting the considered area of floor slabs are specified here):

1. Self-weight of load-bearing elements:
   a. floor slab $g_{k.s}$ = 5.5/7.5 kN/m^2 (for thickness 0.22 m and 0.30 m, respectively),
   b. beams $g_{k.b}$ = 6.39/5.69 kN/mb (without slab),
   c. where γ_f = 1.10 (0.90). Self-weight of elements was considered automatically by computer software.
2. Dead loads: g_k = 2.4 kN/m^2, where γ_f = 1.30 (0.80),
3. Live service loads: q_k = 2.5 kN/m^2 (including 0.5 kN/m^2 from weight of installations), where γ_f = 1.4.

This analysis follows the national standards PN-B.

2.3. Failure of a floor beam

A lot of holes for installations were made in the load-bearing elements during the construction of the building. They were made in slab floors, beams and walls (see Fig. 2a–Fig. 2g). The majority of these holes were made defectively, causing unexpected structural response.

Fig. 2a. Openings in load-bearing elements

Fig. 2b.”Random” openings in a floor slab

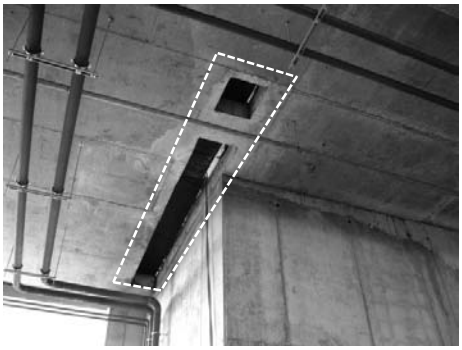

Fig. 2c. Openings designed in floor slab (marked by dashed line)

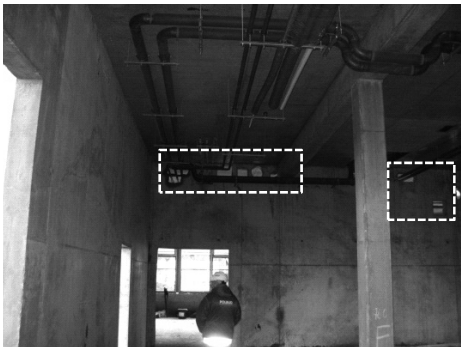

Fig. 2d. Uncontrolled openings in a load-bearing wall

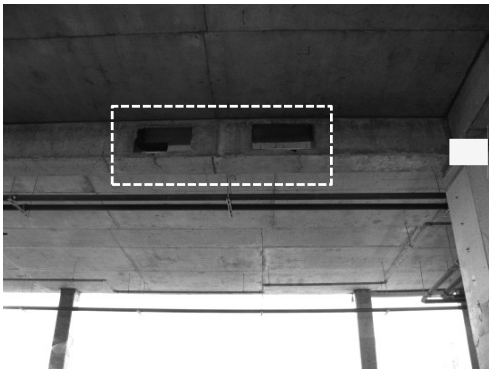

Fig. 2e. Defectively designed openings in beam (cracked lower strip)

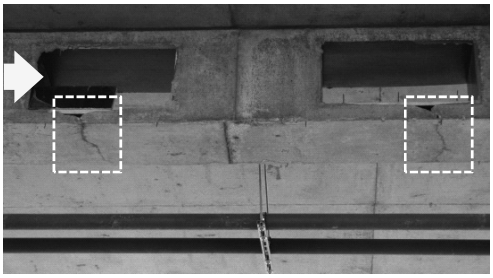

Fig. 2f. Detail of Fig. 2e

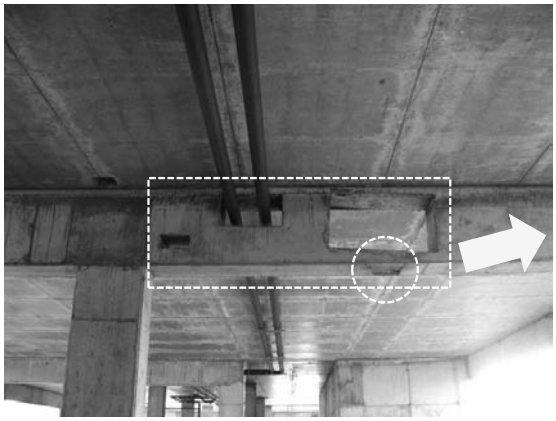

Fig. 2g. Failed beam

Fig. 2h. Detail of Fig. 2g (concrete decrement in lower strip)

Moreover, numerous design-construction mistakes were noticed (cf. Fig. 3a to 3d).

Fig. 3a. Demaged column

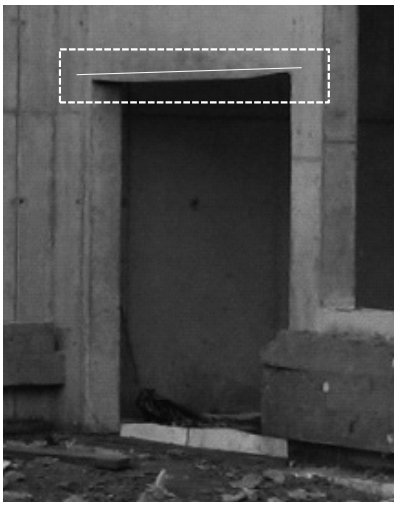

Fig. 3b. Deflection of doorhead due to wrong shoring procedure

Fig. 3c. Defective concrete placement

Fig. 3d. Internal wall made of solid bricks (is it needed?)

3. Structural analysis

3.1. Assumptions

An analysis was performed of selected, critical area of the structure (beam with openings and a floor slab in section J/VII-VIII – Fig. 2g and 4; element number BW-I-3.2, construction drawing no. IP026_PW_DR_2542_RC). Two models were developed:

1) plate model of a floor slab with load-bearing beams and
2) disk model (plane stress state – PSS) of the selected, critical beam.

The "ABC Płyta" and "ABC Tarcza" software was used for analysis. The results of calculations for the model representing the constructed structure (E) (existing state) were compared to corresponding results for the as designed structural model (D).

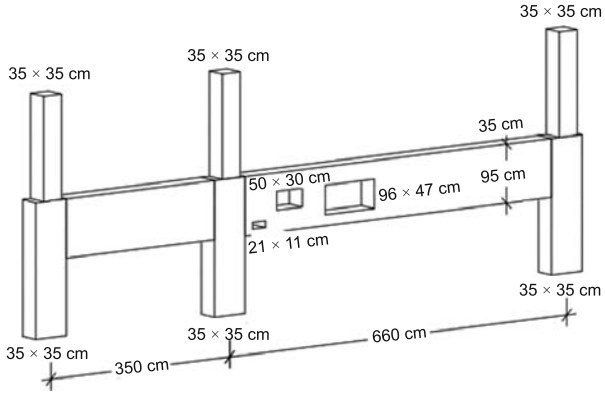

Fig. 4. Designed geometry of beam BW-I-3.2

3.2. Plate model

The differences between constructed state (E) and the designed situation (D) are presented below. Results show an expected modified distribution of displacements (and therefore modified internal forces) and support reactions for slab and analysed beam. Table 1 shows the results for:

– the ultimate limit state (ULS) of moment in fixed support (cf. Fig. 5a and 5b),
– the serviceability limit state (SLS) of displacement of the beam caused by quasi-static actions (confer Fig. 6a and 6b).

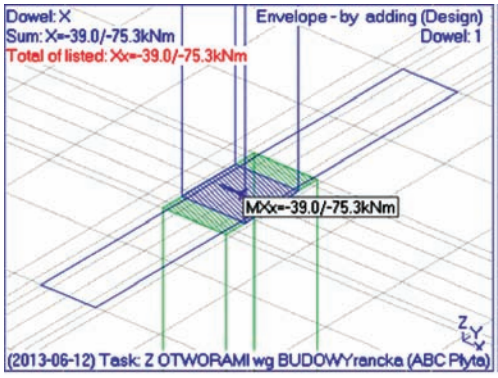

Fig. 5a. Moment in fixed support of beam with constructed openings (E)

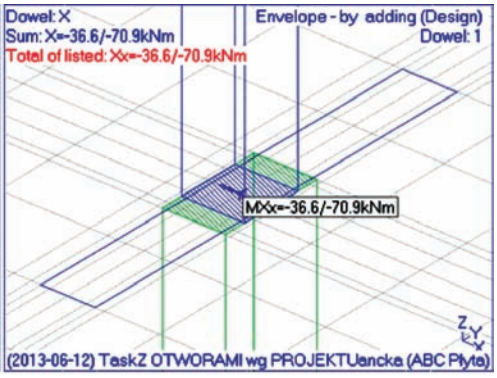

Fig. 5b. Moment in fixed support of beam with designed openings (D)

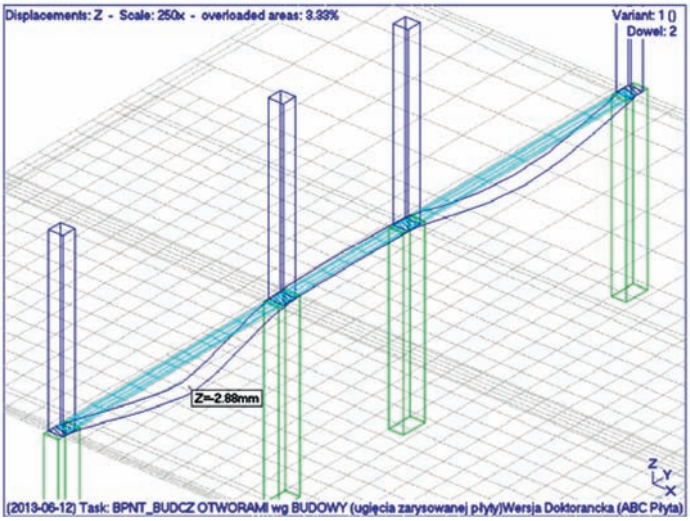

Fig. 6a. Deflection of beam with constructed openings (E)

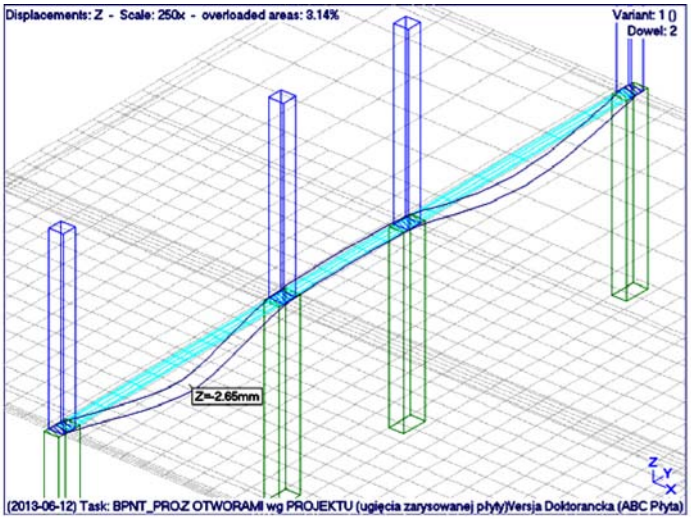

Fig. 6b. Deflection beam with designed openings (D)

The results indicate that the maximum beam deflections in (E) state are larger than deflection in (D) state, and the difference is approximately $\delta_f = 9\%$. In the beam without openings, the deflection equals $f_Z = 1.70$ mm ($\delta_f = -36\%$ in comparison to (D), with a significant observation that this point is not a point of the maximum deflection, which in reality is located in another area of the beam and is equal to $f_{max} = 2.16$ mm). It is caused by a change of the static system of the structure, where a redistribution of internal forces occurs as a result of local stiffness variation. The reduction of bending stiffness of cracked beams is not significantly different between (E) and (P) models – ca. 4%.

Table 1

Values of deflections and moments in fixed support for plate model

Model	Deflection of beam			Deflection of plate		Moment in fixed support		Remark
	f_Z [mm]	δ_f	β	$f_{Z.s}$ [mm]	$\delta_{f.s}$	M_X [kNm]	δ_M	
Constructed beams (E)	2.88	**+9%**	260%	18.08	–1%	–75.3	**6%**	$f_Z = f_{max}$
Designed beams (D)	2.65	–	270%	18.30	–	–70.9	–	$f_Z = f_{max}$
Beams without openings	1.70	–36%	240%	17.57	–4%	–58.4	18%	$f_Z \neq f_{max}$

where: δ_f and δ_M were defined in relevance to (D) state; β – stiffness reduction of cracked section in comparison to (D) state in elastic phase, defined according to equation $\beta = f_Z/f_e$, where f_e – elastic beam deflection from quasi-static loads.

Such relatively slight variations of deflections (and internal forces in analogy) between (E) and (D) models are as a result of the assumed large slab thickness (i.e. 30 cm). This slab takes over the majority of loads and transfers them to the columns without any distinctly visible contribution of the beams.

The maximum deflections of the floor slab do not show any significant variation between (E), (D) and "Beam without openings" models ($\delta_{f.s} < 5\%$; places of maximum deflections are covered for all three models) – again, a considerable influence of floor slab thickness in bearing the loads is observable here.

It is worth paying attention to variation of the moment in fixed support along the beam M_X, (cf. Fig. 4a and 4b) – the value of increment is equal to $\delta_M = 6\%$ (in comparison with model of beams without openings $\delta_M = 18\%$).

3.3. Disk model (plane state of stress)

The disk model allows for the consideration of the shape and scale of deformations of the beam caused by openings (Fig. 7a and 7b). The tensile reinforcement at of the bottom of beam was modelled as an equivalent of 325 mm (cf. point 2.1).

The openings in the beam caused considerable changes in element curvature in the area of reduced stiffness of a section (area around the openings). It leads to a redistribution of internal forces which was not anticipated in the design phase. In the figures below, the principal stresses (σ_1, σ_2) from self-weight loads for beams (Fig. 8a and 8b) with and without openings (Fig. 9a and 9b) models are shown.

The beam openings significantly disturb the distribution of stresses in the considered cross-sections. A particular concentration of stress occurs along the edges of openings and around the corners of openings. The horizontal tension stress σ_X in an area of the largest

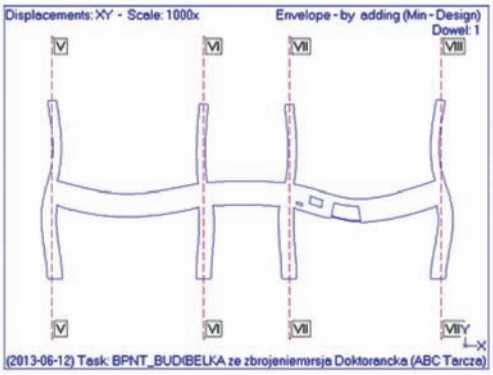

Fig. 7a. Deformation of beam in disk model

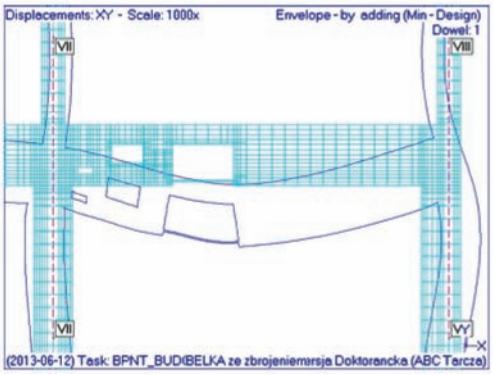

Fig. 7b. Deformation of beam (zoom of Fig. 7a)

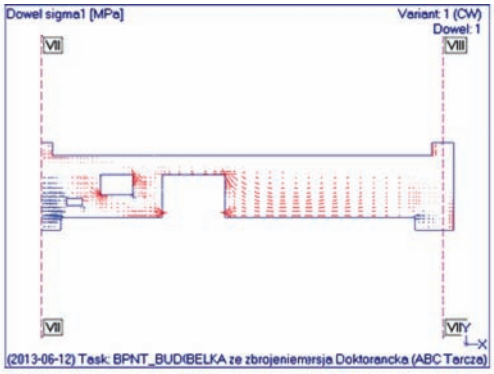

Fig. 8a. Principle stress σ_1 of beam with openings

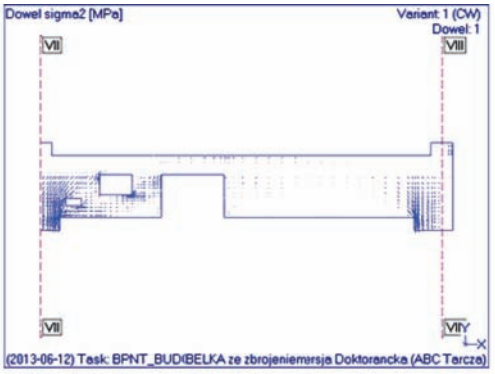

Fig. 8b. Principle stress σ_2 of beam with openings

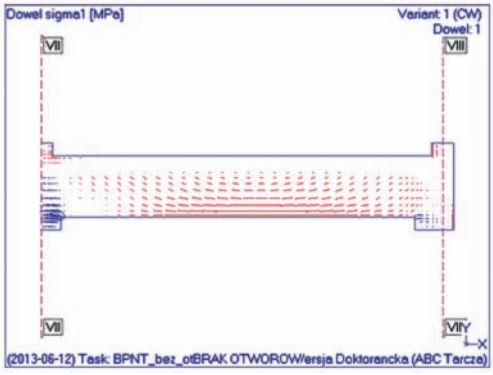

Fig. 9a. Principle stress σ_1 of beam without openings

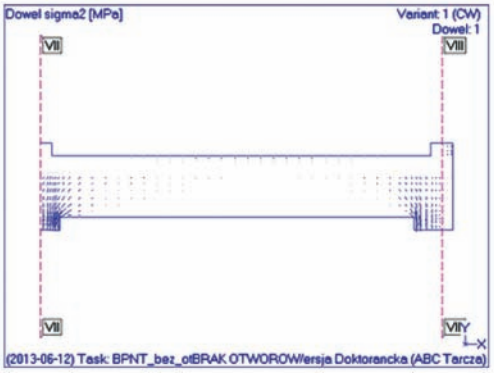

Fig. 9b. Principle stress σ_2 of beam without openings

opening is concentrated at the bottom (represented by steel reinforcement). Simultaneously, the small part of these stresses is taken over by the slab, where the σ_X stress distribution is linear – as shown in Fig. 10. The stress σ_X in the area of the openings (but beyond the slab) is nonlinear (σ_X stress between the openings, Fig. 10). The visible move of the beam neutral axis in top direction (σ_X stress beyond the area of openings) is caused by interaction between the beam and the floor slab, which are monolithically connected. The distribution of vertical stress σ_Y (similar to σ_X) is nonlinear, especially in the corner area of openings where there is a considerable variation of σ_Y (Fig. 11).

Fig. 10–11 show the distribution of σ_X and σ_Y stresses in particular sections of the beam.

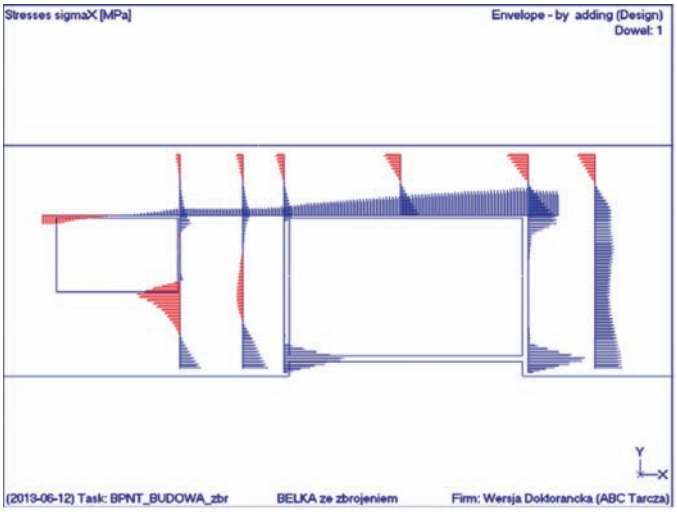

Fig. 10. Stress σ_X

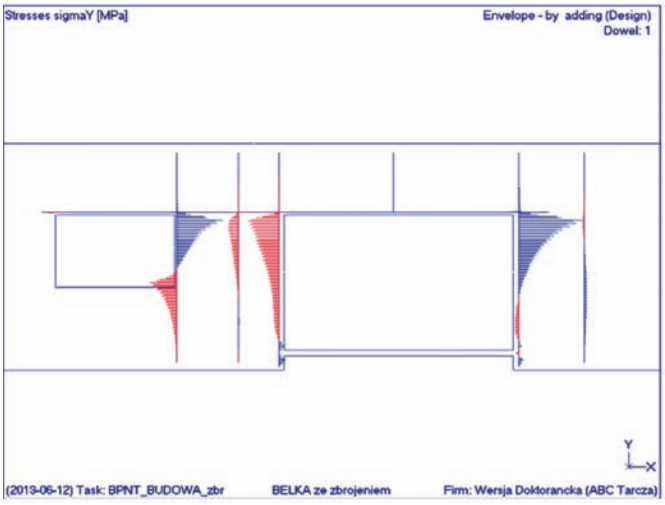

Fig. 11. Stress σ_Y

4. Conclusions from the analysis

The analysis above implies that defectively constructed openings have an impact on the behaviour of load-bearing elements. A structure under loads adapts to a "new" geometry through, among other things, a redistribution of internal forces (confer variations of displacements for slab and beam). However, it causes the risk of unexpected response of a structure due to changed static system. The redistribution is not significant in this case because of the relatively stiff floor slab, which takes over the majority of loads (beam is out of work in the structure) and transfers these loads, to a large extent, directly onto the columns. The recommendation from Designer in point 5.3.3 of the construction project "in the places with insufficient stiffness, reinforced concrete beams connected with floor slabs and columns should be constructed" was not fulfilled, and even missed both during the design and the construction phase – the analysed beams do not have sufficient stiffness.

5. Conclusions

The intention for the presented observations was to voice an opinion about a still timely problem of communication between Designer and Contractor in building projects, and in particular related to supervision, coordination and quality of these works. Despite more and more advanced tools used in engineering, up to now, nothing can replace the human factor (which usually is an adequate experience) [6]. Providing required level of structural reliability does not depend on the use of modern tools – it depends not less on good habits, experience and integrity during everybody's own work. Let the figure below (Fig. 12) be the punchline, which quite clearly illustrates the problem of quality and coordination in the building process.

Fig. 12. „Well-founded" construction of the opening in beams

References

[NI] PN-82/B-02000 Actions on building structures. Principles of the establishment of the values (in Polish).

[N2] PN-82/B-02001 Actions on building structures. Permanent actions (in Polish).

[N3] PN-82/B-02003 Actions on building structures. Variable actions during exploitation and assembling (in Polish).

[N4] PN-B-03264:2002/Ap1:2004 Plain, reinforced and prestressed concrete design – Analysis and structural design (in Polish).

[N5] PN-EN 1992-1-1:2008/Ap1:2010/NA:2010/AC:2011 Eurocode 2: Design of concrete structures – Part 1-1: General rules and rules for buildings (in Polish).

[1] Construction project of building structure, Project no. …026/09, (confidential data), 2010.

[2] Bąk G., *Stress redistribution in result of opening constructed in reinforced concrete beam* [in:] Civil and Environmental Engineering, Vol. 1, No. 2, 2010, 99-110

[3] Knauff M. et al., *Plain, reinforced and prestressed concrete structures. Scientific commentary for PN-B-03264:2002*, Vol. 1, Building Research Institute, Warsaw 2005.

[4] Kobiak J., *Mistakes of reinforced concrete structures*, Arkady, Warsaw 1973.

[5] Starosolski W., *Reinforced concrete structures according to Eurocode 2 and other connected standards*, Vol. 3, PWN, Warsaw 2012.

[6] Starosolski W., *Computational modelling of concrete structures. Selected problems*, Vol. 1 and 2, Silesian University of Technology Publ., Gliwice 2012.

[7] Wojdak R., *Unusual author's building structures*, Gdansk University of Technology Publ., Gdańsk 2010.

[8] Zdanowicz Ł., *Engineer of Tomorrow – Human or Machine?*, 7th Students' Science Conference, Wroclaw 2009.

CONTENTS

TREŚĆ